NASA/CR–2000-209592

Description of Panel Method Code ANTARES

Norbert Ulbrich

Contract NAS2-98083

May 2000

The NASA STI Program Office . . . in Profile

Since its founding, NASA has been dedicated to the advancement of aeronautics and space science. The NASA Scientific and Technical Information (STI) Program Office plays a key part in helping NASA maintain this important role.

The NASA STI Program Office is operated by Langley Research Center, the Lead Center for NASA's scientific and technical information. The NASA STI Program Office provides access to the NASA STI Database, the largest collection of aeronautical and space science STI in the world. The Program Office is also NASA's institutional mechanism for disseminating the results of its research and development activities. These results are published by NASA in the NASA STI Report Series, which includes the following report types:

- TECHNICAL PUBLICATION. Reports of completed research or a major significant phase of research that present the results of NASA programs and include extensive data or theoretical analysis. Includes compilations of significant scientific and technical data and information deemed to be of continuing reference value. NASA's counterpart of peer-reviewed formal professional papers but has less stringent limitations on manuscript length and extent of graphic presentations.

- TECHNICAL MEMORANDUM. Scientific and technical findings that are preliminary or of specialized interest, e.g., quick release reports, working papers, and bibliographies that contain minimal annotation. Does not contain extensive analysis.

- CONTRACTOR REPORT. Scientific and technical findings by NASA-sponsored contractors and grantees.

- CONFERENCE PUBLICATION. Collected papers from scientific and technical conferences, symposia, seminars, or other meetings sponsored or cosponsored by NASA.

- SPECIAL PUBLICATION. Scientific, technical, or historical information from NASA programs, projects, and missions, often concerned with subjects having substantial public interest.

- TECHNICAL TRANSLATION. English-language translations of foreign scientific and technical material pertinent to NASA's mission.

Specialized services that complement the STI Program Office's diverse offerings include creating custom thesauri, building customized databases, organizing and publishing research results . . . even providing videos.

For more information about the NASA STI Program Office, see the following:

- Access the NASA STI Program Home Page at *http://www.sti.nasa.gov*

- E-mail your question via the Internet to help@sti.nasa.gov

- Fax your question to the NASA Access Help Desk at (301) 621-0134

- Telephone the NASA Access Help Desk at (301) 621-0390

- Write to:
  NASA Access Help Desk
  NASA Center for AeroSpace Information
  7121 Standard Drive
  Hanover, MD 21076-1320

NASA/CR–2000-209592

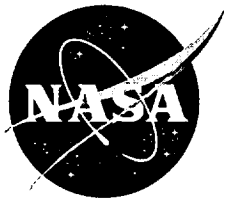

Description of Panel Method Code ANTARES

Norbert Ulbrich
Sverdrup Technology, Inc.
P.O. Box 366, M/S 227-4
Moffett Field, CA 94035-1000

National Aeronautics and
Space Administration

Ames Research Center
Moffett Field, California 94035-1000

Prepared for Ames Research Center
under Contract NAS2-98083

May 2000

Available from:

NASA Center for AeroSpace Information
7121 Standard Drive
Hanover, MD 21076-1320
(301) 621-0390

National Technical Information Service
5285 Port Royal Road
Springfield, VA 22161
(703) 487-4650

PREFACE

Panel method code ANTARES is described in this report. The code computes subsonic wall interference effects in a wind tunnel with rectangular cross–section. Different types of wall boundary conditions may be specified by the user. Blockage effects of a wind tunnel model are represented by point doublets. Lifting effects of a wind tunnel model are represented by line doublets. Compressibility effects are modeled by applying the Prandtl–Glauert transformation. Wall interference correction calculations were successfully verified by comparing panel method code solutions with corresponding classical solutions. A modified version of panel method code ANTARES is used to compute perturbation velocity database files for the real–time wall interference correction system of the NASA Ames 11ft Transonic Wind Tunnel.

I hope that the promising results obtained during the development of panel method code ANTARES will benefit attempts to improve data quality and efficiency of wind tunnel tests in the NASA Ames 11ft Transonic Wind Tunnel.

I want to thank Alan Boone, Mike George, and Don Nickison of NASA and Doug Pena of SVERDRUP Technology for their critical and constructive review of the manuscript. Their careful and competent proofreading and checking has greatly improved the quality of this report.

Moffett Field, California — Norbert Ulbrich

May 2000

TABLE OF CONTENTS

LIST OF SYMBOLS

c	wing chord
c_L	lift coefficient
c_p	pressure coefficient
c_1, c_2, c_3, c_4	coefficients describing wall boundary conditions
Δc_p	pressure coefficient difference
D	width of two–dimensional halfbody
h	half height of two–dimensional tunnel
h_1	width of rectangular tunnel
h_2	height of rectangular tunnel
i	index of wall panel centroid
j	index of wall panel
K	slot constant (see Ref. [6])
k	index of flow field point
L	lift force
l	slot parameter
M_∞	free–stream Mach number
m	summation index in y–direction of image system
m_e	parameter proportional to size of two–dimensional model (see Ref. [6])
N	total number of wall panels
n	summation index in z–direction of image system
R	restriction parameter
r_∞	radius of body of revolution
$r_\circ$	radius of sphere
r_c	radius of cylinder
Δs	span of line doublet
u	perturbation velocity in the x–direction
u_w	velocity correction due to wall interference in the x–direction
u_∞	free–stream velocity
v	perturbation velocity in the y–direction

v_w	velocity correction due to wall interference in the y–direction
w	perturbation velocity in the z–direction
w_w	velocity correction due to wall interference in the z–direction
x	x–coordinate; streamwise direction
$x_\circ$	x–coordinate of point doublet or of line doublet starting point
y	y–coordinate
$y_\circ$	y–coordinate of point doublet or of line doublet starting point
z	z–coordinate
$z_\circ$	z–coordinate of point doublet or of line doublet starting point
$\Delta\alpha$	angle of attack correction due to wall interference effects
β	$= \sqrt{1 - M_\infty^2}$
Γ	circulation
ϵ	blockage factor
ζ	third transformed coordinate; coordinate system rotation
η	second transformed coordinate; coordinate system rotation
Θ	$= \tau(0,0)$; line doublet orientation angle
μ	source strength slope of wall panel
ξ	first transformed coordinate; coordinate system rotation
ρ_∞	free–stream density
σ	singularity strength
τ	line doublet orientation angle of image system element
τ_e	cross–sectional area of two–dimensional model (see Ref. [6])
ϕ	perturbation velocity potential in wind tunnel
ϕ_m	perturbation velocity potential of model
ϕ_w	perturbation velocity potential of walls $\equiv$ wall interference potential
ϕ^*	wall panel potential per unit source strength slope (see Ref. [3])
$\mathbf{n}$	normal vector at wind tunnel wall
$'$ (superscript)	transformed variable (Prandtl–Glauert transformation)

ABSTRACT

Panel method code ANTARES was developed to compute wall interference corrections in a rectangular wind tunnel. The code uses point doublets to represent blockage effects and line doublets to represent lifting effects of a wind tunnel model. Subsonic compressibility effects are modeled by applying the Prandtl–Glauert transformation. The closed wall, open jet, or perforated wall boundary condition may be assigned to a wall panel centroid. The tunnel walls can be represented by using up to 8000 panels. The accuracy of panel method code ANTARES was successfully investigated by comparing solutions for the closed wall and open jet boundary condition with corresponding Method of Images solutions. Fourier transform solutions of a two–dimensional wind tunnel flow field were used to check the application of the perforated wall boundary condition. Studies showed that the accuracy of panel method code ANTARES can be improved by increasing the total number of wall panels in the circumferential direction. It was also shown that the accuracy decreases with increasing free–stream Mach number of the wind tunnel flow field.

CHAPTER 1

INTRODUCTION

The calculation of wind tunnel wall interference corrections in a perforated or slotted wall wind tunnel with rectangular cross–section has always been a challenge due to the complexity of the flow field in the vicinity of the test section walls. Numerical solutions of the wall interference flow field have to be computed by using a sufficiently accurate description of the wall boundary conditions. In addition, compressibility effects have to be included in the wall interference calculation as perforated or slotted wall wind tunnels are frequently operated at high subsonic Mach numbers.

Presently, a real–time wall interference correction system is being developed for the slotted wall test section of the NASA Ames 11ft Transonic Wind Tunnel (TWT). This system is similar to a system that was successfully implemented in the NASA Ames 12ft Pressure Wind Tunnel [1]. The real–time correction system uses a singularity representation of the test article. The system also requires precomputed solutions of the wall interference flow field in the test section and of the pressure coefficient on selected wall pressure ports. Therefore, it became necessary to develop a three–dimensional flow field solver, i.e. panel method code ANTARES, that allows for the calculation of the wind tunnel and wall interference flow field of a singularity in a perforated or slotted wall wind tunnel with rectangular cross–section.

Different numerical techniques are available to compute wall interference in a perforated or slotted wall wind tunnel. After careful review of the existing literature [2] the author decided to use *Keller's* panel method algorithm [3] as a basis for the development of panel method code ANTARES.

Keller [3] developed an incompressible panel method algorithm that computes the upwash velocity (angle of attack correction) caused by line doublets in a wind tunnel with rectangular cross–section. *Keller's* description of the panel method algorithm is exceptionally clear and complete. His algorithm allows the user to assign one of six different types of boundary conditions to each wall panel. The following boundary conditions may be specified: (1) closed wall; (2) open jet; (3) perforated wall; (4) ideal slotted wall (integrated

form); (5) ideal slotted wall (differentiated form); (6) slotted wall including viscosity in slots. Slopes of the source distribution strength of each wall panel are unknowns in the linear system of *Keller's* algorithm. The upwash velocity caused by the effect of the test section walls is computed as soon as the solution of this linear system, i.e. the solution of the boundary value problem, is obtained.

Panel method code ANTARES uses a modified version of *Keller's* algorithm to set up the linear system that describes the wall boundary condition at each wall panel centroid. Several additions and extensions were made to *Keller's* algorithm so that panel method code ANTARES may be used to compute blockage and angle of attack corrections in a subsonic wind tunnel flow field. Point doublets were chosen for the calculation of blockage corrections and the Prandtl–Glauert transformation was selected to model compressibility effects. It was also decided to include features in panel method code ANTARES that allow for the calculation of semispan model wall interference effects.

This report describes basic assumptions and elements of panel method code ANTARES. At first, *Keller's* algorithm [3] is discussed. Then, the modeling of compressibility effects is explained in great detail. A description of the structure of panel method code ANTARES follows. Finally, wall interference calculation results for different types of wall boundary conditions are compared with available classical solutions.

CHAPTER 2

PANEL METHOD CODE ANTARES

2.1 Wall Boundary Condition Description

Panel method code ANTARES was developed to compute the wind tunnel and wall interference flow field in a wind tunnel with rectangular cross–section. ANTARES uses *Keller's* algorithm [3] to set up the matrix equation that allows the user to describe six different types of wall boundary conditions.

In incompressible flow, the wall boundary conditions may be expressed by using the perturbation velocity potential ϕ of the wind tunnel flow field [3]. Then, we get :

$$c_1 \cdot \phi + c_2 \cdot \frac{\partial \phi}{\partial x} + c_3 \cdot \frac{\partial \phi}{\partial \mathbf{n}} + c_4 \cdot \frac{\partial^2 \phi}{\partial x \, \partial \mathbf{n}} = 0 \qquad (1)$$

where x is the streamwise coordinate, $\mathbf{n}$ is the normal vector on the wind tunnel wall, and c_1, c_2, c_3, c_4 are coefficients that describe the different types of wall boundary conditions. The following table lists values of these coefficients for six different types of boundary conditions:

Table 1 : Wall Boundary Condition Coefficients (from Ref. [3])

Type of Boundary Condition	c_1	c_2	c_3	c_4
Closed Wall	0	0	1	0
Open Jet	0	1	0	0
Perforated Wall	0	1	$1/R$	0
Ideal Slotted Wall (Integrated Form)	1	0	l	0
Ideal Slotted Wall (Differentiated Form)	0	1	$\partial l/\partial x$	l
Slotted Wall Including Viscosity in Slots	0	1	$\partial l/\partial x + 1/R$	l

The total perturbation velocity potential ϕ may be written as the sum of the potential ϕ_m caused by the test article in free–air and the potential ϕ_w caused by the wind tunnel

walls, i.e. the wall interference potential. We get :

$$\phi \quad = \quad \phi_m \; + \; \phi_w \tag{2}$$

Combining Eqs. (1) and (2), we get :

$$\begin{aligned} c_1 \cdot \phi_w + c_2 \cdot \frac{\partial\, \phi_w}{\partial\, x} \; + \; c_3 \cdot \frac{\partial\, \phi_w}{\partial\, \mathbf{n}} \; + \; c_4 \cdot \frac{\partial^2\, \phi_w}{\partial\, x\, \partial\, \mathbf{n}} \quad = \\ - \; c_1 \cdot \phi_m \; - \; c_2 \cdot \frac{\partial\, \phi_m}{\partial\, x} \; - \; c_3 \cdot \frac{\partial\, \phi_m}{\partial\, \mathbf{n}} \; - \; c_4 \cdot \frac{\partial^2\, \phi_m}{\partial\, x\, \partial\, \mathbf{n}} \end{aligned} \tag{3}$$

In general, a panel method code is constructed such that boundary conditions are only fulfilled at each wall panel centroid. Each panel may be considered as an infinitesimal wall element with its own boundary condition characteristics. Thus, wall boundary condition coefficients $c_1, \cdots, c_4$ are a function of each wall panel centroid "i". Using Eq. (3), the boundary condition at each panel centroid may be written as :

$$\begin{aligned} c_1(i) \cdot [\phi_w]_i \; + \; c_2(i) \cdot \left[\frac{\partial\, \phi_w}{\partial\, x}\right]_i \; + \; c_3(i) \cdot \left[\frac{\partial\, \phi_w}{\partial\, \mathbf{n}}\right]_i \; + \; c_4(i) \cdot \left[\frac{\partial^2\, \phi_w}{\partial\, x\, \partial\, \mathbf{n}}\right]_i \quad = \\ - \; c_1(i) \cdot [\phi_m]_i \; - \; c_2(i) \cdot \left[\frac{\partial\, \phi_m}{\partial\, x}\right]_i \; - \; c_3(i) \cdot \left[\frac{\partial\, \phi_m}{\partial\, \mathbf{n}}\right]_i \; - \; c_4(i) \cdot \left[\frac{\partial^2\, \phi_m}{\partial\, x\, \partial\, \mathbf{n}}\right]_i \end{aligned} \tag{4}$$

where $[\phi_m]_i$ is the model potential and $[\phi_w]_i$ is the wall potential at the panel centroid "i". The model potential ϕ_m of a point doublet and corresponding derivatives are given in App. 1. The model potential ϕ_m of a line doublet and corresponding derivatives are given in App. 2. It remains to determine the wall potential ϕ_w .

Keller [3] selected a wall panel element in his algorithm that may be used to express the wall potential $[\phi_w]_i$ at each panel centroid as a function of the source strength slope μ_j of all "N" panel elements describing the wind tunnel. Then, we get [3]:

$$[\phi_w]_i \quad = \quad \sum_{j=1}^{N} [\phi^*]_{i,j} \cdot \mu_j \tag{5}$$

where $[\phi^*]_{i,j}$ is the perturbation potential per unit source strength slope at panel centroid "i" due to panel "j", and μ_j is the source strength slope of panel "j". The perturbation potential ϕ^* and its derivatives are given in Ref. [3]. Combining Eqs. (4) and (5), we get :

$$\begin{aligned} \sum_{j=1}^{N} \left[c_1(i) \cdot [\phi^*]_{i,j} + c_2(i) \cdot \left[\frac{\partial\, \phi^*}{\partial\, x}\right]_{i,j} + c_3(i) \cdot \left[\frac{\partial\, \phi^*}{\partial\, \mathbf{n}}\right]_{i,j} + c_4(i) \cdot \left[\frac{\partial^2\, \phi^*}{\partial x\, \partial \mathbf{n}}\right]_{i,j} \right] \cdot \mu_j = \\ - \; c_1(i) \cdot [\phi_m]_i \; - \; c_2(i) \cdot \left[\frac{\partial\, \phi_m}{\partial\, x}\right]_i \; - \; c_3(i) \cdot \left[\frac{\partial\, \phi_m}{\partial\, \mathbf{n}}\right]_i \; - \; c_4(i) \cdot \left[\frac{\partial^2\, \phi_m}{\partial\, x\, \partial\, \mathbf{n}}\right]_i \end{aligned} \tag{6}$$

Equation (6) has to be applied to each wall panel centroid "i" (i.e. $i = 1, \cdots, N$). Thus, a linear system for the unknown source strength slope μ_j of each wall panel "j" (i.e. $\mu_1, \cdots, \mu_N$) is obtained. This linear system may be written as :

$$\begin{pmatrix} a_{11} & \cdots & a_{1j} & \cdots & a_{1N} \\ \vdots & \vdots & \vdots & \vdots & \vdots \\ a_{i1} & \cdots & a_{ij} & \cdots & a_{iN} \\ \vdots & \vdots & \vdots & \vdots & \vdots \\ a_{N1} & \cdots & a_{Nj} & \cdots & a_{NN} \end{pmatrix} \circ \begin{pmatrix} \mu_1 \\ \vdots \\ \mu_j \\ \vdots \\ \mu_N \end{pmatrix} = \begin{pmatrix} b_1 \\ \vdots \\ b_i \\ \vdots \\ b_N \end{pmatrix} \tag{7a}$$

where

$$a_{ij} = c_1(i) \cdot [\phi^*]_{i,j} + c_2(i) \cdot \left[\frac{\partial \phi^*}{\partial x}\right]_{i,j} + c_3(i) \cdot \left[\frac{\partial \phi^*}{\partial \mathbf{n}}\right]_{i,j} + c_4(i) \cdot \left[\frac{\partial^2 \phi^*}{\partial x \, \partial \mathbf{n}}\right]_{i,j} \tag{7b}$$

$$b_i = - c_1(i) \cdot [\phi_m]_i - c_2(i) \cdot \left[\frac{\partial \phi_m}{\partial x}\right]_i - c_3(i) \cdot \left[\frac{\partial \phi_m}{\partial \mathbf{n}}\right]_i - c_4(i) \cdot \left[\frac{\partial^2 \phi_m}{\partial x \, \partial \mathbf{n}}\right]_i \tag{7c}$$

Finally, after the solution of the source strength slope μ_j of each wall panel is obtained by applying a linear system solver to Eq. (7a), it is possible to compute the axial perturbation velocity at a wall panel centroid "i" in the wind tunnel flow field. Combining Eqs. (2) and (5) and differentiating the result in the streamwise direction we get :

$$u(i) = \left[\frac{\partial \phi}{\partial x}\right]_i = \left[\frac{\partial \phi_m}{\partial x}\right]_i + \sum_{j=1}^{N} \left[\frac{\partial \phi^*}{\partial x}\right]_{i,j} \cdot \mu_j \tag{8a}$$

The pressure coefficient at a wall panel centroid may be computed as :

$$c_p(i) = -2 \cdot \frac{u(i)}{u_\infty} = \frac{-2}{u_\infty} \cdot \left(\left[\frac{\partial \phi_m}{\partial x}\right]_i + \sum_{j=1}^{N} \left[\frac{\partial \phi^*}{\partial x}\right]_{i,j} \cdot \mu_j \right) \tag{8b}$$

Similarly, perturbation velocity components of the wall interference flow field at a flow field point "k" may be written as :

$$u_w(k) = \left[\frac{\partial \phi_w}{\partial x}\right]_k = \sum_{j=1}^{N} \left[\frac{\partial \phi^*}{\partial x}\right]_{k,j} \cdot \mu_j \tag{9a}$$

$$v_w(k) = \left[\frac{\partial \phi_w}{\partial y}\right]_k = \sum_{j=1}^{N} \left[\frac{\partial \phi^*}{\partial y}\right]_{k,j} \cdot \mu_j \tag{9b}$$

$$w_w(k) \quad = \quad \left[\frac{\partial\,\phi_w}{\partial\,z}\right]_k \quad = \quad \sum_{j=1}^{N}\left[\frac{\partial\,\phi^*}{\partial\,z}\right]_{k,j}\cdot\mu_j \qquad (9c)$$

Using Eq. (9a), we get the following equation for the blockage factor at a flow field point "k" in the test section :

$$\epsilon(k) \quad = \quad \frac{u_w(k)}{u_\infty} \quad = \quad \frac{1}{u_\infty}\cdot\sum_{j=1}^{N}\left[\frac{\partial\,\phi^*}{\partial\,x}\right]_{k,j}\cdot\mu_j \qquad (10a)$$

Similarly, assuming that the lift force of the test article points in the positive z–direction (see Fig. 1) and using Eq. (9c), we get for the angle of attack correction in degrees :

$$\Delta\alpha(k) \quad = \quad \frac{180}{\pi}\cdot\frac{w_w(k)}{u_\infty} \quad = \quad \frac{180}{\pi}\cdot\frac{1}{u_\infty}\cdot\sum_{j=1}^{N}\left[\frac{\partial\,\phi^*}{\partial\,z}\right]_{k,j}\cdot\mu_j \qquad (10b)$$

2.2 Compressibility Effects

The calculation of wind tunnel and wall interference effects of a point source, point doublet, or line doublet located in a rectangular wind tunnel requires the application of some sort of compressibility correction if tests are conducted at a high subsonic Mach number. Unfortunately, *Keller's* [3] panel method code algorithm is limited to incompressible flow. Therefore, it became necessary to include the Prandtl–Glauert compressibility transformation in panel method code ANTARES.

In general, the Prandtl–Glauert transformation has to be applied to solve the subsonic potential equation in a subsonic flow field. A detailed description of the Prandtl–Glauert transformation may be found in Ref. [4]. The subsonic potential equation is given as :

$$\beta^2\cdot\frac{\partial^2\,\phi}{\partial\,x^2} + \frac{\partial^2\,\phi}{\partial\,y^2} + \frac{\partial^2\,\phi}{\partial\,z^2} \quad = \quad 0 \qquad (11a)$$

$$\beta^2 \quad = \quad 1 - M_\infty^2 \qquad (11b)$$

where ϕ is the perturbation velocity potential, x,y,z are cartesian coordinates of the flow field, and M_∞ is the free–stream Mach number of the subsonic flow field.

The subsonic potential equation is a partial differential equation that has to be solved for the given wind tunnel wall boundary conditions and for the selected singularity (i.e. point source, point doublet, or line doublet) that represents the test article for the purpose of wall interference calculations. This solution is basically obtained in three steps:

(1) The subsonic potential equation and corresponding boundary conditions are transformed by applying the Prandtl–Glauert transformation.

(2) The transformed subsonic potential equation is a Laplace equation; the transformed boundary value problem is solved numerically by using a panel method code.

(3) The solution of the original subsonic potential equation is obtained by reversing the Prandtl–Glauert transformation; perturbation velocity components computed in the transformed coordinate system are transformed back to the original coordinate system.

Variable Transformation

The Prandtl–Glauert transformation maps variables from an original coordinate system x,y,z to a transformed coordinate system x',y',z' . The transformation of the coordinates x,y,z , of the free–stream velocity u_∞, and of the perturbation potential ϕ is given by the following equations (see Eq. (4–10) in Ref. [4]) :

$$x' = x \qquad (12a)$$

$$y' = y \cdot \beta \qquad (12b)$$

$$z' = z \cdot \beta \qquad (12c)$$

$$u'_\infty = u_\infty \qquad (12d)$$

$$\phi' = \phi \cdot \beta^2 \qquad (12e)$$

In the case of a subsonic wind tunnel flow field, it is also necessary to apply the Prandtl–Glauert transformation to variables that are used to describe wind tunnel wall boundary conditions. Thus, it will be shown below that the restriction parameter R (perforated wall boundary condition) has to be transformed using the following equation :

$$R' = \frac{R}{\beta} \qquad (12f)$$

Similarly, it will be shown below that the slot parameter l (slotted wall boundary condition) has to be transformed using the following equation :

$$l' = l \cdot \beta \qquad (12g)$$

The normal vector $\mathbf{n}$ at the wind tunnel wall is located in the y–z–plane. Thus, we get:

$$\mathbf{n} = \begin{pmatrix} N_x \\ N_y \\ N_z \end{pmatrix} = \frac{1}{\sqrt{n_y^2 + n_z^2}} \cdot \begin{pmatrix} 0 \\ n_y \\ n_z \end{pmatrix} \qquad (12h)$$

The transformed normal vector $\mathbf{n}'$ may be written as :

$$\mathbf{n}' = \begin{pmatrix} N_x' \\ N_y' \\ N_z' \end{pmatrix} = \frac{1}{\sqrt{n_y'^2 + n_z'^2}} \cdot \begin{pmatrix} 0 \\ n_y' \\ n_z' \end{pmatrix} \qquad (12i)$$

Combining Eqs. (12b), (12c), with Eq. (12i), we get :

$$\mathbf{n}' = \frac{1}{\sqrt{(n_y \cdot \beta)^2 + (n_z \cdot \beta)^2}} \cdot \begin{pmatrix} 0 \\ n_y \cdot \beta \\ n_z \cdot \beta \end{pmatrix} = \frac{1}{\sqrt{n_y^2 + n_z^2}} \cdot \begin{pmatrix} 0 \\ n_y \\ n_z \end{pmatrix} \qquad (12j)$$

Comparing Eq. (12j) with Eq. (12h), we get :

$$\mathbf{n}' = \mathbf{n} \qquad (12k)$$

Wall interference calculations may use singularities to represent the blockage and lifting effect of a test article. The Prandtl–Glauert transformation has to be applied to the location of the singularities. The strength σ of the singularities is connected with the test article geometry and has to be transformed as well. The transformed singularity strength σ' may be expressed as :

$$\sigma' = \sigma \cdot F(\beta) \qquad (12l)$$

where $F(\beta)$ is a transformation function. The value of this transformation function is rigorously derived in App. 3 for different types of singularities (see also Table 7 on p.54).

Subsonic Potential Equation Transformation

The subsonic potential equation given in Eq. (11a) may now be transformed. Differentiating Eqs. (12a), (12b), and (12c), we get :

$$\frac{\partial x'}{\partial x} = 1 \qquad (13a)$$

$$\frac{\partial y'}{\partial y} = \beta \qquad (13b)$$

$$\frac{\partial z'}{\partial z} = \beta \qquad (13c)$$

Applying the chain rule to Eq. (12e) twice and using Eqs. (13a), (13b), (13c), we get :

$$\frac{\partial^2 \phi}{\partial x^2} = \frac{\partial^2 (\phi' / \beta^2)}{\partial x^2} = \frac{1}{\beta^2} \cdot \left(\frac{\partial x'}{\partial x} \right)^2 \cdot \frac{\partial^2 \phi'}{\partial x'^2} = \frac{1}{\beta^2} \cdot \frac{\partial^2 \phi'}{\partial x'^2} \qquad (14a)$$

$$\frac{\partial^2 \phi}{\partial y^2} = \frac{\partial^2 (\phi' / \beta^2)}{\partial y^2} = \frac{1}{\beta^2} \cdot \left(\frac{\partial y'}{\partial y} \right)^2 \cdot \frac{\partial^2 \phi'}{\partial y'^2} = \frac{\partial^2 \phi'}{\partial y'^2} \qquad (14b)$$

$$\frac{\partial^2 \phi}{\partial z^2} = \frac{\partial^2 (\phi' / \beta^2)}{\partial z^2} = \frac{1}{\beta^2} \cdot \left(\frac{\partial z'}{\partial z} \right)^2 \cdot \frac{\partial^2 \phi'}{\partial z'^2} = \frac{\partial^2 \phi'}{\partial z'^2} \qquad (14c)$$

Finally, the transformed subsonic potential equation is obtained by combining Eqs. (11a), (14a), (14b), and (14c) . We get :

$$\frac{\partial^2 \phi'}{\partial x'^2} + \frac{\partial^2 \phi'}{\partial y'^2} + \frac{\partial^2 \phi'}{\partial z'^2} = 0 \qquad (15)$$

In the next step it is necessary to apply the Prandtl–Glauert transformation to the wall boundary conditions.

Wall Boundary Condition Transformation

Keller [3] discusses six different types of wall boundary conditions. The Prandtl-Glauert transformation has to be applied to each type before a solution of the subsonic flow field can be found.

Type 1 / Closed Wall : The closed wall boundary condition may be written as :

$$\boxed{\frac{\partial \phi}{\partial \mathbf{n}} = 0 \qquad (16a)}$$

The normal derivative operator may be written as :

$$\frac{\partial}{\partial \mathbf{n}} \equiv \mathbf{n} \circ \nabla \equiv N_x \cdot \frac{\partial}{\partial x} + N_y \cdot \frac{\partial}{\partial y} + N_z \cdot \frac{\partial}{\partial z} \qquad (16b)$$

From Eq. (12h) we know that $N_x = 0$ on the wind tunnel wall. Thus, we get for Eq. (16b) :

$$\frac{\partial}{\partial \mathbf{n}} \equiv N_y \cdot \frac{\partial}{\partial y} + N_z \cdot \frac{\partial}{\partial z} \qquad (16c)$$

Similarly, the transformed normal derivative operator may be written as :

$$\frac{\partial}{\partial \mathbf{n}'} \equiv N'_y \cdot \frac{\partial}{\partial y'} + N'_z \cdot \frac{\partial}{\partial z'} \qquad (16d)$$

Applying the chain rule to Eq. (16d), we get :

$$\frac{\partial}{\partial \mathbf{n}'} \equiv N'_y \cdot \frac{\partial y}{\partial y'} \cdot \frac{\partial}{\partial y} + N'_z \cdot \frac{\partial z}{\partial z'} \cdot \frac{\partial}{\partial z} \qquad (16e)$$

Combining Eqs. (13b), (13c), with Eq. (16e), we get :

$$\frac{\partial}{\partial \mathbf{n}'} \equiv N'_y \cdot \frac{1}{\beta} \cdot \frac{\partial}{\partial y} + N'_z \cdot \frac{1}{\beta} \cdot \frac{\partial}{\partial z} \qquad (16e)$$

From Eq. (12k), we know that $N'_y = N_y$ and $N'_z = N_z$. Thus, using Eq. (16c), we get for Eq. (16e) :

$$\frac{\partial}{\partial \mathbf{n}'} \equiv \frac{1}{\beta} \cdot \left[N_y \cdot \frac{\partial}{\partial y} + N_z \cdot \frac{\partial}{\partial z} \right] \equiv \frac{1}{\beta} \cdot \frac{\partial}{\partial \mathbf{n}} \qquad (16f)$$

$$\Longrightarrow \quad \frac{\partial}{\partial \mathbf{n}} \equiv \beta \cdot \frac{\partial}{\partial \mathbf{n}'} \tag{16g}$$

Combining Eq. (16a) with Eqs. (12e) and (16g), we get :

$$\frac{\partial \phi}{\partial \mathbf{n}} = \beta \cdot \frac{\partial (\phi' / \beta^2)}{\partial \mathbf{n}'} = \frac{1}{\beta} \cdot \frac{\partial \phi'}{\partial \mathbf{n}'} = 0 \tag{16h}$$

$$\boxed{\Longrightarrow \quad \frac{\partial \phi'}{\partial \mathbf{n}'} = 0 \qquad (16i)}$$

Type 2 / Open Jet : The open jet boundary condition may be written as :

$$\boxed{\frac{\partial \phi}{\partial x} = 0 \qquad (17a)}$$

Applying the chain rule to Eq. (17a), we get :

$$\frac{\partial \phi}{\partial x} = \frac{\partial x'}{\partial x} \cdot \frac{\partial \phi}{\partial x'} = 0 \tag{17b}$$

Combining Eqs. (12e), (13a) with Eq. (17b), we get :

$$\frac{\partial \phi}{\partial x} = \frac{\partial x'}{\partial x} \cdot \frac{\partial (\phi' / \beta^2)}{\partial x'} = \frac{1}{\beta^2} \cdot \frac{\partial \phi'}{\partial x'} = 0 \tag{17c}$$

$$\boxed{\Longrightarrow \quad \frac{\partial \phi'}{\partial x'} = 0 \qquad (17d)}$$

Type 3 / Perforated Wall : The perforated wall boundary condition may be written as :

$$\boxed{\frac{\partial \phi}{\partial x} + \frac{1}{R} \cdot \frac{\partial \phi}{\partial \mathbf{n}} = 0 \qquad (18a)}$$

Applying the chain rule to Eq. (18a) and using Eq. (16g), we get :

$$\frac{\partial\, x'}{\partial\, x} \cdot \frac{\partial\, \phi}{\partial\, x'} + \frac{1}{R} \cdot \beta \cdot \frac{\partial\, \phi}{\partial\, \mathbf{n}'} = 0 \qquad (18b)$$

Combining Eqs. (12e), (13a), with Eq. (18b), we get :

$$\frac{\partial\, (\, \phi' \,/\, \beta^2 \,)}{\partial\, x'} + \frac{\beta}{R} \cdot \frac{\partial\, (\, \phi' \,/\, \beta^2 \,)}{\partial\, \mathbf{n}'} = \frac{1}{\beta^2} \cdot \frac{\partial\, \phi'}{\partial\, x'} + \frac{1}{R \cdot \beta} \cdot \frac{\partial\, \phi'}{\partial\, \mathbf{n}'} = 0 \qquad (18c)$$

$$\Longrightarrow \quad \frac{\partial\, \phi'}{\partial\, x'} + \frac{1}{(\, R \,/\, \beta \,)} \cdot \frac{\partial\, \phi'}{\partial\, \mathbf{n}'} = 0 \qquad (18d)$$

It is possible to define a transformed restriction parameter $R' = R/\beta$. Then, the transformed boundary condition for a perforated wall becomes :

$$\Longrightarrow \quad \frac{\partial\, \phi'}{\partial\, x'} + \frac{1}{R'} \cdot \frac{\partial\, \phi'}{\partial\, \mathbf{n}'} = 0 \qquad (18e)$$

Type 4 / Ideal Slotted Wall (integrated form) : The ideal slotted wall boundary condition in integrated form may be written as :

$$\phi + l \cdot \frac{\partial\, \phi}{\partial\, \mathbf{n}} = 0 \qquad (19a)$$

Using Eq. (16g) in Eq. (19a), we get :

$$\phi + l \cdot \beta \cdot \frac{\partial\, \phi}{\partial\, \mathbf{n}'} = 0 \qquad (19b)$$

Combining Eq. (12e) with Eq. (19b), we get :

$$\frac{\phi'}{\beta^2} + l \cdot \beta \cdot \frac{\partial\, (\, \phi' \,/\, \beta^2 \,)}{\partial\, \mathbf{n}'} = \frac{1}{\beta^2} \cdot \left[\phi' + l \cdot \beta \cdot \frac{\partial\, \phi'}{\partial\, \mathbf{n}'} \right] = 0 \qquad (19c)$$

$$\Longrightarrow \quad \phi' + (\, l \cdot \beta \,) \cdot \frac{\partial\, \phi'}{\partial\, \mathbf{n}'} = 0 \qquad (19d)$$

A transformed slot parameter $l' = l \cdot \beta$ is introduced in Eq. (19d). Then, comparing Eqs. (19a) and (19d), the transformed boundary condition for an ideal slotted wall in integrated form becomes :

$$\Longrightarrow \quad \phi' + l' \cdot \frac{\partial \phi'}{\partial \mathbf{n}'} = 0 \qquad (19e)$$

Type 5 / Ideal Slotted Wall (differentiated form) : The ideal slotted wall boundary condition in differentiated form may be written as :

$$\frac{\partial \phi}{\partial x} + \frac{\partial l}{\partial x} \cdot \frac{\partial \phi}{\partial \mathbf{n}} + l \cdot \frac{\partial^2 \phi}{\partial x \, \partial \mathbf{n}} = 0 \qquad (20a)$$

Applying the chain rule to Eq. (20a) and using Eq. (16g), we get :

$$\frac{\partial x'}{\partial x} \cdot \frac{\partial \phi}{\partial x'} + \frac{\partial x'}{\partial x} \cdot \frac{\partial l}{\partial x'} \cdot \beta \cdot \frac{\partial \phi}{\partial \mathbf{n}'} + l \cdot \frac{\partial x'}{\partial x} \cdot \beta \cdot \frac{\partial^2 \phi}{\partial x' \, \partial \mathbf{n}'} = 0 \quad (20b)$$

Combining Eqs. (12e), (13a), with Eq. (20b), we get :

$$\frac{\partial (\phi' / \beta^2)}{\partial x'} + \frac{\partial l}{\partial x'} \cdot \beta \cdot \frac{\partial (\phi' / \beta^2)}{\partial \mathbf{n}'} + l \cdot \beta \cdot \frac{\partial^2 (\phi' / \beta^2)}{\partial x' \, \partial \mathbf{n}'} = 0 \quad (20c)$$

$$\Longrightarrow \quad \frac{\partial \phi'}{\partial x'} + \frac{\partial (l \cdot \beta)}{\partial x'} \cdot \frac{\partial \phi'}{\partial \mathbf{n}'} + (l \cdot \beta) \cdot \frac{\partial^2 \phi'}{\partial x' \, \partial \mathbf{n}'} = 0 \qquad (20d)$$

A transformed slot parameter $l' = l \cdot \beta$ is introduced in Eq. (20d). Then, the transformed boundary condition for an ideal slotted wall in differentiated form becomes :

$$\Longrightarrow \quad \frac{\partial \phi'}{\partial x'} + \frac{\partial l'}{\partial x'} \cdot \frac{\partial \phi'}{\partial \mathbf{n}'} + l' \cdot \frac{\partial^2 \phi'}{\partial x' \, \partial \mathbf{n}'} = 0 \qquad (20e)$$

Type 6 / Slotted Wall Including Viscosity : The slotted wall boundary condition including viscosity in slots may be written as :

$$\frac{\partial \phi}{\partial x} + \left[\frac{\partial l}{\partial x} + \frac{1}{R} \right] \cdot \frac{\partial \phi}{\partial \mathbf{n}} + l \cdot \frac{\partial^2 \phi}{\partial x \, \partial \mathbf{n}} = 0 \qquad (21a)$$

Applying the chain rule to Eq. (21a) and using Eq. (16g), we get :

$$\frac{\partial x'}{\partial x} \cdot \frac{\partial \phi}{\partial x'} + \left[\frac{\partial x'}{\partial x} \cdot \frac{\partial l}{\partial x'} + \frac{1}{R} \right] \cdot \beta \cdot \frac{\partial \phi}{\partial \mathbf{n}'} + l \cdot \frac{\partial x'}{\partial x} \cdot \beta \cdot \frac{\partial^2 \phi}{\partial x' \, \partial \mathbf{n}'} = 0 \quad (21b)$$

Combining Eqs. (12e), (13a), with Eq. (21b), we get :

$$\frac{\partial (\phi' / \beta^2)}{\partial x'} + \left[\frac{\partial l}{\partial x'} + \frac{1}{R} \right] \cdot \beta \cdot \frac{\partial (\phi' / \beta^2)}{\partial \mathbf{n}'} + l \cdot \beta \cdot \frac{\partial^2 (\phi' / \beta^2)}{\partial x' \, \partial \mathbf{n}'} = 0 \quad (21c)$$

$$\Longrightarrow \quad \frac{\partial \phi'}{\partial x'} + \left[\frac{\partial (l \cdot \beta)}{\partial x'} + \frac{1}{(R / \beta)} \right] \cdot \frac{\partial \phi'}{\partial \mathbf{n}'} + (l \cdot \beta) \cdot \frac{\partial^2 \phi'}{\partial x' \, \partial \mathbf{n}'} = 0 \quad (21d)$$

Now a transformed restriction parameter $R' = R/\beta$ and a transformed slot parameter $l' = l \cdot \beta$ are introduced. Then, comparing Eqs. (21a) and (21d), the transformed boundary condition for a slotted wall including viscosity in slots becomes :

$$\Longrightarrow \quad \frac{\partial \phi'}{\partial x'} + \left[\frac{\partial l'}{\partial x'} + \frac{1}{R'} \right] \cdot \frac{\partial \phi'}{\partial \mathbf{n}'} + l' \cdot \frac{\partial^2 \phi'}{\partial x' \, \partial \mathbf{n}'} = 0 \qquad (21e)$$

Reversal of the Prandtl–Glauert Transformation

The solution of the transformed subsonic potential equation (Eq. (15)) may be computed by using the panel method code algorithm developed by *Keller* [3]. After the solution is found, it is only necessary to reverse the Prandtl–Glauert transformation to obtain the solution of the subsonic wind tunnel flow field. Perturbation velocities computed in the transformed coordinate system have to be transformed back to the original coordinate system. Thus, applying the chain rule to Eq. (12e), we get for the perturbation velocity components in the subsonic flow field :

$$u = \frac{\partial \phi}{\partial x} = \frac{1}{\beta^2} \cdot \frac{\partial x'}{\partial x} \cdot \frac{\partial \phi'}{\partial x'} \qquad (22a)$$

$$v = \frac{\partial \phi}{\partial y} = \frac{1}{\beta^2} \cdot \frac{\partial y'}{\partial y} \cdot \frac{\partial \phi'}{\partial y'} \qquad (22b)$$

$$w = \frac{\partial \phi}{\partial z} = \frac{1}{\beta^2} \cdot \frac{\partial z'}{\partial z} \cdot \frac{\partial \phi'}{\partial z'} \qquad (22c)$$

Finally, combining Eqs. (13a), (13b), (13c) with Eqs. (22a), (22b), (22c), we get the perturbation velocity components in the subsonic flow field :

$$u = \frac{1}{\beta^2} \cdot \frac{\partial \phi'}{\partial x'} = \frac{u'}{\beta^2} \qquad (23a)$$

$$v = \frac{1}{\beta} \cdot \frac{\partial \phi'}{\partial y'} = \frac{v'}{\beta} \qquad (23b)$$

$$w = \frac{1}{\beta} \cdot \frac{\partial \phi'}{\partial z'} = \frac{w'}{\beta} \qquad (23c)$$

where u', v', w' are the perturbation velocity components in the transformed coordinate system x', y', z' .

In general, the application of the Prandtl–Glauert transformation in a panel method code may be summarized as follows :

(1) In a first step, the original coordinate system (x,y,z) maps to a transformed coordinate system (x',y', z', see Eqs. (12a), (12b), (12c)). Restriction parameter R and slot parameter l have to be transformed by using Eqs. (12f), (12g). Strengths σ of singularities representing the test article have to be transformed by using Eq. (12l) and Table 7 on p.54 .

(2) In the next step, the solution of the transformed subsonic potential equation is found by using the algorithm given by *Keller* [3].

(3) Finally, perturbation velocities in the subsonic wind tunnel flow field are computed by reversing the Prandtl–Glauert transformation (Eqs. (23a), (23b), (23c)). The following flow chart summarizes different solution steps :

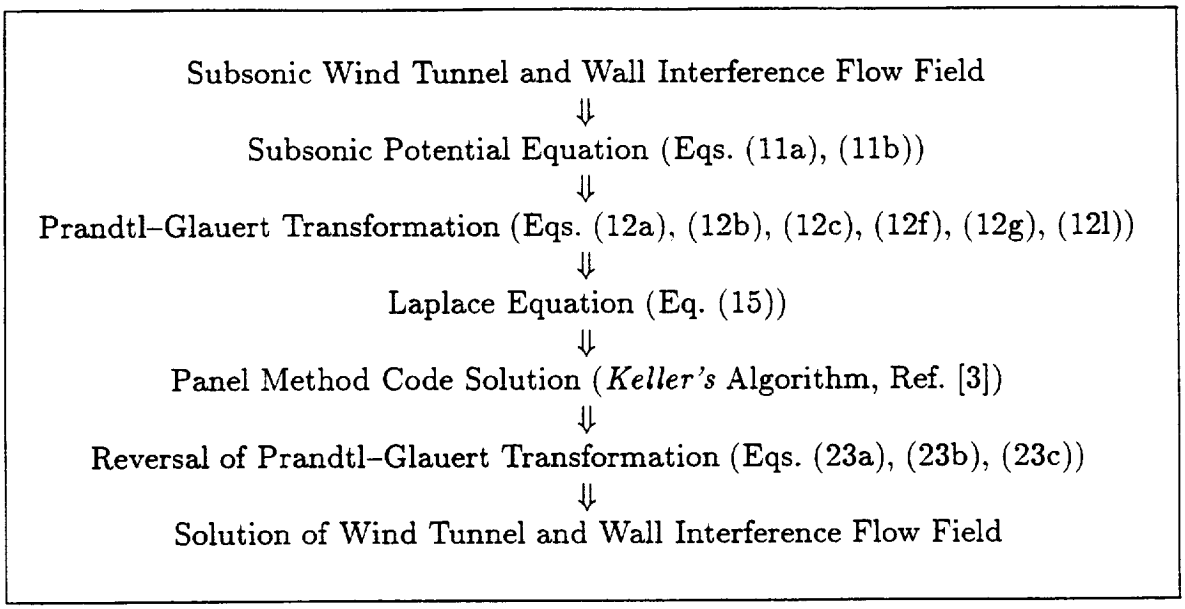

2.3 Panel Method Code Structure

Panel method code ANTARES computes the wall interference flow field in a wind tunnel with rectangular cross–section. ANTARES allows the user to represent the test article by using two types of singularities. Point doublets represent blockage effects of the test article. Line doublets represent lifting effects of the test article. Currently, ANTARES allows the user to select three different types of wall boundary conditions (closed wall, open jet, or perforated wall). Other boundary conditions listed in Table 1 on p.3 may easily be implemented as the code computes all derivatives required for the application of *Keller's* algorithm [3]. The internal structure of panel method code ANTARES can be divided into three parts (see Fig. 2) :

(i) Preparation of Linear System: In the first part, the linear system describing the wall boundary conditions is prepared. At first, the wall boundary condition type of each wall panel centroid "i" has to be specified by selecting coefficients $c_1(i)$ to $c_4(i)$. These coefficients are required for the calculation of matrix coefficients a_{ij} and the right hand side vector b_i of the linear system (see Eqs. (7b),(7c)). The Prandtl–Glauert transformation has to be applied to the restriction parameter "R" and to the slot parameter "l" if they are used to compute coefficients $c_3(i)$ and $c_4(i)$. The reciprocal of restriction parameter "R" is used to compute coefficient $c_3(i)$. Therefore, panel method code ANTARES checks

if the absolute value of "R" is greater than 0.0001 .

In the next step the panel model of the wind tunnel walls has to be prepared. Equal panel spacing is selected in the circumferential direction of the test section. Cosine panel spacing is selected in the streamwise direction of the test section with smaller panels near the location of the test article. Experience has shown that a total number of 60 panels in the streamwise direction is sufficient as *Keller's* algorithm uses a wall panel type that linearly varies the source strength over each panel in the steamwise direction [3]. However, a relatively large number of panels is required in the circumferential direction of the test section as *Keller's* panel type keeps the source strength constant over each panel in the circumferential direction. Thus, a total number of 4800 panels (80 panels in the circumferential direction and 60 panels in the streamwise direction) is selected to represent the test section for a fullspan model configuration (see Fig. 4). A total number of 7200 panels (120 panels in the circumferential direction and 60 panels in the streamwise direction) is selected to represent the test section for a semispan model configuration (see Fig. 8). For a fullspan model configuration, the length of the paneled test section geometry is about eight tunnel widths. Finally, after the Prandtl–Glauert transformation is applied to the wall panel coordinates, it is possible to compute matrix coefficients a_{ij} using Eq. (7b).

Type and location of singularities representing the test article have to be specified as well so that the right hand side vector b_i of the linear system can be computed. The Prandtl–Glauert transformation has to be applied to singularity coordinates and the singularity strength. Afterwards it is possible to apply Eq. (7c) and compute the right hand side vector b_i of the linear system given in Eq. (7a).

(ii) Solution of Linear System: In this part a linear system solver is used to solve the boundary value problem. Numerical studies have shown that a standard off–the–shelve LU–Decomposition algorithm [5] may be used to solve the linear system. It is recommended to use "DOUBLE PRECISION" arithmetic in an effort to avoid finite digit arithmetic problems. ANTARES stores all matrix coefficients in arrays and therefore storage requirements can be large. For example, the storage of coefficients a_{ij} for 4800 panels requires approximately 184 [Mbytes]. ANTARES takes advantage of symmetry in the case of the test section panel model for a semispan model configuration. This reduces

the number of unknowns in the linear system from 7200 to 3600.

(iii) Calculation of Wall Interference Flow Field: After the solution of the linear system defined by Eq. (7a) is found wall interference perturbation velocity components may easily be computed by adding all velocity contributions of wall panels using Eqs. (9a), (9b), (9c). Finally, the Prandtl–Glauert transformation has to be reversed using Eqs. (23a), (23b), (23c) so that perturbation velocity components in the compressible subsonic wall interference flow field may be obtained.

The real–time wall interference correction system currently being developed for the NASA Ames 11ft TWT requires the calculation of the pressure coefficient at each wall panel centroid. ANTARES uses Eq. (8b) to compute this pressure coefficient.

2.4 Closed Wall Boundary Condition

The accuracy of panel method code ANTARES is investigated in this chapter. Therefore, solutions of the wall interference calculation for a closed wall rectangular wind tunnel are compared with corresponding Method of Images solutions provided in App. 4 and App. 5. In addition, solutions of the wind tunnel flow field on the wind tunnel walls are investigated.

In general, panel method code ANTARES may be used to compute the wall interference flow field caused by a point doublet or line doublet in a closed wall wind tunnel. The user only has to specify the panel representation of the test section geometry and the location of the selected point doublet or line doublet inside of the test section. Coefficients related to the wall boundary condition type on each of the four test section walls (see nomenclature in Fig. 1) have to be specified as well. These coefficients are defined in Eq. (1). The table below lists the coefficients for the closed wall boundary condition :

Table 2 : Wall Boundary Condition Coefficients (Closed Wall)

Wall No.	Panel Index Range	$c_1(i)$	$c_2(i)$	$c_3(i)$	$c_4(i)$
1	$1 \leq i \leq 1200$	0	0	1	0
2	$1201 \leq i \leq 2400$	0	0	1	0
3	$2401 \leq i \leq 3600$	0	0	1	0
4	$3601 \leq i \leq 4800$	0	0	1	0

Two different wind tunnel cross–sections are selected for the study of the accuracy of panel method code ANTARES. Compressibility effects are investigated as well by computing wall interference for two different Mach numbers (0.00 and 0.80).

Wind Tunnel Cross–Section No.1 : The first wind tunnel used for the accuracy study has a square cross–section (see Fig. 3). The panel representation of the test section boundary is depicted in Fig. 4. The wall panel index range of each wall is given in Table 2 . A total number of 4800 panels was selected for the panel model (60 panels in the streamwise direction and 80 panels in the circumferential direction). Cosine panel spacing was selected in the streamwise direction and equal panel spacing in the circumferential direction. The total length of the paneled test section was chosen to be eight tunnel widths. The calculation of wall interference effects caused by a fullspan model is simulated. Therefore, a single point doublet or line doublet is placed inside of the tunnel to represent blockage or lifting effects of the wind tunnel model (see Fig. 3). The selected tunnel width and height is 10 [ft]. For the present study it was decided to compute the wall interference flow field on the tunnel centerline (see Line 1 in Fig. 3). The wind tunnel flow field on selected locations on the wind tunnel wall is computed as well (see Row 1 and Row 2 in Fig. 3).

Figures 5a, 5b, and 5c depict the result of the wall interference calculation for the selected unit point doublet representing test article blockage. The dimensionless wall interference perturbation velocity components are depicted as a function of the tunnel centerline coordinate. The overall agreement between panel method code solution (abbreviated P.M.) and Method of Images solution (abbreviated M.I.) for both Mach numbers is excellent. It appears that the difference between the panel method code solution and the Method of Images solution (exact solution) is small for the y and z component of the wall interference velocity vector (see Fig. 5b and 5c). Differences between panel method code solution and the Method of Images solution (exact solution) increase with increasing Mach number only for the axial interference velocity component (see Fig. 5a).

Figures 5d and 5e compare the wind tunnel flow field solution on Row 1 and Row 2 for the selected unit point doublet. Again, the overall agreement between the panel method code solution and the Method of Images solution for the two selected Mach numbers is good.

Figures 6a, 6b, and 6c depict the result of the wall interference calculation for a unit line doublet representing test article lifting effects. The line doublet orientation angle is selected to be 0.0°. Again, dimensionless wall interference perturbation velocity components are shown. The agreement between panel method code solution and Method of Images solution for all three components of the wall interference velocity vector and for both Mach numbers is good. Differences between the panel method code solution and the Method of Images solution (exact solution) are smaller than in the case of the unit point doublet.

Figures 6d and 6e compare the wind tunnel flow field solution on Row 1 and Row 2 for the selected unit line doublet. Again, the agreement between the panel method code solution and the Method of Images solution for the two selected Mach numbers is good.

Wind Tunnel Cross–Section No.2 : The second wind tunnel geometry used for the present accuracy study has a rectangular cross–section (see Fig. 7). The corresponding panel representation of the test section is depicted in Fig. 8. A total number of 7200 panels was selected for the panel model (60 panels in the streamwise direction and 120 panels in the circumferential direction). Cosine panel spacing was selected in the streamwise direction and equal panel spacing in the circumferential direction. The total length of the paneled test section was chosen to be eight tunnel widths. The calculation of wall interference effects of a semispan model configuration is simulated in this example assuming that the reflection plane is located halfway between Wall 3 and Wall 4. A point doublet or line doublet and its corresponding mirror image are placed inside of the tunnel to represent lifting or blockage effects of a semispan wind tunnel model (see Fig. 7). The selected tunnel width is 10 [ft]. Wall interference of a semispan model mounted on the floor of a 10 [ft] by 10 [ft] test section is being computed (see Line 2 in Fig. 7). Therefore, the tunnel height has to be chosen 20 [ft]. The wind tunnel flow field on selected locations on the wind tunnel wall is computed as well (see Row 1 and Row 2 in Fig. 7).

Figures 9a, 9b, and 9c depict the result of the wall interference calculation for the selected two unit point doublets representing test article blockage. Dimensionless wall interference perturbation velocity components are depicted. The overall agreement between panel method code solution and Method of Images solution for both Mach numbers is excellent.

Figures 9d and 9e compare the wind tunnel flow field solution on Row 1 and Row 2

for the selected two unit point doublets. Again, the overall agreement between the panel method code solution and the Method of Images solution for the two selected Mach numbers is good.

Figures 10a, 10b, and 10c depict the result of the wall interference calculation for the selected two unit line doublets representing lifting effects of the semispan model. The line doublet orientation angle is selected to be 90.0° and therefore the lift force of the semispan model points in the positive y–coordinate direction (see Fig. 7). The dimensionless wall interference perturbation velocity components are depicted. The overall agreement between panel method code solution and Method of Images solution for both Mach numbers is good.

Figures 10d and 10e compare the wind tunnel flow field solution on Row 1 and Row 2 for the selected two unit line doublets. Again, the overall agreement is good.

2.5 Open Jet Boundary Condition

Panel method code ANTARES allows the user to compute the wind tunnel wall interference flow field of a test article in an open jet. Method of Images solutions of a point doublet or line doublet in a rectangular open jet are used to study the accuracy of these panel method code solutions (see App. 4 and App. 5).

The calculation of wall interference in an open jet using panel method code ANTARES is similar to calculations described in the previous chapter. Coefficients describing the wall boundary condition on the four test section walls are assigned such that the open jet boundary condition is imposed. The following table lists values of these coefficients for the open jet boundary condition :

Table 3 : Wall Boundary Condition Coefficients (Open Jet)

Wall No.	Panel Index Range	$c_1(i)$	$c_2(i)$	$c_3(i)$	$c_4(i)$
1	$1 \leq i \leq 1200$	0	1	0	0
2	$1201 \leq i \leq 2400$	0	1	0	0
3	$2401 \leq i \leq 3600$	0	1	0	0
4	$3601 \leq i \leq 4800$	0	1	0	0

An open jet with square cross–section is selected for the study of the accuracy of panel method code ANTARES. An open jet width and height of 10 [ft] is selected. The open jet boundaries are represented by using 4800 panels (60 panels in the streamwise direction and 80 panels in the circumferential direction, see Fig. 4). The paneled test section length is equal to eight tunnel widths. Compressibility effects are investigated by computing wall interference for two different Mach numbers (0.00 and 0.90).

A single point doublet or line doublet is placed inside of the tunnel to represent blockage or lifting effects of the wind tunnel model (see Fig. 3). Panel method code ANTARES and the Method of Images are used to compute the wall interference flow field on the tunnel centerline (see Line 1 in Fig. 3).

Figures 11a, 11b, and 11c depict the result of the wall interference calculation for the selected unit point doublet representing test article blockage in an open jet. The dimensionless wall interference perturbation velocity components are depicted. The overall agreement between panel method code solution (abbreviated P.M.) and Method of Images solution (abbreviated M.I.) for both Mach numbers is excellent. Differences between panel method code solution and Method of Images solution of the axial interference velocity component are smaller than for a corresponding calculation using the closed wall boundary condition (compare Fig. 11a with Fig. 5a)

Figures 12a, 12b, and 12c depict the result of the wall interference calculation for a unit line doublet representing test article lifting effects in an open jet. The line doublet orientation angle is selected to be 0.0°. The dimensionless wall interference perturbation velocity components are depicted. Again, the agreement between panel method code solution (abbreviated P.M.) and Method of Images solution (abbreviated M.I.) for both Mach numbers is excellent.

2.6 Perforated Wall Boundary Condition

Classical solutions of blockage and lift interference effects in a two–dimensional perforated wall wind tunnel may be used to check the application of perforated wall boundary conditions in panel method code ANTARES. The classical solution of the perturbation potential and the blockage factor caused by a two–dimensional point doublet on the cen-

terline of a two–dimensional perforated wall wind tunnel is given by *Baldwin et al.* [6]. Similarly, the classical solution of the lift interference caused by a two–dimensional vortex on the centerline of a two–dimensional perforated wall wind tunnel is given by *Pindzola and Lo* [7].

In the first part of this chapter, classical solutions are described in greater detail. Afterwards classical and panel method code solutions for blockage and lift interference are compared and discussed.

Classical Blockage Factor : *Baldwin et al.* [6] use the Fourier transform technique to compute the perturbation potential ϕ_w due to tunnel walls (φ^* in their nomenclature). The blockage factor on the tunnel centerline may easily be computed by differentiating Eq. (19) of Ref. [6] with respect to the streamwise coordinate. It is assumed that the walls of the two–dimensional tunnel are "ideal porous" ($K = 0$) and that wall interference is computed on the tunnel centerline ($y = 0$). Then, Eq. (19) of Ref. [6] becomes :

$$\phi_w(x) \;=\; \frac{-\,m_e}{2\,\pi\,\beta\,h} \cdot \left[\int_0^\infty I_1(q)\,d\,q \;+\; \int_0^\infty I_2(q)\,d\,q \right] \tag{24a}$$

where

$$I_1 \;=\; \frac{\beta}{R} \cdot \frac{1}{[\,cosh(q)\,]^2 \;+\; [\,(\beta/R)\cdot sinh(q)\,]^2} \cdot cos\left(\frac{q\,x}{\beta\,h}\right) \tag{24b}$$

$$I_2 \;=\; \frac{1}{2} \cdot \frac{[\,1 \;-\; (\beta/R)^2\,] \;+\; [\,1 \;+\; (\beta/R)^2\,]\cdot e^{-2q}}{[\,cosh(q)\,]^2 \;+\; [\,(\beta/R)\cdot sinh(q)\,]^2} \cdot sin\left(\frac{q\,x}{\beta\,h}\right) \tag{24c}$$

Parameter m_e in Eq. (24a) may be expressed as a function of the point doublet strength σ by using Eq. (2.43) from Ref. [2] or Eq. (11) from Ref. [6]. Then, we get :

$$m_e \;=\; \frac{\tau_e \cdot u_\infty}{\beta} \;=\; \frac{\sigma}{\beta} \tag{25}$$

The perturbation potential due to tunnel walls (Eq. (24a)) may be differentiated with respect to the streamwise coordinate x. Combining the corresponding result with Eq. (25) and with the definition of the blockage factor we get :

$$\begin{aligned} \epsilon(x) \;&=\; \frac{1}{u_\infty} \cdot \frac{\partial\,\phi_w(x)}{\partial\,x} \\ &=\; \frac{1}{u_\infty} \cdot \frac{-\,\sigma}{2\,\pi\,\beta^2\,h} \cdot \left[\int_0^\infty \frac{\partial\,I_1(q)}{\partial\,x}\,d\,q \;+\; \int_0^\infty \frac{\partial\,I_2(q)}{\partial\,x}\,d\,q \right] \end{aligned} \tag{26a}$$

where

$$\frac{\partial I_1}{\partial x} = \frac{-q}{R\,h} \cdot \frac{1}{[\,cosh(q)\,]^2 + [\,(\beta/R)\cdot sinh(q)\,]^2} \cdot sin\left(\frac{q\,x}{\beta\,h}\right) \qquad (26b)$$

$$\frac{\partial I_2}{\partial x} = \frac{q}{2\,\beta\,h} \cdot \frac{[\,1 - (\beta/R)^2\,] + [\,1 + (\beta/R)^2\,]\cdot e^{-2q}}{[\,cosh(q)\,]^2 + [\,(\beta/R)\cdot sinh(q)\,]^2} \cdot cos\left(\frac{q\,x}{\beta\,h}\right) \qquad (26c)$$

Baldwin et al. [6] give a solution for the blockage factor at the location of the two–dimensional point doublet (see Eq. (22) in Ref. [6]). This solution may be used to check the above result. Using the above equations, we get for blockage factor ϵ at the location of the point doublet ($x = 0$) :

$$\epsilon(0) = \frac{1}{u_\infty} \cdot \frac{-\sigma}{2\,\pi\,\beta^2\,h} \cdot \int_0^\infty I_3\,d\,q = \frac{1}{u_\infty} \cdot \frac{-m_e}{2\,\pi\,\beta\,h} \cdot \int_0^\infty I_3\,d\,q \qquad (27a)$$

where

$$I_3 = \frac{1}{\beta\,h} \cdot \frac{[\,1 - (\beta/R)^2\,] + [\,1 + (\beta/R)^2\,]\cdot e^{-2q}}{[\,cosh(q)\,]^2 + [\,(\beta/R)\cdot sinh(q)\,]^2} \cdot \frac{q}{2} \qquad (27b)$$

We also know that :

$$\begin{aligned} & \left([\,1 - (\beta/R)^2\,] + [\,1 + (\beta/R)^2\,]\cdot e^{-2q} \right) \cdot \frac{q}{2} \\ = & \left([\,1 - (\beta/R)^2\,]\cdot e^{q} + [\,1 + (\beta/R)^2\,]\cdot e^{-q} \right) \cdot e^{-q} \cdot \frac{q}{2} \\ = & \left(\frac{e^q + e^{-q}}{2} - (\beta/R)^2 \cdot \frac{e^q - e^{-q}}{2} \right) \cdot e^{-q} \cdot q \\ = & \left(cosh(q) - (\beta/R)^2 \cdot sinh(q) \right) \cdot e^{-q} \cdot q \end{aligned} \qquad (28)$$

Combining Eqs. (27a), (27b), and (28), we get the blockage factor at the location of the point doublet :

$$\epsilon(0) = \frac{1}{u_\infty} \cdot \frac{-m_e}{2\,\pi\,\beta^2\,h^2} \cdot \int_0^\infty \frac{[\,cosh(q) - (\beta/R)^2 \cdot sinh(q)\,]\cdot e^{-q}\cdot q}{[\,cosh(q)\,]^2 + [\,(\beta/R)\cdot sinh(q)\,]^2}\,d\,q \qquad (29)$$

Equation (29) is equal to Eq. (22) of Ref. [6]. Thus, Eqs. (26a), (26b), (26c) reduce to Eq. (22) of Ref. [6] if the blockage factor is computed at the location of the two–dimensional point doublet.

Classical Lift Interference : *Pindzola and Lo* [7] also use the Fourier transform technique to compute the lift interference caused by a two–dimensional vortex in a two–dimensional perforated wall wind tunnel. They express lift interference in terms of upwash

velocity w_w (w in their nomenclature). Using Eq. (3.65) of Ref. [7], the dimensionless upwash perturbation velocity component caused by a two–dimensional vortex on the centerline ($z = 0$) of a two–dimensional perforated wall wind tunnel may be written as :

$$\frac{w_w}{u_\infty} = \frac{1}{u_\infty} \cdot \frac{-\Gamma}{2\,\pi\,h} \cdot \left[\int_0^\infty I_4\, d\,q + \int_0^\infty I_5\, d\,q \right] \qquad (30a)$$

where

$$I_4 = \frac{\beta}{R} \cdot \frac{1}{[\,sinh(q)\,]^2 + [\,(\beta/R) \cdot cosh(q)\,]^2} \cdot cos\left(\frac{q\,x}{\beta\,h}\right) \qquad (30b)$$

$$I_5 = \frac{[\,sinh(q) - (\beta/R)^2 \cdot cosh(q)\,] \cdot e^{-q}}{[\,sinh(q)\,]^2 + [\,(\beta/R) \cdot cosh(q)\,]^2} \cdot sin\left(\frac{q\,x}{\beta\,h}\right) \qquad (30c)$$

Comparison of Wall Interference : Boundary conditions in panel method code ANTARES may be modified so that the flow field of a two–dimensional tunnel is computed. It is only required to impose the "closed wall" boundary condition on the tunnel sidewalls (Wall 1 and Wall 2 in Fig. 1) and the "perforated wall" boundary condition on the tunnel floor and ceiling (Wall 3 and Wall 4 in Fig. 1) of a tunnel with square cross–section. Table 4 lists wall boundary condition coefficients selected for the simulation of a two–dimensional perforated wall wind tunnel (see Eq. (1)).

Table 4 : Wall Boundary Condition Coefficients (2D Perforated Wall)

Wall No.	Panel Index Range	$c_1(i)$	$c_2(i)$	$c_3(i)$	$c_4(i)$
1	$1 \le i \le 1200$	0	0	1	0
2	$1201 \le i \le 2400$	0	0	1	0
3	$2401 \le i \le 3600$	0	1	$1/R$	0
4	$3601 \le i \le 4800$	0	1	$1/R$	0

The potential and derivatives of the three–dimensional point doublet in panel code ANTARES have to be replaced by corresponding equations of a two–dimensional point doublet (see Ref. [8], p.67/68). It is also required to replace the potential and derivatives of the three–dimensional line doublet by corresponding equations of a two–dimensional vortex (see Ref. [8], p.70/71).

A square tunnel ($10\ [ft] \times 10\ [ft]$, see Fig. 3 and Fig. 4) is selected for the comparison between classical solutions (Eqs. (26a), (26b), (26c) for blockage and Eqs. (30a), (30b),

(30c) for lift interference) and corresponding panel method code solutions computed by ANTARES. The restriction parameter R of the perforated floor and ceiling of the square tunnel is set to 1.14 (restriction parameter of NASA Ames 11ft TWT, see Ref. [2], p.3-25). Two different Mach numbers (0.00 and 0.90) are selected to investigate compressibility effects on the wall interference calculation.

At first, blockage corrections are investigated. A two–dimensional unit point doublet pointing upstream is placed on the tunnel centerline at the coordinate system origin ($\sigma = 1, x = y = z = 0$). Results of the panel method code calculation are compared in Fig. 13 with the corresponding exact solution (Eqs. (26a), (26b), (26c)). The agreement between panel method code solution and exact solution is excellent for both Mach numbers.

In the next step, upwash corrections are investigated. A two–dimensional unit vortex is placed on the tunnel centerline at the coordinate system origin ($\Gamma = 1, x = y = z = 0$). Results of the panel method code calculation are compared in Fig. 14 with the corresponding exact solution (Eqs. (30a), (30b), (30c)). Again, the agreement between panel method solution and exact solution is excellent for both Mach numbers.

CHAPTER 3

CONCLUSION AND REMARKS

Panel method code ANTARES was developed to determine wall interference effects of point doublets and line doublets in a wind tunnel with rectangular cross–section. The code is based on *Keller's* algorithm [3] that allows the user to describe up to six different types of wall boundary conditions.

At the present time ANTARES can assign the closed wall, open jet, or perforated wall boundary condition to the centroid of each wall panel. Blockage effects of the test article are represented by using point doublets. Test article lifting effects are represented by using line doublets. Compressibility effects are taken into account by applying the Prandtl–Glauert transformation to the test section geometry, the point doublet or line doublet coordinates, and to the singularity strength.

The accuracy of the panel method code calculation for a given panel representation of the test section geometry was investigated by using available classical solutions. Panel method code solutions of the closed wall and open jet boundary condition were successfully compared with corresponding Method of Images solutions. Panel method code solutions of the perforated wall boundary condition were successfully compared with corresponding Fourier transform solutions.

Studies have shown that the accuracy of a wall interference calculation depends on the number of wall panels used to represent the test section walls. The accuracy also depends on the free–stream Mach number that is used to transform the test section geometry. For a fullspan model test section configuration, a total number of 4800 panels (60 in the streamwise direction and 80 in the circumferential direction) seems to provide a good representation of the test section geometry. For a semispan model test, a total number of 7200 panels (60 in the streamwise direction and 120 in the circumferential direction) should be selected. In both cases it is recommended to use cosine panel spacing in the streamwise direction and equal panel spacing in the circumferential direction. Accuray improvements were achieved by increasing the number of panels in the circumferential direction. The length of the paneled test section should be about eight tunnel widths.

ANTARES computes sufficiently accurate corrections up to a Mach number of 0.80 if the closed wall boundary condition is applied to the selected panel representation of the wind tunnel walls. The Mach number limit seems to be close to 0.90 if the open jet or perforated wall boundary condition is applied.

Panel method code ANTARES does not model the effect of shocks that may occur during the test of a wind tunnel model at high subsonic Mach numbers. Mach number limits for the closed wall, open jet, or perforated wall boundary condition are therefore only valid as long as no shocks touch the test section walls during the wind tunnel test.

Derivatives required for the application of the ideal slotted wall boundary condition and of the slotted wall boundary condition that includes viscous effects in slots have already been included in ANTARES (see Table 1 on p.3 and Appendices 1 and 2). An implementation of these boundary conditions in ANTARES will be considered in a future release of the software.

REFERENCES

LIST OF REFERENCES

[1] Ulbrich, N., "The Real–Time Wall Interference Correction System of the NASA Ames 12–Foot Pressure Wind Tunnel," NASA/CR–1998–208537, Ames Research Center, Moffett Field, California, July 1998 .

[2] Ewald, B. F. R. (editor), "Wind Tunnel Wall Correction," AGARDograph 336, North Atlantic Treaty Organization, October 1998, p.(2–12) to p.(2–31), and p.(3–23) to p.(3–27) .

[3] Keller, J. D., "Numerical Calculation of Boundary–Induced Interference in Slotted or Perforated Wind Tunnels Including Viscous Effects in Slots," NASA TN D–6871, Langley Research Center, Hampton, Virginia, August 1972.

[4] Schlichting, H. and Truckenbroth, E., "Aerodynamics of the Airplane," translated by H. J. Ramm, McGraw–Hill International Book Company, 1979, Eqs. (2–10), (3–54a), (4–10), (4–22), p.217 to p.223 and p.348 to p.351 .

[5] Press, W. H., Teukolsky, S. A., Vetterling, W. T., Flannery, B. P., "Numerical Recipes in FORTRAN 77," Cambridge University Press, reprint of second edition with corrections, 1996, p.34 to p.40 .

[6] Baldwin, B. S., Turner, J. B., Knechtel, E. D., "Wall Interference in Wind Tunnels with Slotted and Porous Boundaries at Subsonic Speeds," NACA TN 3176, Ames Aeronautical Laboratory, Moffett Field, California, May 1954, Eqs. (11), (19), (22) .

[7] Pindzola, M. and Lo, C. F., "Boundary Interference at Subsonic Speeds in Wind Tunnels with Ventilated Walls," AEDC-TR-69-47, Arnold Engineering Development Center, Arnold Air Force Station, Tennessee, May 1969, Eq. (3.65) .

[8] Katz, J. and Plotkin, A., "Low–Speed Aerodynamics: From Wing Theory to Panel Methods," McGraw–Hill Series in Aeronautical and Aerospace Engineering, New York, 1991, Eqs. (3.37), (3.43), (3.44), (3.45), (3.71), (3.72), (3.73), (3.80), (3.81), (3.82), (3.96), (3.119) .

[9] Duncan, W. J., Thom, A. S., Young, A. D., "Mechanics of Fluids," American Elsevier Publishing Company, Inc., New York, New York, 2nd Ed., 1970, p.62, p.65 .

APPENDICES

APPENDIX 1

POINT DOUBLET POTENTIAL AND DERIVATIVES

Panel method code ANTARES uses point doublets pointing upstream to describe blockage effects of a test article in a rectangular wind tunnel. ANTARES describes wind tunnel wall boundary conditions by applying *Keller's* algorithm (see Ref. [3]). Therefore, it is necessary to specify the point doublet potential and its derivatives in the tunnel coordinate system x,y,z .

A point doublet is located at point x_o,y_o,z_o in the tunnel coordinate system. The point doublet is pointing upstream, i.e. in the negative x–direction (see Fig. 1). Then, the potential of the point doublet may be written as [8]:

$$\phi_m = \frac{\sigma}{4\,\pi} \cdot \frac{x - x_o}{\left[\,(x-x_o)^2 + (y-y_o)^2 + (z-z_o)^2\,\right]^{3/2}} \tag{1.1}$$

First and second order derivatives may easily be obtained by differentiating Eq. (1.1). For the first order derivatives we get :

$$\frac{\partial\,\phi_m}{\partial\,x} = \frac{\sigma}{4\,\pi} \cdot \frac{(y-y_o)^2 + (z-z_o)^2 - 2\cdot(x-x_o)^2}{\left[\,(x-x_o)^2 + (y-y_o)^2 + (z-z_o)^2\,\right]^{5/2}} \tag{1.2a}$$

$$\frac{\partial\,\phi_m}{\partial\,y} = \frac{(-3)\cdot\sigma}{4\cdot\pi} \cdot \frac{(x-x_o)\cdot(y-y_o)}{\left[\,(x-x_o)^2 + (y-y_o)^2 + (z-z_o)^2\,\right]^{5/2}} \tag{1.2b}$$

$$\frac{\partial\,\phi_m}{\partial\,z} = \frac{(-3)\cdot\sigma}{4\cdot\pi} \cdot \frac{(x-x_o)\cdot(z-z_o)}{\left[\,(x-x_o)^2 + (y-y_o)^2 + (z-z_o)^2\,\right]^{5/2}} \tag{1.2c}$$

Similarly, for the second order derivatives we get :

$$\frac{\partial^2\,\phi_m}{\partial\,x\,\partial\,y} = \frac{(-3)\cdot\sigma}{4\cdot\pi} \cdot \frac{(y-y_o)\cdot\left[\,(y-y_o)^2 + (z-z_o)^2 - 4\cdot(x-x_o)^2\,\right]}{\left[\,(x-x_o)^2 + (y-y_o)^2 + (z-z_o)^2\,\right]^{7/2}} \tag{1.3a}$$

$$\frac{\partial^2\,\phi_m}{\partial\,x\,\partial\,z} = \frac{(-3)\cdot\sigma}{4\cdot\pi} \cdot \frac{(z-z_o)\cdot\left[\,(y-y_o)^2 + (z-z_o)^2 - 4\cdot(x-x_o)^2\,\right]}{\left[\,(x-x_o)^2 + (y-y_o)^2 + (z-z_o)^2\,\right]^{7/2}} \tag{1.3b}$$

Derivatives normal to the walls of the rectangular wind tunnel are required as panel method code ANTARES uses *Keller's* algorithm [3] to model different types of wall boundary conditions. In general, the normal derivative operator may be written as :

$$\frac{\partial}{\partial \mathbf{n}} \equiv \mathbf{n} \circ \nabla \equiv \begin{pmatrix} N_x \\ N_y \\ N_z \end{pmatrix} \circ \begin{pmatrix} \partial / \partial x \\ \partial / \partial y \\ \partial / \partial z \end{pmatrix} \tag{1.4}$$

The scalar product defined in Eq. (1.4) may also be written as :

$$\frac{\partial}{\partial \mathbf{n}} \equiv N_x \cdot \frac{\partial}{\partial x} + N_y \cdot \frac{\partial}{\partial y} + N_z \cdot \frac{\partial}{\partial z} \tag{1.5}$$

Now it is possible to determine the normal derivatives if the outward normal vector $\mathbf{n}$ on each wind tunnel wall is identified. Using Fig. 1 and Eq. (1.5), we get :

Table 5 : Normal Derivatives on the Wind Tunnel Wall (Point Doublet)

Wall No.	$\mathbf{n}$	$\frac{\partial}{\partial \mathbf{n}}$	$\frac{\partial \phi_m}{\partial \mathbf{n}}$	$\frac{\partial^2 \phi_m}{\partial x \partial \mathbf{n}}$
1	$\begin{pmatrix} 0 \\ 1 \\ 0 \end{pmatrix}$	$\frac{\partial}{\partial y}$	$\frac{\partial \phi_m}{\partial y}$ Eq.(1.2b)	$\frac{\partial^2 \phi_m}{\partial x \partial y}$ Eq.(1.3a)
2	$\begin{pmatrix} 0 \\ -1 \\ 0 \end{pmatrix}$	$-\frac{\partial}{\partial y}$	$-\frac{\partial \phi_m}{\partial y}$ Eq.(1.2b)	$-\frac{\partial^2 \phi_m}{\partial x \partial y}$ Eq.(1.3a)
3	$\begin{pmatrix} 0 \\ 0 \\ 1 \end{pmatrix}$	$\frac{\partial}{\partial z}$	$\frac{\partial \phi_m}{\partial z}$ Eq.(1.2c)	$\frac{\partial^2 \phi_m}{\partial x \partial z}$ Eq.(1.3b)
4	$\begin{pmatrix} 0 \\ 0 \\ -1 \end{pmatrix}$	$-\frac{\partial}{\partial z}$	$-\frac{\partial \phi_m}{\partial z}$ Eq.(1.2c)	$-\frac{\partial^2 \phi_m}{\partial x \partial z}$ Eq.(1.3b)

APPENDIX 2

LINE DOUBLET POTENTIAL AND DERIVATIVES

Panel method code ANTARES uses line doublets to model lifting effects of a test article in a rectangular wind tunnel. Wind tunnel wall boundary conditions are described by applying *Keller's* algorithm [3]. Therefore, it is necessary to specify the line doublet potential and its derivatives in the tunnel coordinate system x,y,z .

Figure 15a shows the location of a line doublet in a rectangular wind tunnel. The line doublet is oriented such that the corresponding lift force points in the ζ direction of the line doublet fixed coordinate system ξ,η,ζ . Line doublet orientation angle Θ is used to describe the line doublet orientation in the tunnel coordinate system x,y,z .

The calculation of the line doublet potential and its derivatives in the tunnel coordinate system x,y,z may be done in three steps:

(1) A coordinate system transformation from the tunnel coordinate system x,y,z to the line doublet fixed coordinate system ξ,η,ζ is introduced which will greatly simplify the calculation of the line doublet potential and its derivatives.

(2) The line doublet potential and its derivatives are determined in the line doublet fixed coordinate system ξ,η,ζ .

(3) The line doublet potential and its derivatives are transformed from the line doublet fixed coordinate system ξ,η,ζ to the tunnel coordinate system x,y,z .

Coordinate System Transformation

In general, it is easier to compute the line doublet potential and its derivatives in the line doublet fixed coordinate system ξ,η,ζ . Therefore, the following transformation may be used to transform coordinates from the tunnel coordinate system x,y,z to the line doublet fixed coordinate system ξ,η,ζ . Thus, we get for a flow field point x,y,z in the tunnel coordinate system :

$$\xi(x) = x \tag{2.1a}$$

$$\eta(y,z,\Theta) = y \cdot cos\ \Theta - z \cdot sin\ \Theta \tag{2.1b}$$

$$\zeta(y,z,\Theta) = y \cdot sin\ \Theta + z \cdot cos\ \Theta \tag{2.1c}$$

Similary, starting point coordinates x_o,y_o,z_o of the line doublet have to be transformed to

the line doublet fixed coordinate system ξ,η,ζ . We get :

$$\xi_o = x_o \tag{2.2a}$$

$$\eta_o = y_o \cdot cos\ \Theta - z_o \cdot sin\ \Theta \tag{2.2b}$$

$$\zeta_o = y_o \cdot sin\ \Theta + z_o \cdot cos\ \Theta \tag{2.2c}$$

Potential and Derivatives in Line Doublet Fixed Coordinate System

The line doublet potential in the line doublet fixed coordinate system ξ,η,ζ may be written as [1]:

$$\phi_m = \frac{\sigma}{4\,\pi} \cdot \frac{\zeta - \zeta_o}{(\eta - \eta_o)^2 + (\zeta - \zeta_o)^2} \cdot A \tag{2.3a}$$

where

$$A = 1 + \frac{\xi - \xi_o}{\left[\,(\xi - \xi_o)^2 + (\eta - \eta_o)^2 + (\zeta - \zeta_o)^2\,\right]^{1/2}} \tag{2.3b}$$

Derivatives of the line doublet potential in the line doublet fixed coordinate system ξ,η,ζ may now be obtained by differentiating Eq. (2.3a). For the first order derivatives we get :

$$\frac{\partial\,\phi_m}{\partial\,\xi} = \frac{\sigma}{4\,\pi} \cdot \frac{\zeta - \zeta_o}{\left[\,(\xi - \xi_o)^2 + (\eta - \eta_o)^2 + (\zeta - \zeta_o)^2\,\right]^{3/2}} \tag{2.4}$$

$$\frac{\partial\,\phi_m}{\partial\,\eta} = \frac{-\,\sigma}{4\,\pi} \cdot \frac{(\eta - \eta_o)\cdot(\zeta - \zeta_o)}{(\eta - \eta_o)^2 + (\zeta - \zeta_o)^2} \cdot \left[\frac{2\cdot B}{(\eta - \eta_o)^2 + (\zeta - \zeta_o)^2} + C\right] \tag{2.5a}$$

where

$$B = 1 + \frac{\xi - \xi_o}{\left[\,(\xi - \xi_o)^2 + (\eta - \eta_o)^2 + (\zeta - \zeta_o)^2\,\right]^{1/2}} \tag{2.5b}$$

$$C = \frac{\xi - \xi_o}{\left[(\xi - \xi_o)^2 + (\eta - \eta_o)^2 + (\zeta - \zeta_o)^2 \right]^{3/2}} \tag{2.5c}$$

$$\frac{\partial \phi_m}{\partial \zeta} = \frac{\sigma}{4\pi} \cdot \frac{1}{(\eta - \eta_o)^2 + (\zeta - \zeta_o)^2} \cdot \left[\frac{(\eta - \eta_o)^2 - (\zeta - \zeta_o)^2}{(\eta - \eta_o)^2 + (\zeta - \zeta_o)^2} \cdot D + E \right] \tag{2.6a}$$

where

$$D = 1 + \frac{\xi - \xi_o}{\left[(\xi - \xi_o)^2 + (\eta - \eta_o)^2 + (\zeta - \zeta_o)^2 \right]^{1/2}} \tag{2.6b}$$

$$E = \frac{(-1) \cdot (\xi - \xi_o) \cdot (\zeta - \zeta_o)^2}{\left[(\xi - \xi_o)^2 + (\eta - \eta_o)^2 + (\zeta - \zeta_o)^2 \right]^{3/2}} \tag{2.6c}$$

For the second order derivatives we get :

$$\frac{\partial^2 \phi_m}{\partial \xi \, \partial \eta} = \frac{(-3)\,\sigma}{4\pi} \cdot \frac{(\eta - \eta_o) \cdot (\zeta - \zeta_o)}{\left[(\xi - \xi_o)^2 + (\eta - \eta_o)^2 + (\zeta - \zeta_o)^2 \right]^{5/2}} \tag{2.7}$$

$$\frac{\partial^2 \phi_m}{\partial \xi \, \partial \zeta} = \frac{\sigma}{4\pi} \cdot \frac{(\xi - \xi_o)^2 + (\eta - \eta_o)^2 - 2 \cdot (\zeta - \zeta_o)^2}{\left[(\xi - \xi_o)^2 + (\eta - \eta_o)^2 + (\zeta - \zeta_o)^2 \right]^{5/2}} \tag{2.8}$$

Potential and Derivatives in Tunnel Coordinate System

The line doublet potential and its derivatives in the tunnel coordinate system may easily be obtained by reversing the coordinate system transformation defined by Eqs. (2.1a) to (2.1c). The line doublet potential is a scalar function and depends only on the coordinates of the selected flow field point. Thus, combining Eqs. (2.1a) to (2.1c) with Eqs. (2.3a), (2.3b), we get for the potential :

$$\phi_m(x, y, z) = \phi_m(\xi(x), \eta(y, z, \Theta), \zeta(y, z, \Theta)) \tag{2.9}$$

Derivatives in the tunnel coordinate system may be obtained by reversing the coordinate system rotation (see Fig. 15b). Then, we get for the first order derivatives of the line doublet potential :

$$\frac{\partial \phi_m}{\partial x} = \frac{\partial \phi_m}{\partial \xi} \tag{2.10a}$$

$$\frac{\partial \phi_m}{\partial y} = \frac{\partial \phi_m}{\partial \eta} \cdot cos\,\Theta + \frac{\partial \phi_m}{\partial \zeta} \cdot sin\,\Theta \tag{2.10b}$$

$$\frac{\partial \phi_m}{\partial z} = \frac{\partial \phi_m}{\partial \eta} \cdot (-sin\,\Theta) + \frac{\partial \phi_m}{\partial \zeta} \cdot cos\,\Theta \tag{2.10c}$$

The higher order derivatives may be obtained in a similar manner. We know from Eq. (2.1a) :

$$\xi = x \quad \Longrightarrow \quad \frac{\partial}{\partial \xi} \equiv \frac{\partial}{\partial x} \tag{2.11a}$$

Thus, we get :

$$\frac{\partial^2 \phi_m}{\partial x\, \partial y} = \frac{\partial}{\partial \xi} \cdot \frac{\partial \phi_m}{\partial y} \tag{2.11b}$$

$$\frac{\partial^2 \phi_m}{\partial x\, \partial z} = \frac{\partial}{\partial \xi} \cdot \frac{\partial \phi_m}{\partial z} \tag{2.11c}$$

Combining Eq. (2.10b) and (2.11b), we get :

$$\frac{\partial^2 \phi_m}{\partial x\, \partial y} = \frac{\partial^2 \phi_m}{\partial \xi\, \partial \eta} \cdot cos\,\Theta + \frac{\partial^2 \phi_m}{\partial \xi\, \partial \zeta} \cdot sin\,\Theta \tag{2.12a}$$

Combining Eq. (2.10c) and (2.11c), we get :

$$\frac{\partial^2 \phi_m}{\partial x\, \partial z} = \frac{\partial^2 \phi_m}{\partial \xi\, \partial \eta} \cdot (-sin\,\Theta) + \frac{\partial^2 \phi_m}{\partial \xi\, \partial \zeta} \cdot cos\,\Theta \tag{2.12b}$$

Derivatives normal to the walls of the rectangular wind tunnel are required as panel method code ANTARES uses *Keller's* algorithm [3] to model different types of wall boundary conditions. From App. 1 we know that the normal derivative operator is equal to :

$$\frac{\partial}{\partial \mathbf{n}} \equiv N_x \cdot \frac{\partial}{\partial x} + N_y \cdot \frac{\partial}{\partial y} + N_z \cdot \frac{\partial}{\partial z} \tag{2.13}$$

Now it is possible to determine the normal derivatives if the outward normal vector **n** on each wind tunnel wall is identified. Using Fig. 1 and Eq. (2.13), we get :

Table 6 : Normal Derivatives on the Wind Tunnel Wall (Line Doublet)

Wall No.	$\mathbf{n}$	$\frac{\partial}{\partial \mathbf{n}}$	$\frac{\partial \phi_m}{\partial \mathbf{n}}$	$\frac{\partial^2 \phi_m}{\partial x \partial \mathbf{n}}$
1	$\begin{pmatrix} 0 \\ 1 \\ 0 \end{pmatrix}$	$\frac{\partial}{\partial y}$	$\frac{\partial \phi_m}{\partial y}$ Eq.(2.10b)	$\frac{\partial^2 \phi_m}{\partial x \partial y}$ Eq.(2.12a)
2	$\begin{pmatrix} 0 \\ -1 \\ 0 \end{pmatrix}$	$-\frac{\partial}{\partial y}$	$-\frac{\partial \phi_m}{\partial y}$ Eq.(2.10b)	$-\frac{\partial^2 \phi_m}{\partial x \partial y}$ Eq.(2.12a)
3	$\begin{pmatrix} 0 \\ 0 \\ 1 \end{pmatrix}$	$\frac{\partial}{\partial z}$	$\frac{\partial \phi_m}{\partial z}$ Eq.(2.10c)	$\frac{\partial^2 \phi_m}{\partial x \partial z}$ Eq.(2.12b)
4	$\begin{pmatrix} 0 \\ 0 \\ -1 \end{pmatrix}$	$-\frac{\partial}{\partial z}$	$-\frac{\partial \phi_m}{\partial z}$ Eq.(2.10c)	$-\frac{\partial^2 \phi_m}{\partial x \partial z}$ Eq.(2.12b)

The calculation of the line doublet potential and its derivatives in the tunnel coordinate system is complex as the line doublet orientation angle has to be taken into account. A coordinate system transformation from the tunnel coordinate system to a line doublet fixed coordinate system is required. Then, the potential and its derivatives are computed in the line doublet fixed coordinate system. Finally, the potential and its derivatives are computed in the tunnel coordinate system by reversing the coordinate system transformation. The following flow chart summarizes different solution steps :

Selection of flow field point (x, y, z) in tunnel coordinate system.

$\Downarrow$

Selection of line doublet (x_o, y_o, z_o, Θ) in tunnel coordinate system.

$\Downarrow$

Transformation from tunnel coordinate system to line doublet fixed coordinate system (Eqs. (2.1a) to (2.2c))

$\Downarrow$

Calculation of potential and its derivatives in line doublet fixed coordinate system (Eqs. (2.3a) to (2.8))

$\Downarrow$

Calculation of potential and its derivatives in tunnel coordinate system (Eqs. (2.9) to (2.12b))

APPENDIX 3

SINGULARITY STRENGTH TRANSFORMATION

In general, the Prandtl–Glauert transformation has to be applied if the subsonic wind tunnel and wall interference flow field of a singularity located in a wind tunnel is calculated. This transformation requires a stretching of the wind tunnel coordinates from an original coordinate system (x,y,z) to a corresponding transformed coordinate system (x',y',z'). The transformation of the coordinates, of the free–stream velocity, and of the perturbation potential is given by the following equations (see Ref. [4], p.217–223 and p.348–351) :

$$x' = x \qquad (3.1a)$$

$$y' = y \cdot \beta \qquad (3.1b)$$

$$z' = z \cdot \beta \qquad (3.1c)$$

$$u'_\infty = u_\infty \qquad (3.1d)$$

$$\phi' = \phi \cdot \beta^2 \qquad (3.1e)$$

$$\beta = \sqrt{1 - M_\infty^2} \qquad (3.1f)$$

where u_∞ is the free–stream velocity, ϕ is the perturbation velocity potential, and M_∞ is the free–stream Mach number of the subsonic flow field. After the application of the transformation, the flow field solution is found in the transformed coordinate system by solving the Laplace equation. Finally, a back–transformation has to be applied to the solution of the Laplace equation in the transformed coordinate system to obtain the solution of the subsonic potential equation in the original coordinate system.

Singularities are used to represent a test article during a wind tunnel wall interference calculation. Point sources or point doublets represent blockage effects of the test article. Vortices or line doublets represent lifting effects of the test article. The geometry of the test

article is related to the strength of these singularities. The Prandtl–Glauert transformation changes the test article geometry. Thus, the Prandtl–Glauert transformation also has to change the strength of singularities representing the test article. The transformation of the singularity strength has to be a function of scale factor β, i.e.

$$\sigma' = \sigma \cdot F(\beta) \qquad (3.1g)$$

The particular form of the transformation function $F(\beta)$ for each type of singularity is rigorously derived in the following parts of this section.

Two–Dimensional Point Source

A two–dimensional point source may be used to describe the blockage effect of a halfbody in a two–dimensional flow field. The strength σ of this point source in the original coordinate system (x,z) may be written as (see Ref. [9], p.62) :

$$\sigma = u_\infty \cdot D \qquad (3.2)$$

where u_∞ is the free–stream velocity and D is the width of the two–dimensional halfbody. The singularity strength in the transformed coordinate system (x',z') may be written as :

$$\sigma' = u'_\infty \cdot D' \qquad (3.3)$$

Applying the Prandtl–Glauert transformation, i.e. Eq. (3.1c) and (3.1d), to the width of the two–dimensional halfbody and to the free–stream velocity, we get :

$$u'_\infty \cdot D' = u_\infty \cdot D \cdot \beta \qquad (3.4)$$

Finally, combining Eqs. (3.2), (3.3), and (3.4), we get :

$$\sigma' = \sigma \cdot \beta \qquad (3.5a)$$

where σ' is the transformed strength and σ is the original strength of a two–dimensional point source. Thus, for a two–dimensional point source, the transformation function $F(\beta)$ as defined in Eq. (3.1g) is given as :

$$F(\beta) \quad = \quad \beta \qquad (3.5b)$$

It is possible to verify the singularity strength transformation given in Eq. (3.5b). Therefore, a Method of Images solution for the blockage factor caused by a 2D point source at a high subsonic Mach number was developed using derivatives of the singularity potential in combination with Eqs. (3.5a), (12a), (12c), and (23a). This solution for the blockage factor showed good agreement with a classical solution given by Eq. (2.56) in Ref. [2].

Two–Dimensional Point Doublet

A two–dimensional point doublet may be used to represent blockage effects of a cylinder in a two–dimensional flow field. The strength σ of this point doublet may be written as (see Ref. [2], Eq. (2.43) or Ref. [8], Eq. (3.96)) :

$$\sigma \quad = \quad u_\infty \cdot 2 \cdot \pi \cdot r_c^2 \qquad (3.6)$$

where u_∞ is the free–stream velocity and r_c is the radius of the cylinder. The product $\pi \cdot r_c^2$ in Eq. (3.6) may be interpreted as the cross–sectional area of the cylinder. This area can also be written in integral form as :

$$\pi \cdot r_c^2 \quad = \quad \int_{-r_c}^{+r_c} z(x)\, d\, x \qquad (3.7)$$

where $z(x)$ is the width of the cylinder for a given streamwise location x . Combining Eqs. (3.6) and (3.7), the singularity strength in the original coordinate system (x,z) may be written as :

$$\sigma \quad = \quad u_\infty \cdot 2 \cdot \int_{-r_c}^{+r_c} z(x)\, d\, x \qquad (3.8)$$

Thus, the singularity strength in the transformed coordinate system (x',z') may be written as :

$$\sigma' \quad = \quad u'_\infty \cdot 2 \cdot \int_{-r'_c}^{+r'_c} z'(x')\, d\, x' \qquad (3.9)$$

Applying the Prandtl–Glauert transformation, i.e. Eqs. (3.1a) and (3.1c), to the streamwise coordinate x and the width $z(x)$ of the cylinder we get :

$$d\,x' \;=\; d\,x \qquad \Longrightarrow \qquad r_c' \;=\; r_c \tag{3.10a}$$

$$z'(x') \;=\; z(x)\cdot\beta \tag{3.10b}$$

Combining Eqs. (3.1d), (3.9), (3.10a), and (3.10b), we get :

$$\sigma' \;=\; \left[\, u_\infty \cdot 2 \cdot \int_{-r_c}^{+r_c} z(x)\; d\,x \,\right] \cdot \beta \tag{3.11}$$

Combining Eqs. (3.8) and (3.11), we get :

$$\sigma' \;=\; \sigma\cdot\beta \tag{3.12a}$$

where σ' is the transformed strength and σ is the original strength of a two–dimensional point doublet. Thus, for a two–dimensional point doublet, the transformation function $F(\beta)$ as defined in Eq. (3.1g) is given as :

$$\boxed{F(\beta) \;=\; \beta \qquad (3.12b)}$$

It is possible to verify the singularity strength transformation given in Eq. (3.12b). Therefore, a Method of Images solution for the blockage factor caused by a 2D point doublet at a high subsonic Mach number was constructed using derivatives of the singularity potential in combination with Eqs. (3.12a), (12a), (12c), and (23a). This solution for the blockage factor showed good agreement with a classical solution given by Eq. (2.45) in Ref. [2].

Three–Dimensional Point Source

A three–dimensional point source and point sink may be used to represent solid volume blockage effects of a fuselage in a three–dimensional flow field. The strength σ of a three–dimensional point source may be written as (see Ref. [9], p.65) :

$$\sigma = u_\infty \cdot \pi \cdot r_\infty^2 \qquad (3.13)$$

where r_∞ is the downstream radius of the three–dimensional body of revolution that corresponds to a single source in a flow field and u_∞ is the free–stream velocity. The downstream radius of the three–dimensional body of revolution may be written as :

$$r_\infty^2 = y(x)^2 + z(x)^2 \qquad (3.14)$$

where $y(x)$ and $z(x)$ describe the cross–sectional shape of the body of revolution far downstream of the source. Combining Eqs. (3.13), (3.14) we get the strength σ of a three–dimensional point source in the original coordinate system (x,y,z) :

$$\sigma = u_\infty \cdot \pi \cdot \left[y(x)^2 + z(x)^2 \right] \qquad (3.15)$$

The singularity strength in the transformed coordinate system (x',y',z') may be written as :

$$\sigma' = u'_\infty \cdot \pi \cdot \left[y'(x')^2 + z'(x')^2 \right] \qquad (3.16)$$

Applying the Prandtl–Glauert transformation, i.e. Eqs. (3.1a), (3.1b), (3.1c), we get :

$$y'(x') = y(x) \cdot \beta \qquad (3.17a)$$

$$z'(x') = z(x) \cdot \beta \qquad (3.17b)$$

Combining Eqs. (3.1d), (3.16), (3.17a), (3.17b), we get :

$$\sigma' = \left[u_\infty \cdot \pi \cdot \left[y(x)^2 + z(x)^2 \right] \right] \cdot \beta^2 \qquad (3.18)$$

Finally, combining Eqs. (3.15) and (3.18), we get :

$$\sigma' = \sigma \cdot \beta^2 \qquad (3.19a)$$

where σ' is the transformed strength and σ is the original strength of a three–dimensional point source. Thus, for a three–dimensional point source, the transformation function $F(\beta)$ as defined in Eq. (3.1g) is given as :

$$F(\beta) \quad = \quad \beta^2 \qquad (3.19b)$$

It is possible to verify the singularity strength transformation given in Eq. (3.19b). Therefore, a Method of Images solution for the blockage factor caused by a 3D point source at a high subsonic Mach number was constructed using derivatives of the singularity potential in combination with Eqs. (3.19a), (12a), (12b), (12c), and (23a). This solution for the blockage factor showed good agreement with a classical solution given by Eq. (2.72) in Ref. [2].

Three–Dimensional Point Doublet

A three–dimensional point doublet may be used to represent solid volume blockage effects of a small fuselage in a three–dimensional flow field. The strength σ of a three–dimensional point doublet may be written as (see Ref. [8], p.80) :

$$\sigma \quad = \quad u_\infty \cdot 2 \cdot \pi \cdot r_\circ^3 \qquad (3.20)$$

where $r_\circ$ is the radius of the sphere and u_∞ is the free–stream velocity. The product $2 \cdot \pi \cdot r_\circ^3$ in Eq. (3.20) may be interpreted as a multiple of the volume of a sphere. Therefore, we can write :

$$2 \cdot \pi \cdot r_\circ^3 \quad = \quad \frac{3}{2} \cdot \left[\frac{4}{3} \cdot \pi \cdot r_\circ^3 \right] \quad = \quad \frac{3}{2} \cdot \int_{-r_\circ}^{+r_\circ} \pi \cdot \left[\, y(x)^2 \, + \, z(x)^2 \, \right] d\, x \qquad (3.21)$$

where $y(x), z(x)$ describes the cross–sectional shape of the sphere as a function of the streamwise coordinate. Combining Eqs. (3.20) and (3.21), we get for the singularity strength in the original coordinate system (x,y,z) :

$$\sigma \quad = \quad u_\infty \cdot \frac{3}{2} \cdot \int_{-r_\circ}^{+r_\circ} \pi \cdot \left[\, y(x)^2 \, + \, z(x)^2 \, \right] d\, x \qquad (3.22)$$

The singularity strength in the transformed coordinate system (x',y',z') may be writ-

ten as :

$$\sigma' \quad = \quad u'_\infty \cdot \frac{3}{2} \cdot \int_{-r'_\circ}^{+r'_\circ} \pi \cdot \left[\, y'(x')^2 \, + \, z'(x')^2 \, \right] d\, x' \tag{3.23}$$

Applying the Prandtl–Glauert transformation, i.e. Eqs. (3.1a), (3.1b), (3.1c), we get :

$$d\, x' \quad = \quad d\, x \qquad \Longrightarrow \qquad r'_\circ \quad = \quad r_\circ \tag{3.24a}$$

$$y'(x') \quad = \quad y(x) \cdot \beta \tag{3.24b}$$

$$z'(x') \quad = \quad z(x) \cdot \beta \tag{3.24c}$$

Combining Eqs. (3.1d), (3.23), (3.24a), (3.24b), (3.24c), we get :

$$\sigma' \quad = \quad \left[u_\infty \cdot \frac{3}{2} \cdot \int_{-r_\circ}^{+r_\circ} \pi \cdot \left[\, y(x)^2 \, + \, z(x)^2 \, \right] d\, x \right] \cdot \beta^2 \tag{3.25}$$

Finally, combining Eqs. (3.22), (3.25), we get :

$$\sigma' \quad = \quad \sigma \cdot \beta^2 \tag{3.26a}$$

where σ' is the transformed strength and σ is the original strength of a three–dimensional point doublet. Thus, for a three–dimensional point doublet, the transformation function $F(\beta)$ as defined in Eq. (3.1g) is given as :

$$\boxed{F(\beta) \quad = \quad \beta^2 \qquad (3.26b)}$$

It is possible to verify the singularity strength transformation given in Eq. (3.26b). Therefore, a Method of Images solution for the blockage factor caused by a 3D point doublet at a high subsonic Mach number was constructed using derivatives of the singularity potential in combination with Eqs. (3.26a), (12a), (12b), (12c), and (23a). This solution for the blockage factor showed good agreement with a classical solution given by Eq. (2.64) in Ref. [2].

Two–Dimensional Vortex

A two–dimensional vortex may be used to represent lifting effects of an airfoil in a two–dimensional flow field. The strength σ of a two–dimensional vortex may be derived by using the Kutta–Joukowski formula. The Kutta–Joukowski formula may be written as :

$$L \,/\, \Delta s \quad = \quad \rho_\infty \cdot u_\infty \cdot \Gamma \tag{3.27}$$

where $L/\Delta s$ is the lift force per unit wing span, ρ_∞ is the free–stream density, u_∞ is the free–stream velocity, and Γ is the circulation. Thus, in case of a two–dimensional vortex, we may define the strength as :

$$\boxed{\sigma \quad = \quad \frac{L}{\rho_\infty \cdot u_\infty \cdot \Delta s} \quad = \quad \Gamma \qquad (3.28)}$$

The lift force per unit wing span, i.e. $L/\Delta s$, may also be written by using the lift coefficient definition. Then, we get :

$$L \,/\, \Delta s \quad = \quad \frac{\rho_\infty}{2} \cdot u_\infty^2 \cdot c_L \cdot c \tag{3.29}$$

where c is the chord of the airfoil. Combining Eqs. (3.28), (3.29) we get :

$$\sigma \quad = \quad \frac{u_\infty}{2} \cdot c_L \cdot c \tag{3.30}$$

The lift coefficient c_L may be rewritten by considering the pressure coefficient difference Δc_p between upper and lower surface of an airfoil as a function of the streamwise coordinate x. Using Eq. (2–10) from Ref. [4], we get :

$$c_L \quad = \quad \frac{1}{c} \cdot \int_0^c \Delta c_p(x) \; d\, x \tag{3.31}$$

Combining Eq. (3.30) and (3.31), we get for the vortex strength in the original coordinate system (x,y,z) :

$$\sigma \quad = \quad \frac{u_\infty}{2} \cdot \int_0^c \Delta c_p(x) \; d\, x \tag{3.32}$$

The singularity strength in the transformed coordinate system (x',y',z') may be written as :

$$\sigma' \quad = \quad \frac{u'_\infty}{2} \cdot \int_0^{c'} \Delta c'_p(x')\, d\, x' \tag{3.33}$$

The streamwise coordinate x and chord c are transformed by using Eq. (3.1a) :

$$d\, x' \quad = \quad d\, x \qquad \Longrightarrow \qquad c' \quad = \quad c \tag{3.34a}$$

The transformed pressure coefficient difference may be written as a function of the original pressure coefficient difference. Assuming small perturbations, we know for the pressure coefficient in the original coordinate system :

$$c_p(x) \quad = \quad \frac{-2}{u_\infty} \cdot \frac{\partial\, \phi}{\partial\, x} \tag{3.34b}$$

Similarly, we know for the pressure coefficient in the transformed coordinate system :

$$c'_p(x') \quad = \quad \frac{-2}{u'_\infty} \cdot \frac{\partial\, \phi'}{\partial\, x'} \tag{3.34c}$$

Using Eq. (3.1a), (3.1d), (3.1e) and applying the chain rule to Eq. (3.34c), we get :

$$c'_p(x') \quad = \quad \frac{-2}{u_\infty} \cdot \frac{\partial\, x}{\partial\, x'} \cdot \frac{\partial\, (\, \phi \cdot \beta^2\,)}{\partial\, x} \quad = \quad \left[\frac{-2}{u_\infty} \cdot \frac{\partial\, \phi}{\partial\, x} \right] \cdot \beta^2 \tag{3.34d}$$

Combining Eqs. (3.34b) and (3.34d), we get :

$$c'_p(x') \quad = \quad c_p(x) \cdot \beta^2 \tag{3.34e}$$

Equation (3.34e) agrees with Eq. (4–22) from Ref. [4]. Thus, we may write the pressure coefficient difference in the transformed coordinate system as :

$$\Delta c'_p(x') \quad = \quad \Delta c_p(x) \cdot \beta^2 \tag{3.34f}$$

Combining Eqs. (3.1d), (3.33), (3.34a), and (3.34f), we get :

$$\sigma' \quad = \quad \left[\frac{u_\infty}{2} \cdot \int_0^{c} \Delta c_p(x)\, d\, x \right] \cdot \beta^2 \tag{3.35}$$

Finally, combining Eqs. (3.32), (3.35), we get :

$$\sigma' = \sigma \cdot \beta^2 \qquad (3.36a)$$

where σ' is the transformed strength and σ is the original strength of a two–dimensional vortex. Thus, for a two–dimensional vortex, the transformation function $F(\beta)$ as defined in Eq. (3.1g) is given as :

$$\boxed{F(\beta) = \beta^2 \qquad (3.36b)}$$

It is possible to verify the singularity strength transformation given in Eq. (3.36b). Therefore, a Method of Images solution for the upwash velocity caused by a 2D vortex at a high subsonic Mach number was constructed using derivatives of the singularity potential in combination with Eqs. (3.36a), (12a), (12c), and (23c). This solution for the upwash velocity showed good agreement with a classical solution given by Eq. (2.13) in Ref. [2].

Three–Dimensional Line Doublet

A three–dimensional line doublet may be used to represent lifting effects of a wing in a three–dimensional flow field. The strength σ of a three–dimensional line doublet is defined as lift force divided by density and free–stream velocity :

$$\boxed{\sigma = \frac{L}{\rho_\infty \cdot u_\infty} = \Gamma \cdot \Delta s \qquad (3.37)}$$

where u_∞ is the free–stream velocity, ρ_∞ is the density, Γ is the circulation, and Δs is the span of a wing span element. The lift force L, may also be written by using the lift coefficient definition. Then, we get :

$$L = \frac{\rho_\infty}{2} \cdot u_\infty^2 \cdot c_L \cdot c \cdot \Delta s \qquad (3.38)$$

where c is the chord of the airfoil. Combining Eqs. (3.37), (3.38) we get :

$$\sigma = \frac{u_\infty}{2} \cdot c_L \cdot c \cdot \Delta s \qquad (3.39a)$$

The lift coefficient may be expressed as a function of the pressure coefficient difference on the surface of the wing span element. Using Eq. (3–54a) from Ref. [4], we get :

$$c_L = \frac{1}{c \cdot \Delta s} \cdot \int_0^c \int_{-\Delta s/2}^{\Delta s/2} \Delta c_p(x,y)\; d\,x\; d\,y \qquad (3.39b)$$

Combining Eq. (3.39a) and (3.39b), we get for the line doublet strength in the original coordinate system (x,y,z) :

$$\sigma = \frac{u_\infty}{2} \cdot \int_0^c \int_{-\Delta s/2}^{\Delta s/2} \Delta c_p(x,y)\; d\,x\; d\,y \qquad (3.40)$$

The singularity strength in the transformed coordinate system (x',y',z') may be written as :

$$\sigma' = \frac{u'_\infty}{2} \cdot \int_0^{c'} \int_{-\Delta s'/2}^{\Delta s'/2} \Delta c'_p(x',y')\; d\,x'\; d\,y' \qquad (3.41)$$

The y coordinate and wing span Δs are transformed by using Eq. (3.1b). Then, we get :

$$d\,y' = d\,y \cdot \beta \quad \Longrightarrow \quad \Delta s' = \Delta s \cdot \beta \qquad (3.42)$$

Combining Eqs. (3.1d), (3.34a), (3.34f), (3.41), and (3.42), we get :

$$\sigma' = \left[\frac{u_\infty}{2} \cdot \int_0^c \int_{-\Delta s/2}^{\Delta s/2} \Delta c_p(x,y)\; d\,x\; d\,y \right] \cdot \beta^3 \qquad (3.43)$$

Finally, combining Eqs. (3.40), (3.43), we get :

$$\sigma' = \sigma \cdot \beta^3 \qquad (3.44a)$$

where σ' is the transformed strength and σ is the original strength of a three–dimensional line doublet as defined in Eq. (3.37). Thus, for a three–dimensional line doublet strength as defined in Eq. (3.37), the transformation function $F(\beta)$ as defined in Eq. (3.1g) is given as :

$$\boxed{F(\beta) = \beta^3 \qquad (3.44b)}$$

It is possible to verify the singularity strength transformation given in Eq. (3.44b). Therefore, a Method of Images solution for the upwash velocity caused by a 3D line doublet at a high subsonic Mach number was constructed using derivatives of the singularity potential in combination with Eqs. (3.44a), (12a), (12b), (12c), and (23c). This solution for the upwash velocity showed good agreement with a classical solution given by Eq. (2.30) in Ref. [2].

Summary

Singularities like point sources, point doublets, vortices, and line doublets may be used to compute wind tunnel wall interference effects. These singularities represent blockage and lifting effects of a wind tunnel model. Their location and strength is closely related to the geometry of the test article. Therefore, it is necessary to apply the Prandtl–Glauert transformation to the singularity strength as well, if wall interference effects are computed in a subsonic flow field. The table below summarizes the particular form of the Prandtl–Glauert transformation for each singularity type that is discussed in this section.

Table 7 : Singularity Strength Transformation ($\sigma' = \sigma \cdot F(\beta)$)

Singularity Type	Singularity Strength (σ)	$F(\beta)$
Point Source (2D)	$u_\infty \cdot D$	β
Point Doublet (2D)	$u_\infty \cdot 2 \cdot \pi \cdot r_c^2$	β
Point Source (3D)	$u_\infty \cdot \pi \cdot r_\infty^2$	β^2
Point Doublet (3D)	$u_\infty \cdot 2 \cdot \pi \cdot r_\circ^3$	β^2
Vortex (2D)	$L \;/\; (\rho_\infty \cdot u_\infty \cdot \Delta s) = \Gamma$	β^2
Line Doublet (3D)	$L \;/\; (\rho_\infty \cdot u_\infty) = \Gamma \cdot \Delta s$	β^3

Important Remark : Previously, the derivation of the singularity strength transformation for a three–dimensional line doublet was performed erroneously by the author (Eq. (22) in Ref. [1] is not valid for a line doublet). The correct singularity strength transformation for a line doublet is now given in Eq. (3.44a). The author added a corresponding errata page to Ref. [1].

APPENDIX 4

METHOD OF IMAGES – POINT DOUBLET

The Method of Images may be applied to compute the wind tunnel and wall interference flow field caused by a point doublet that is located inside of a rectangular wind tunnel with "closed wall" or "open jet" boundary conditions. Figure 16a shows the image system for the "closed wall" boundary condition. All unit point doublet strength values have the same sign in this case. Figure 16b shows the image system for the "open jet" boundary condition. Point doublet strength sign changes are indicated in Fig. 16b.

It is assumed that a point doublet points in the negative x–direction and is located at x_o,y_o,z_o inside of a rectangular tunnel of width h_1 and height h_2 (see Fig. 16a). Then, we get for the velocity components $u = \partial\phi/\partial x$, $v = \partial\phi/\partial y$, $w = \partial\phi/\partial z$ of the wind tunnel flow field at a flow field point x,y,z :

$$u(x,y,z) = \sum_{m=-\infty}^{\infty} \sum_{n=-\infty}^{\infty} U(m,n) \cdot F(m,n) \tag{4.1a}$$

$$v(x,y,z) = \sum_{m=-\infty}^{\infty} \sum_{n=-\infty}^{\infty} V(m,n) \cdot F(m,n) \tag{4.1b}$$

$$w(x,y,z) = \sum_{m=-\infty}^{\infty} \sum_{n=-\infty}^{\infty} W(m,n) \cdot F(m,n) \tag{4.1c}$$

where

$$U(m,n) = \frac{\sigma}{4\,\pi} \cdot \frac{(Y(m)-y_o)^2 + (Z(n)-z_o)^2 - 2\cdot(x-x_o)^2}{\left[\,(x-x_o)^2 + (Y(m)-y_o)^2 + (Z(n)-z_o)^2\,\right]^{5/2}} \tag{4.2a}$$

$$V(m,n) = \frac{(-3)\cdot\sigma}{4\cdot\pi} \cdot \frac{(x-x_o)\cdot(Y(m)-y_o)}{\left[\,(x-x_o)^2 + (Y(m)-y_o)^2 + (Z(n)-z_o)^2\,\right]^{5/2}} \tag{4.2b}$$

$$W(m,n) = \frac{(-3)\cdot\sigma}{4\cdot\pi} \cdot \frac{(x-x_o)\cdot(Z(n)-z_o)}{\left[\,(x-x_o)^2 + (Y(m)-y_o)^2 + (Z(n)-z_o)^2\,\right]^{5/2}} \tag{4.2c}$$

$$F(m,n) = \begin{cases} 1 & ; \ \textit{closed wall} \\ (-1)^{m+n} & ; \ \textit{open jet} \end{cases} \tag{4.2d}$$

and

$$Y(m) \;=\; y \;+\; m \cdot h_1 \;+\; [\,1 \;-\; (-1)^m\,] \cdot y_o \tag{4.3a}$$

$$Z(n) \;=\; z \;+\; n \cdot h_2 \;+\; [\,1 \;-\; (-1)^n\,] \cdot z_o \tag{4.3b}$$

The velocity components $u_w = \partial\phi_w/\partial x$, $v_w = \partial\phi_w/\partial y$, $w_w = \partial\phi_w/\partial z$ of the wall interference flow field at a flow field point x,y,z may be obtained by only considering summation terms in Eqs. (4.1a), (4.1b), (4.1c) that are caused by image point doublets. Then, we get :

$$u_w(x,y,z) \;=\; \sum_{\substack{m=-\infty \\ (m,n)\neq(0,0)}}^{\infty} \sum_{n=-\infty}^{\infty} U(m,n) \cdot F(m,n) \tag{4.4a}$$

$$v_w(x,y,z) \;=\; \sum_{\substack{m=-\infty \\ (m,n)\neq(0,0)}}^{\infty} \sum_{n=-\infty}^{\infty} V(m,n) \cdot F(m,n) \tag{4.4b}$$

$$w_w(x,y,z) \;=\; \sum_{\substack{m=-\infty \\ (m,n)\neq(0,0)}}^{\infty} \sum_{n=-\infty}^{\infty} W(m,n) \cdot F(m,n) \tag{4.4c}$$

Perturbation velocity components $U(m,n)$, $V(m,n)$, $W(m,n)$, are given by Eqs. (4.2a), (4.2b), and (4.2c) . Factor $F(m,n)$ is given by Eq. (4.2d) .

Numerical studies have shown that summation terms in Eqs. (4.1a), (4.1b), (4.1c), (4.4a), (4.4b), and (4.4c) should be computed using "DOUBLE PRECISION" arithmetic ("-r8" compiler flag). A summation index range of $-200 \leq m \leq 200$ and $-200 \leq n \leq 200$ is recommended.

APPENDIX 5

METHOD OF IMAGES – LINE DOUBLET

The Method of Images may be applied to compute the wind tunnel and wall interference flow field caused by a semi–infinite line doublet that is located inside of a rectangular wind tunnel with "closed wall" boundary condition. The Method of Images adds perturbation velocity components of each line doublet of the image system to obtain a wind tunnel and wall interference flow field solution (see Fig. 17a). Unfortunately, perturbation velocity components of a line doublet are a function of the line doublet orientation angle Θ. This angle is defined as 0 $[rad]$ if the lift force caused by the line doublet points in the positive z–axis direction of the tunnel coordinate system x, y, z (see Fig. 17a). A coordinate system transformation may be used to simplify the application of the Method of Images to a line doublet (for more detail see App. 2) . This transformation is essentially a coordinate system rotation that uses line doublet orientation angle Θ.

It is assumed that a semi–infinite line doublet with starting point $x_\circ$,$y_\circ$,$z_\circ$ and orientation angle Θ is located inside of a rectangular wind tunnel of width h_1 and height h_2 (see Fig. 17a). Then, based on the Method of Images and Eqs. (2.10a), (2.10b), (2.10c) in App. 2, we get for velocity components $u = \partial\phi/\partial x$, $v = \partial\phi/\partial y$, $w = \partial\phi/\partial z$ of the wind tunnel flow field at a flow field point x,y,z :

$$u(x,y,z) \;=\; \sum_{m=-\infty}^{\infty} \sum_{n=-\infty}^{\infty} U(m,n) \tag{5.1a}$$

$$v(x,y,z) \;=\; \sum_{m=-\infty}^{\infty} \sum_{n=-\infty}^{\infty} \Big[\; V(m,n)\cdot cos[\tau(m,n)] \;+\; W(m,n)\cdot sin[\tau(m,n)] \;\Big] \tag{5.1b}$$

$$w(x,y,z) \;=\; \sum_{m=-\infty}^{\infty} \sum_{n=-\infty}^{\infty} \Big[\; -V(m,n)\cdot sin[\tau(m,n)] \;+\; W(m,n)\cdot cos[\tau(m,n)] \;\Big] \tag{5.1c}$$

where velocity components $U(m,n)$, $V(m,n)$, and $W(m,n)$ are computed in the line doublet fixed coordinate system ξ, η, ζ of each line doublet of the image system. Using Eqs. (2.4), (2.5a), (2.5b), (2.5c), (2.6a), (2.6b), (2.6c), from App. 2, line doublet velocity components may be written as :

$$U(m,n) \;=\; \frac{\sigma}{4\,\pi} \cdot \frac{\zeta - \zeta_\circ}{\Big[\; (\xi-\xi_\circ)^2 + (\eta-\eta_\circ)^2 + (\zeta-\zeta_\circ)^2 \;\Big]^{3/2}} \tag{5.2}$$

$$V(m,n) = \frac{-\sigma}{4\pi} \cdot \frac{(\eta-\eta_o)\cdot(\zeta-\zeta_o)}{(\eta-\eta_o)^2+(\zeta-\zeta_o)^2} \cdot \left[\frac{2\cdot B}{(\eta-\eta_o)^2+(\zeta-\zeta_o)^2} + C \right] \quad (5.3a)$$

where

$$B = 1 + \frac{\xi-\xi_o}{\left[(\xi-\xi_o)^2+(\eta-\eta_o)^2+(\zeta-\zeta_o)^2 \right]^{1/2}} \quad (5.3b)$$

$$C = \frac{\xi-\xi_o}{\left[(\xi-\xi_o)^2+(\eta-\eta_o)^2+(\zeta-\zeta_o)^2 \right]^{3/2}} \quad (5.3c)$$

$$W(m,n) = \frac{\sigma}{4\pi} \cdot \frac{1}{(\eta-\eta_o)^2+(\zeta-\zeta_o)^2} \cdot \left[\frac{(\eta-\eta_o)^2-(\zeta-\zeta_o)^2}{(\eta-\eta_o)^2+(\zeta-\zeta_o)^2} \cdot D + E \right] \quad (5.4a)$$

where

$$D = 1 + \frac{\xi-\xi_o}{\left[(\xi-\xi_o)^2+(\eta-\eta_o)^2+(\zeta-\zeta_o)^2 \right]^{1/2}} \quad (5.4b)$$

$$E = \frac{(-1)\cdot(\xi-\xi_o)\cdot(\zeta-\zeta_o)^2}{\left[(\xi-\xi_o)^2+(\eta-\eta_o)^2+(\zeta-\zeta_o)^2 \right]^{3/2}} \quad (5.4c)$$

The coordinates of the flow field point x, y, z in the tunnel coordinate system are transformed to the line doublet fixed coordinate system ξ, η, ζ using the following equations (see also Eqs. (2.1a), (2.1b), (2.1c)) :

$$\xi = x \quad (5.5a)$$

$$\eta = \eta(m,n) = Y(m)\cdot\cos[\tau(m,n)] - Z(n)\cdot\sin[\tau(m,n)] \quad (5.5b)$$

$$\zeta = \zeta(m,n) = Y(m)\cdot\sin[\tau(m,n)] + Z(n)\cdot\cos[\tau(m,n)] \quad (5.5c)$$

The Y and Z coordinate of a flow field point have to be computed using the following equations :

$$Y(m) = y + m\cdot h_1 + [\,1 - (-1)^m\,]\cdot y_o \quad (5.6a)$$

$$Z(n) = z + n\cdot h_2 + [\,1 - (-1)^n\,]\cdot z_o \quad (5.6b)$$

Similarly, coordinates of the line doublet starting point x_o, y_o, z_o are transformed to the line doublet fixed coordinate system ξ, η, ζ using the following equations (see also Eqs. (2.2a), (2.2b), (2.2c)) :

$$\xi_o = x_o \quad (5.7a)$$

$$\eta_o(m,n) \;=\; y_o \cdot \cos[\tau(m,n)] \;-\; z_o \cdot \sin[\tau(m,n)] \qquad (5.7b)$$

$$\zeta_o(m,n) \;=\; y_o \cdot \sin[\tau(m,n)] \;+\; z_o \cdot \cos[\tau(m,n)] \qquad (5.7c)$$

The line doublet orientation angle of each line doublet of the image system is a function of line doublet orientation angle Θ and image system indices (m,n). By inspection (Fig. 17a), we see that the line doublet orientation angle of each image system element for the "closed wall" boundary condition is given as :

$$\tau(m,n) \;=\; (-1)^m \cdot [\,(-1)^n \cdot \Theta \;+\; n \cdot \pi\,] \quad ; \quad \textit{closed wall} \qquad (5.8)$$

where $\Theta = \tau(0,0)$ is the angle between the z–axis of the tunnel coordinate system x,y,z and the ζ–axis of the line doublet fixed coordinate system ξ,η,ζ .

The velocity components $u_w = \partial\phi_w/\partial x$, $v_w = \partial\phi_w/\partial y$, $w_w = \partial\phi_w/\partial z$ of the wall interference flow field at a flow field point x,y,z may be obtained by only considering velocity components in Eqs. (5.1a), (5.1b), (5.1c) that are caused by image line doublets. Then, we get :

$$u_w(x,y,z) \;=\; \sum_{\substack{m=-\infty \\ (m,n)\neq(0,0)}}^{\infty} \sum_{n=-\infty}^{\infty} U(m,n) \qquad (5.9a)$$

$$v_w(x,y,z) \;=\; \sum_{\substack{m=-\infty \\ (m,n)\neq(0,0)}}^{\infty} \sum_{n=-\infty}^{\infty} \Big[\, V(m,n)\cdot cos[\tau(m,n)] + W(m,n)\cdot sin[\tau(m,n)] \,\Big] \qquad (5.9b)$$

$$w_w(x,y,z) = \sum_{\substack{m=-\infty \\ (m,n)\neq(0,0)}}^{\infty} \sum_{n=-\infty}^{\infty} \Big[\, -V(m,n)\cdot sin[\tau(m,n)] + W(m,n)\cdot cos[\tau(m,n)] \,\Big] \qquad (5.9c)$$

Velocity components $U(m,n)$, $V(m,n)$, $W(m,n)$, and orientation angle $\tau(m,n)$ are computed using Eqs. (5.2), (5.3a), (5.3b), (5.3c), (5.4a), (5.4b), (5.4c), and (5.8) .

Numerical studies have shown that summation terms in Eqs. (5.1a), (5.1b), (5.1c), (5.9a), (5.9b), and (5.9c) should be computed using "DOUBLE PRECISION" arithmetic ("-r8" compiler flag). A summation index range of $-200 \le m \le 200$ and $-200 \le n \le 200$ is recommended.

The Method of Images may also be used to compute the wall interference flow field of a line doublet located in a rectangular "open jet" if the line doublet orientation angle Θ

is equal to 0, $\pi/2$, π, or $3\pi/2$. Figure 17b shows the image system of a rectangular "open jet" for $\Theta = 0$. The orientation angle of each image system element of the "open jet" becomes :

$$\tau(m,n) = \begin{cases} \Theta + m \cdot \pi & for \quad \Theta = 0 \quad or \quad \pi \\ \Theta + n \cdot \pi & for \quad \Theta = \pi/2 \quad or \quad 3\pi/2 \end{cases} \quad ; \quad open\ jet \qquad (5.10)$$

Thus, Eq. (5.8) has to be replaced by Eq. (5.10) if the interference flow field of a line doublet in an open jet for any of the four possible values of Θ is computed by using Eqs. (5.9a), (5.9b), and (5.9c) .

FIGURES

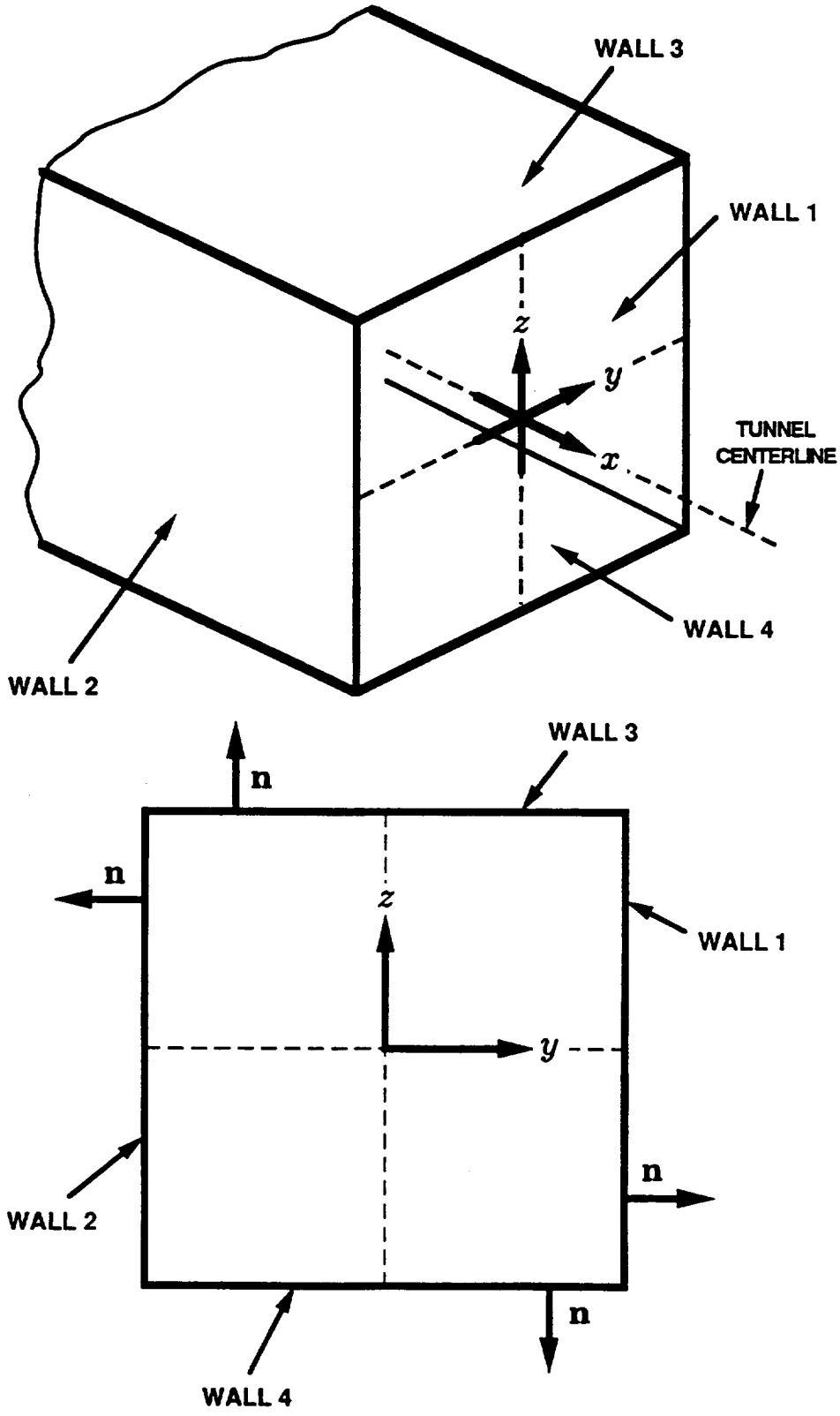

Fig. 1 Coordinate system definition of rectangular wind tunnel.

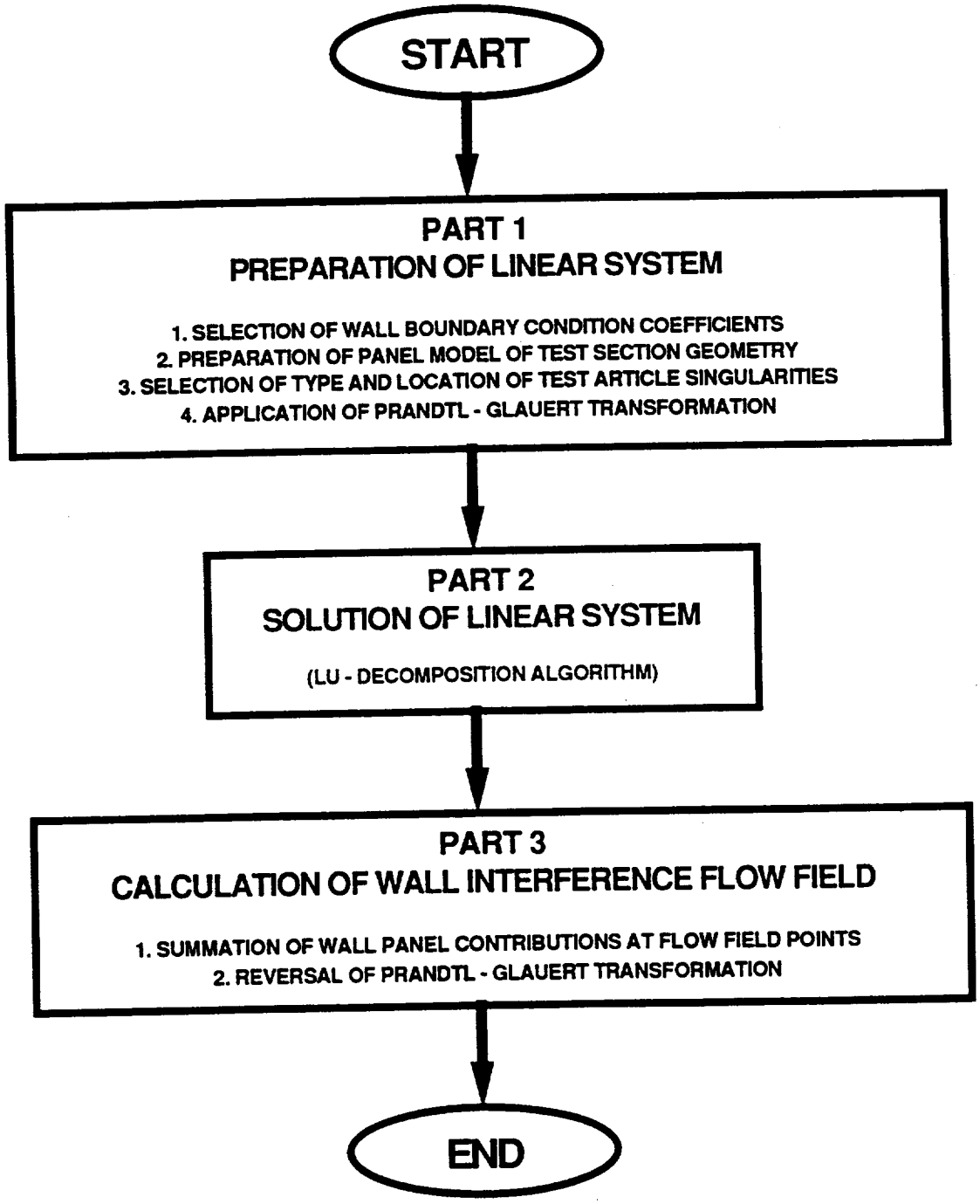

Fig. 2 Basic structure of panel method code ANTARES.

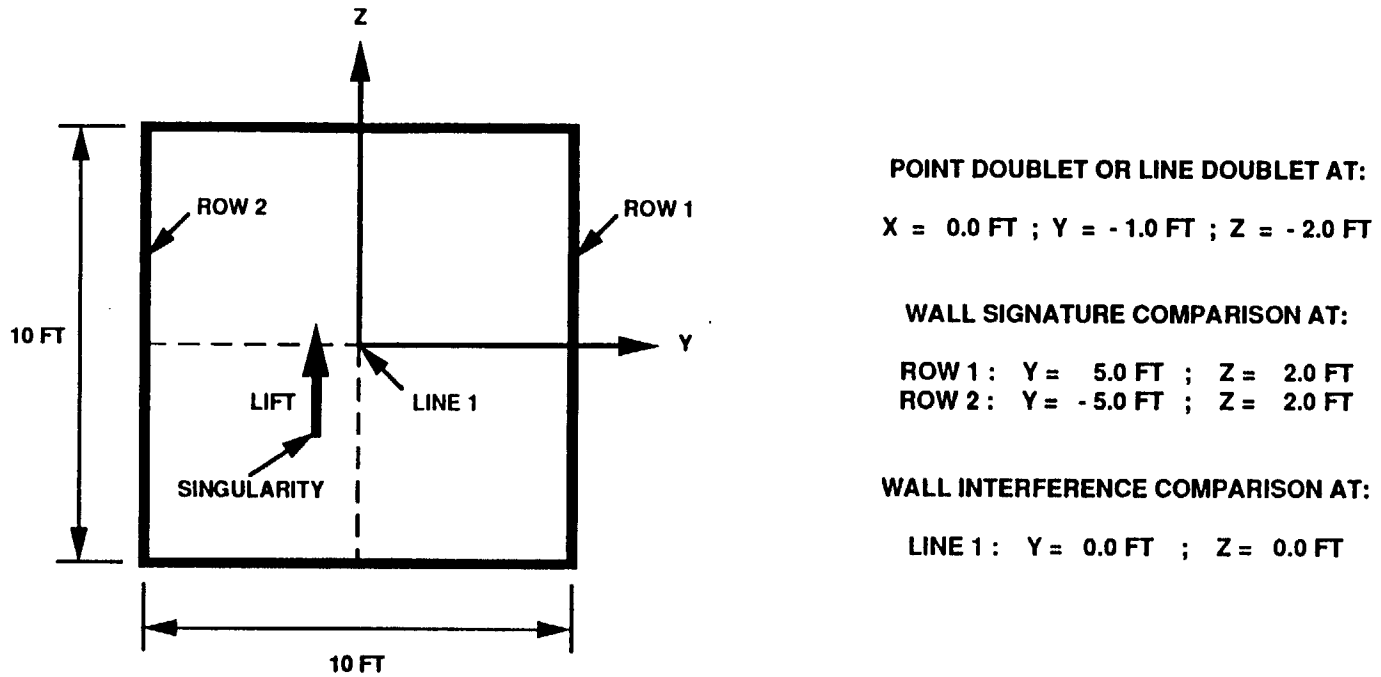

Fig. 3 Geometry of square wind tunnel and location of singularity.

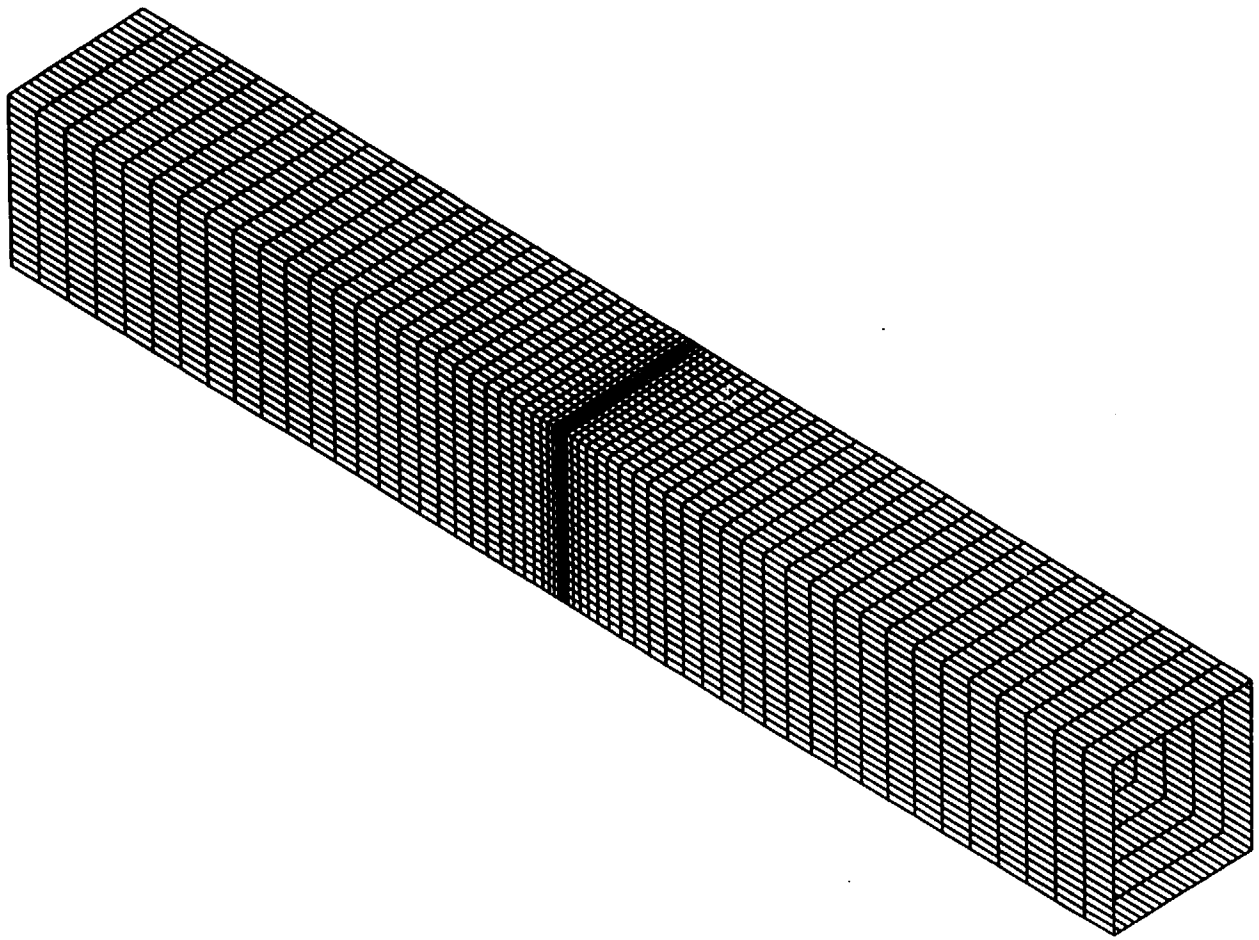

Fig. 4 Panel representation of square wind tunnel.

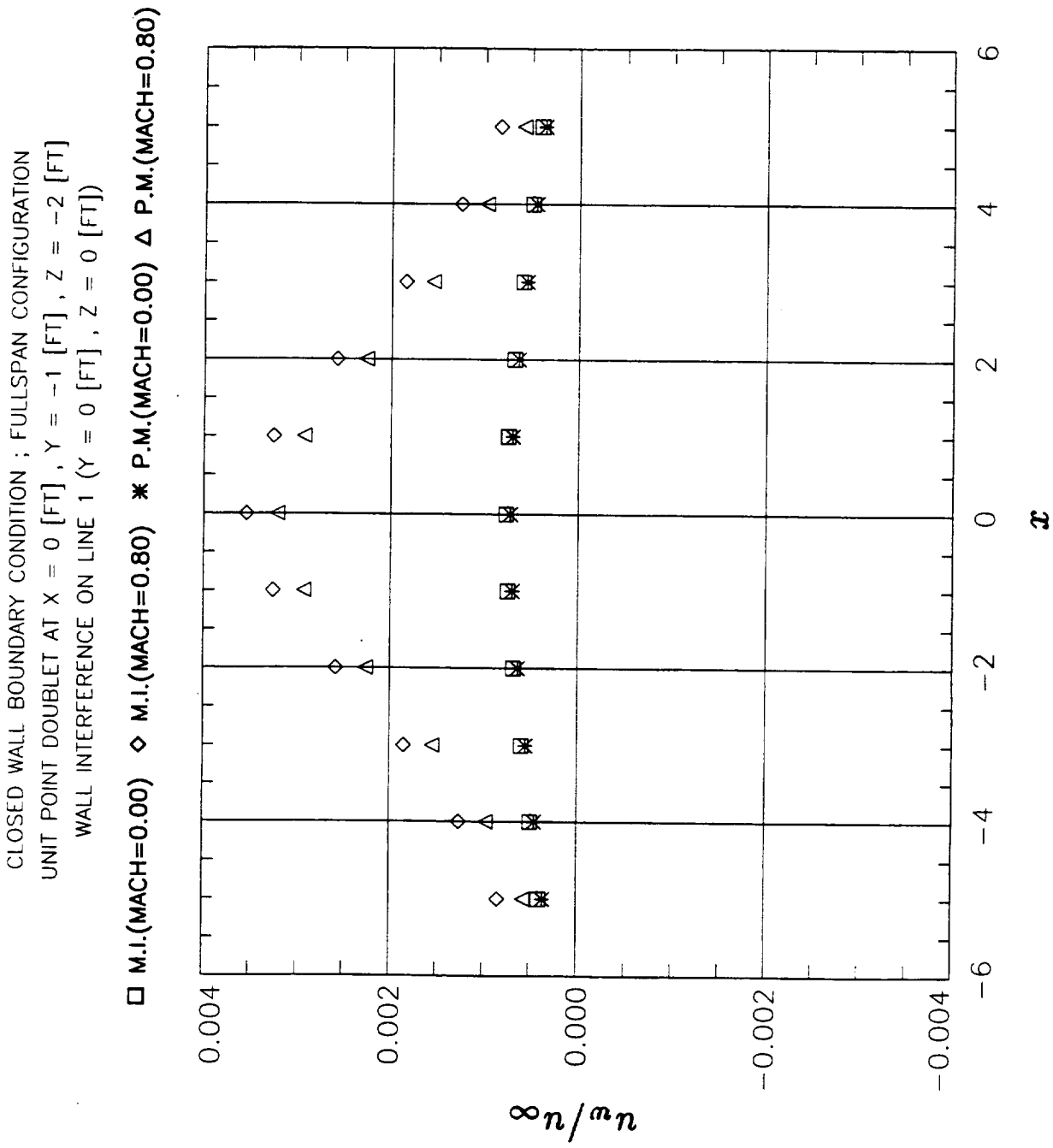

Fig. 5a Wall interference velocity component u_w/u_∞ due to unit point doublet in square tunnel; Method of Images (M.I.) versus panel method code (P.M.).

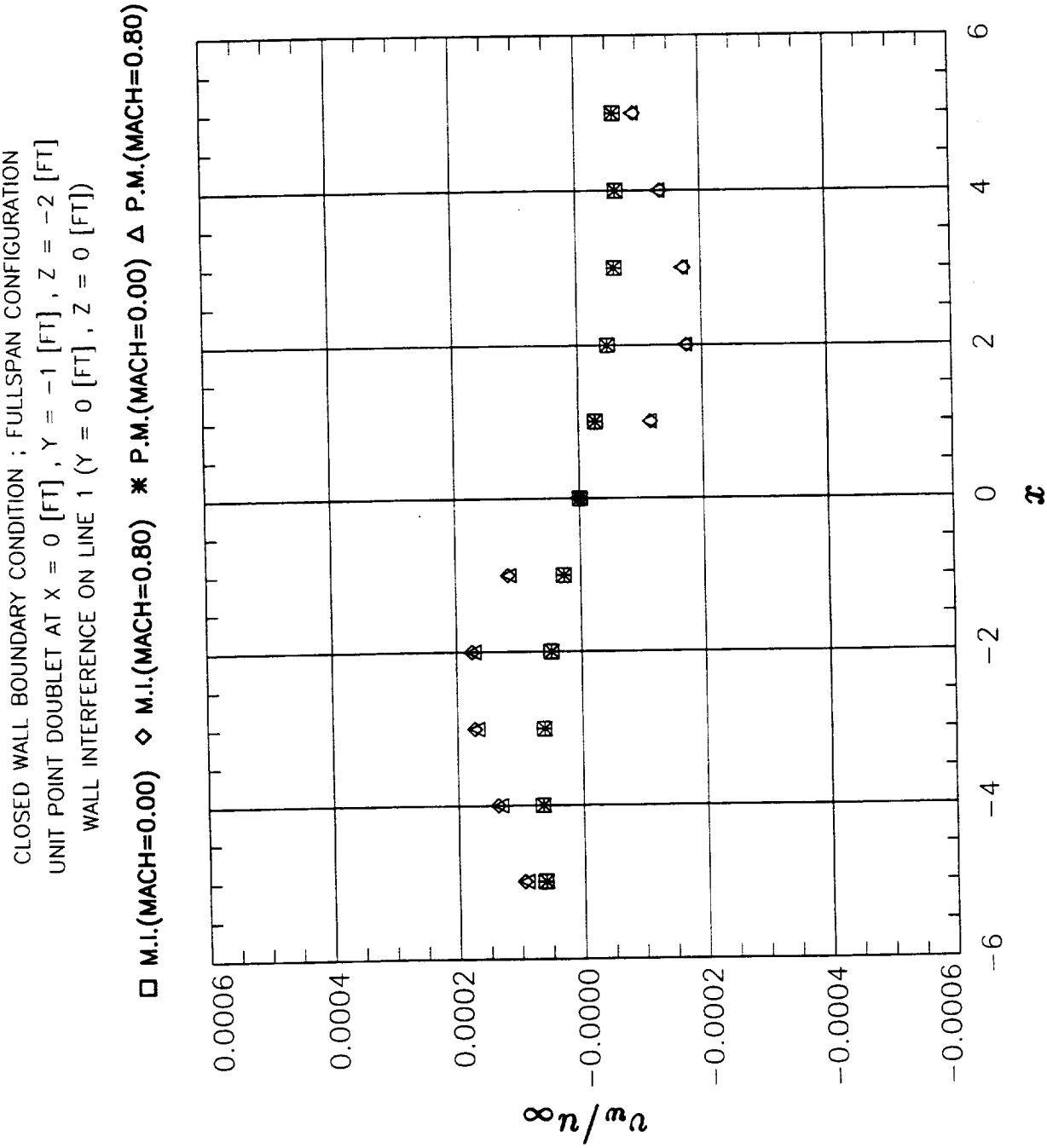

Fig. 5b Wall interference velocity component v_w/u_∞ due to unit point doublet in square tunnel; Method of Images (M.I.) versus panel method code (P.M.).

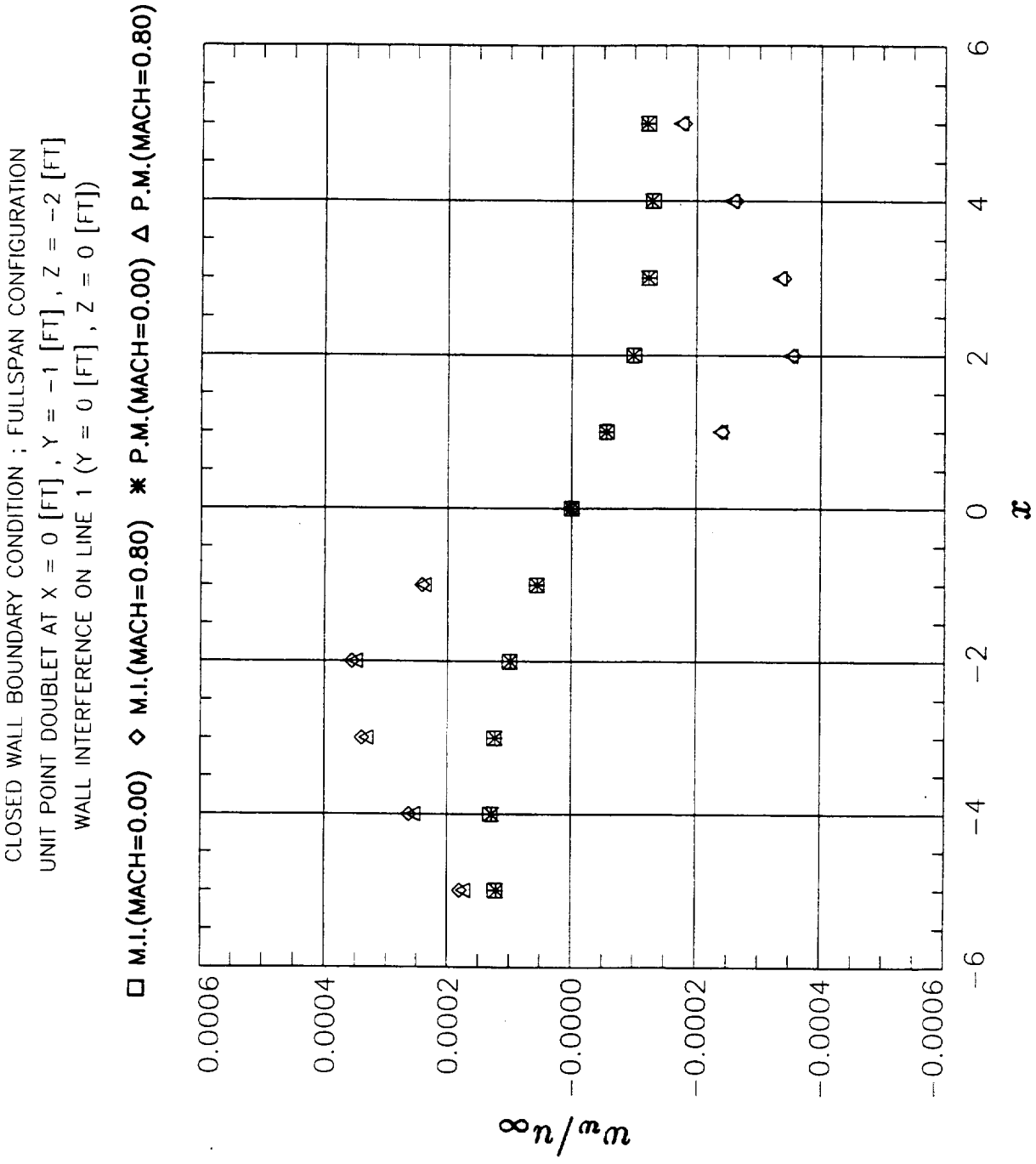

Fig. 5c Wall interference velocity component w_w/u_∞ due to unit point doublet in square tunnel; Method of Images (M.I.) versus panel method code (P.M.).

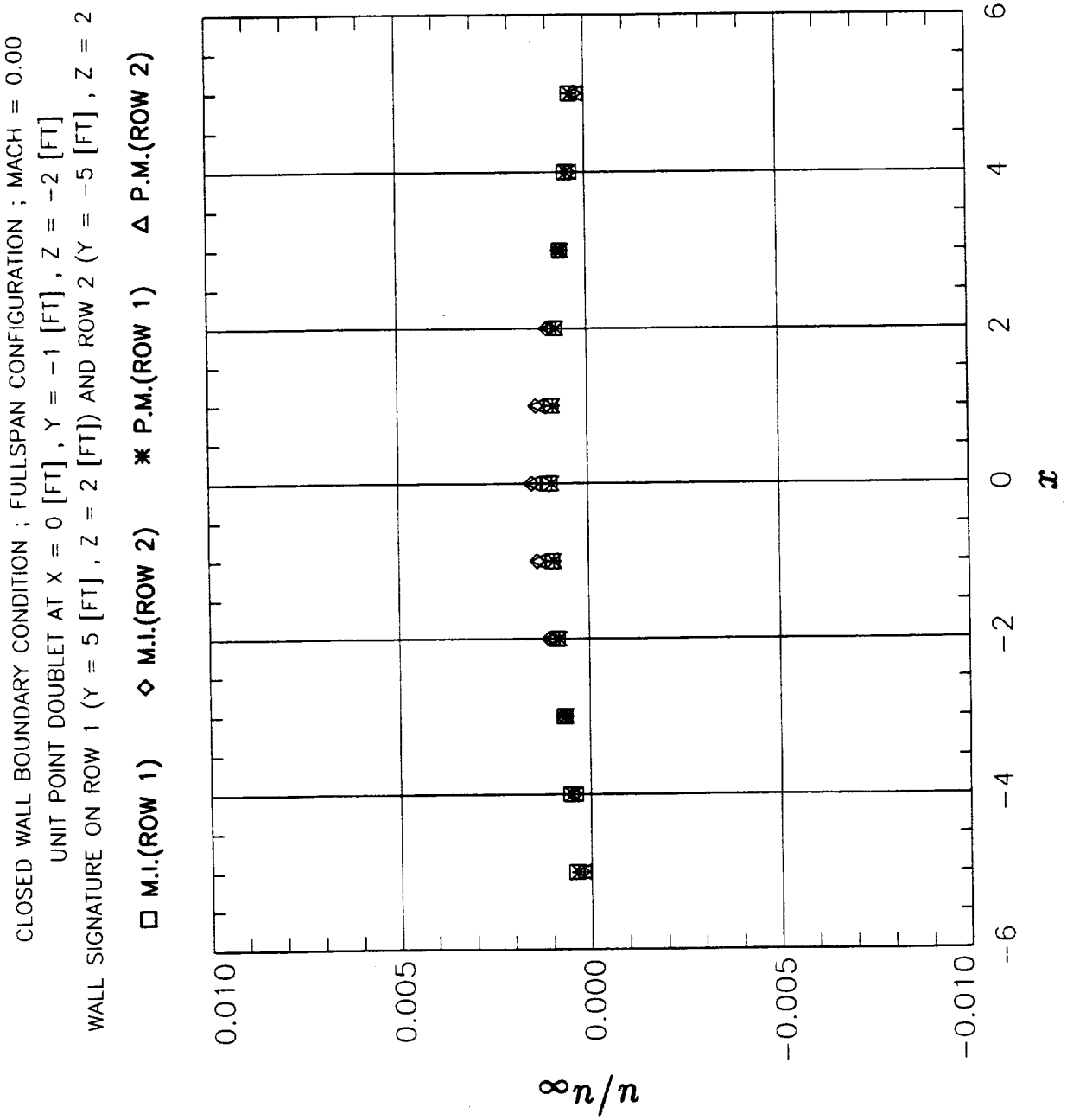

Fig. 5d Velocity component u/u_∞ ($M_\infty = 0.00$) due to unit point doublet in square tunnel; Method of Images (M.I.) versus panel method code (P.M.).

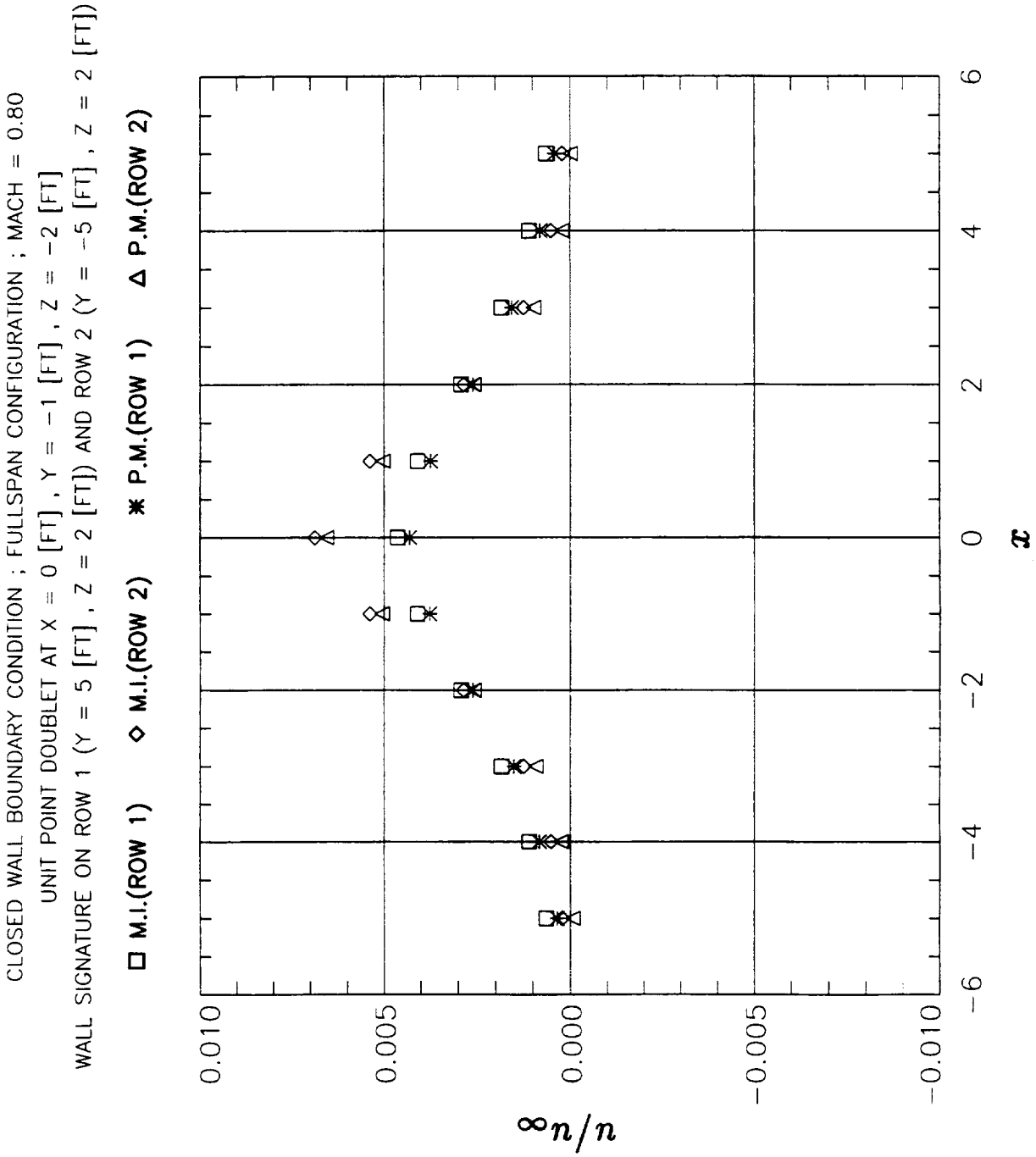

Fig. 5e Velocity component u/u_∞ ($M_\infty = 0.80$) due to unit point doublet in square tunnel; Method of Images (M.I.) versus panel method code (P.M.).

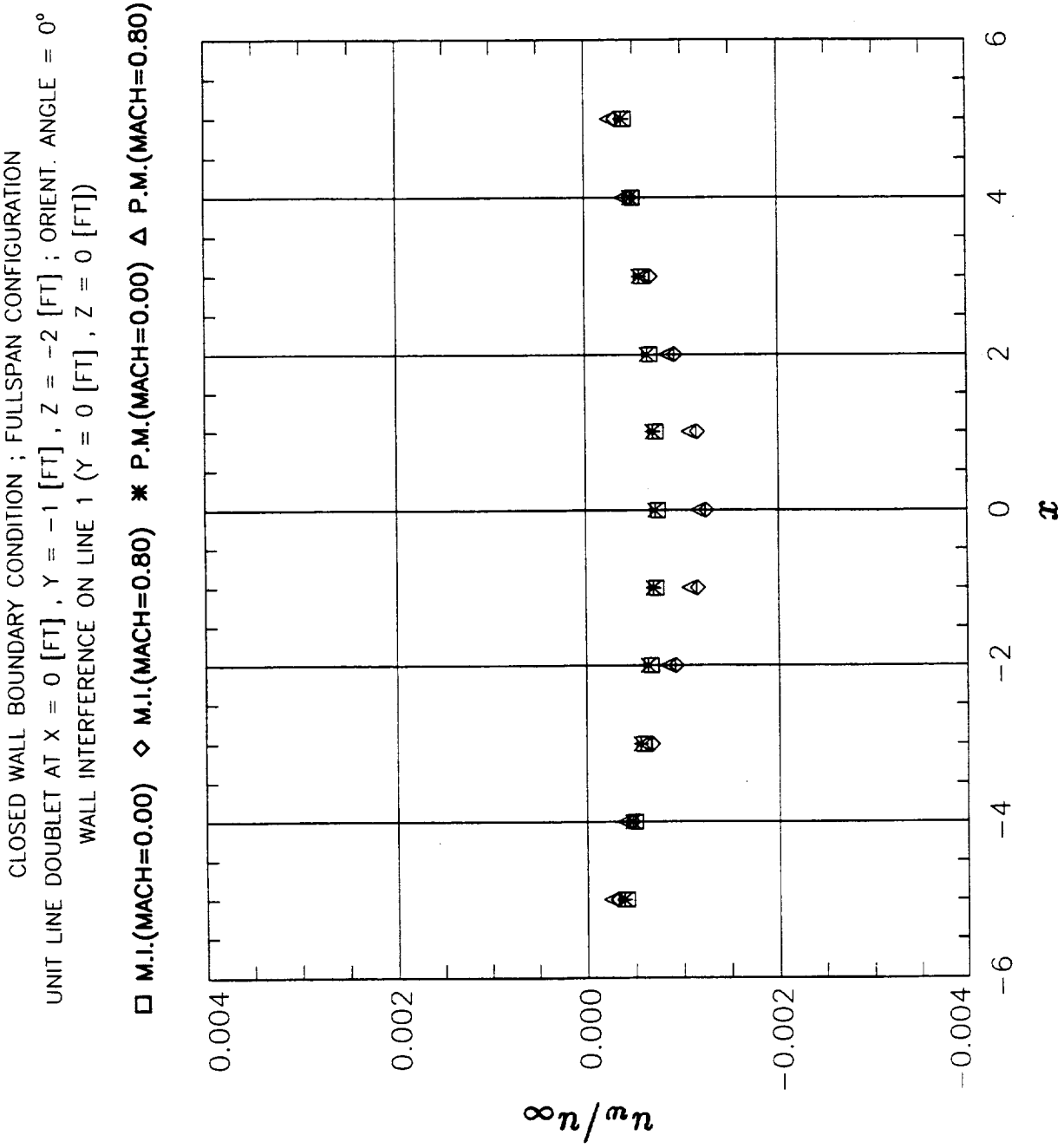

Fig. 6a Wall interference velocity component u_w/u_∞ due to unit line doublet in square tunnel; Method of Images (M.I.) versus panel method code (P.M.).

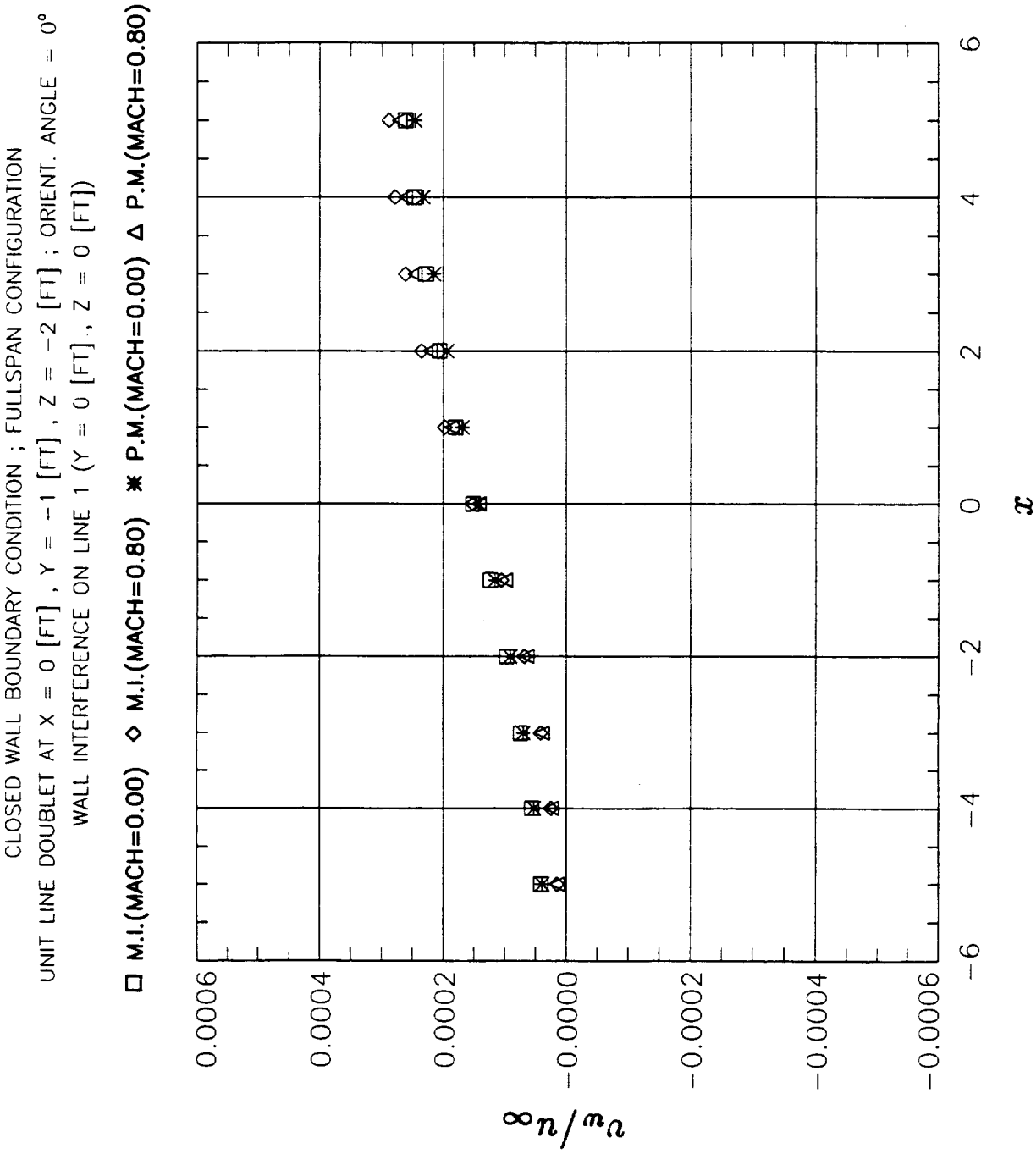

Fig. 6b Wall interference velocity component v_w/u_∞ due to unit line doublet in square tunnel; Method of Images (M.I.) versus panel method code (P.M.).

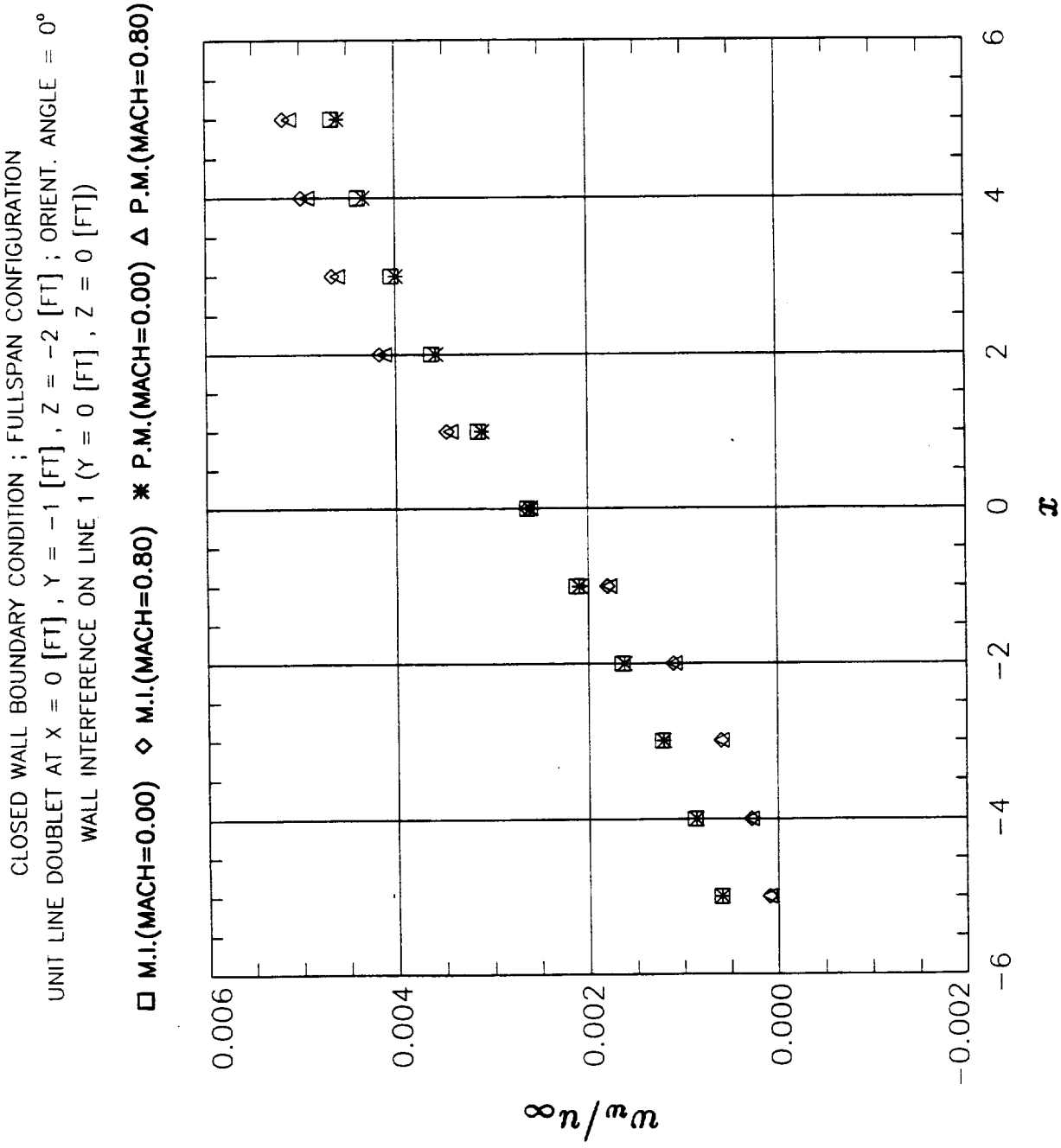

Fig. 6c Wall interference velocity component w_w/u_∞ due to unit line doublet in square tunnel; Method of Images (M.I.) versus panel method code (P.M.).

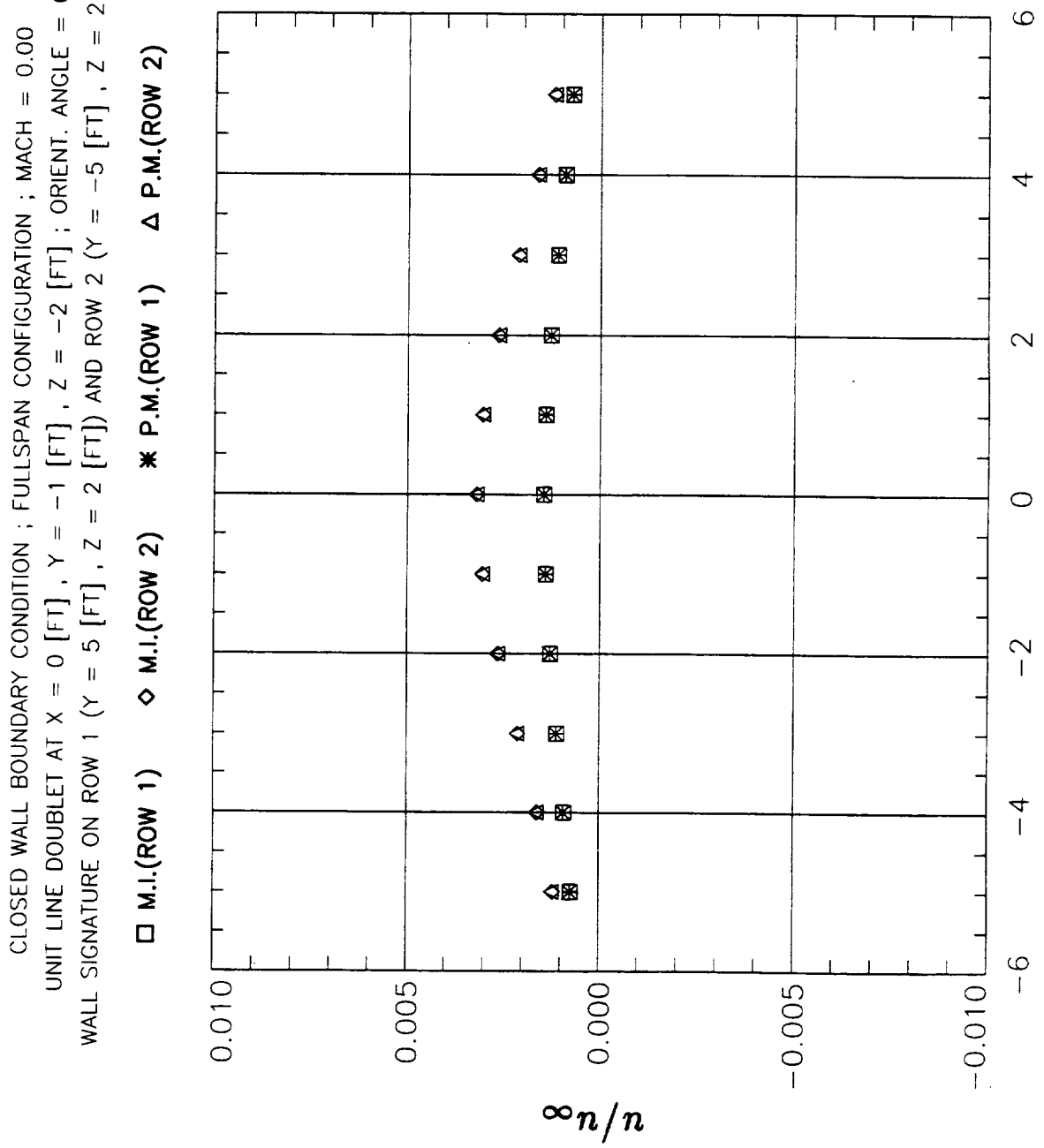

Fig. 6d Velocity component u/u_∞ ($M_\infty = 0.00$) due to unit line doublet in square tunnel; Method of Images (M.I.) versus panel method code (P.M.).

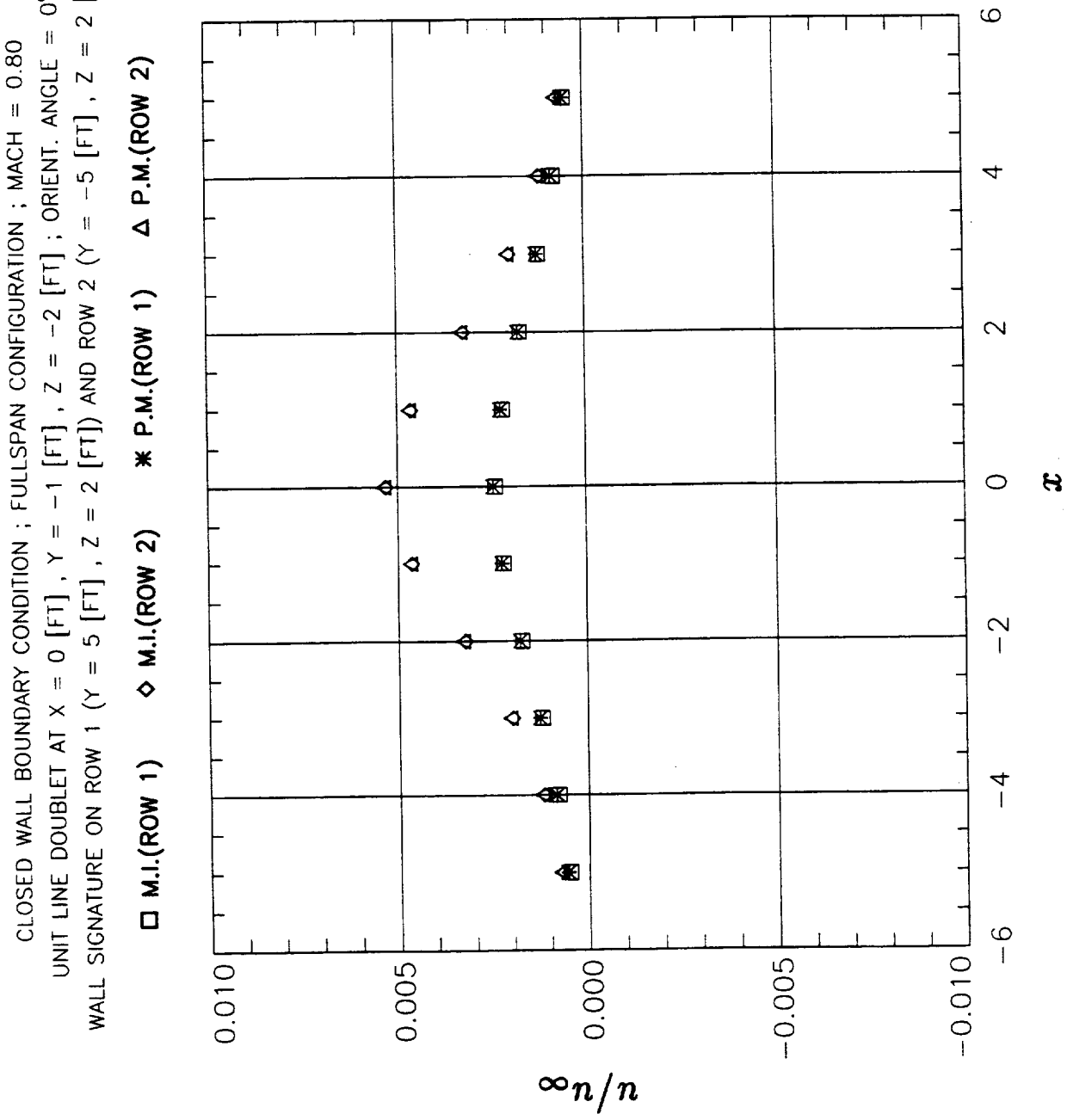

Fig. 6e Velocity component u/u_∞ ($M_\infty = 0.80$) due to unit line doublet in square tunnel; Method of Images (M.I.) versus panel method code (P.M.).

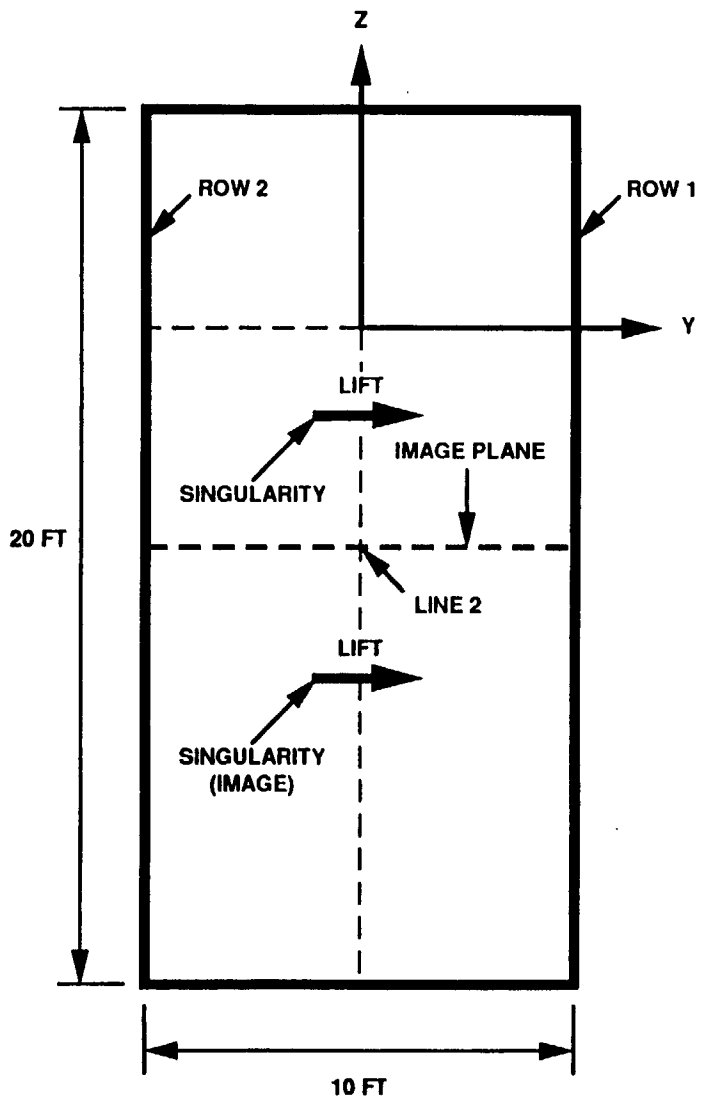

POINT DOUBLET OR LINE DOUBLET AT:

X = 0.0 FT ; Y = - 1.0 FT ; Z = - 2.0 FT
AND AT
X = 0.0 FT ; Y = - 1.0 FT ; Z = - 8.0 FT

WALL SIGNATURE COMPARISON AT:

ROW 1 : Y = 5.0 FT ; Z = 2.0 FT
ROW 2 : Y = - 5.0 FT ; Z = 2.0 FT

WALL INTERFERENCE COMPARISON AT:

LINE 2 : Y = 0.0 FT ; Z = - 5.0 FT

Fig. 7 Geometry of rectangular wind tunnel and location of singularities.

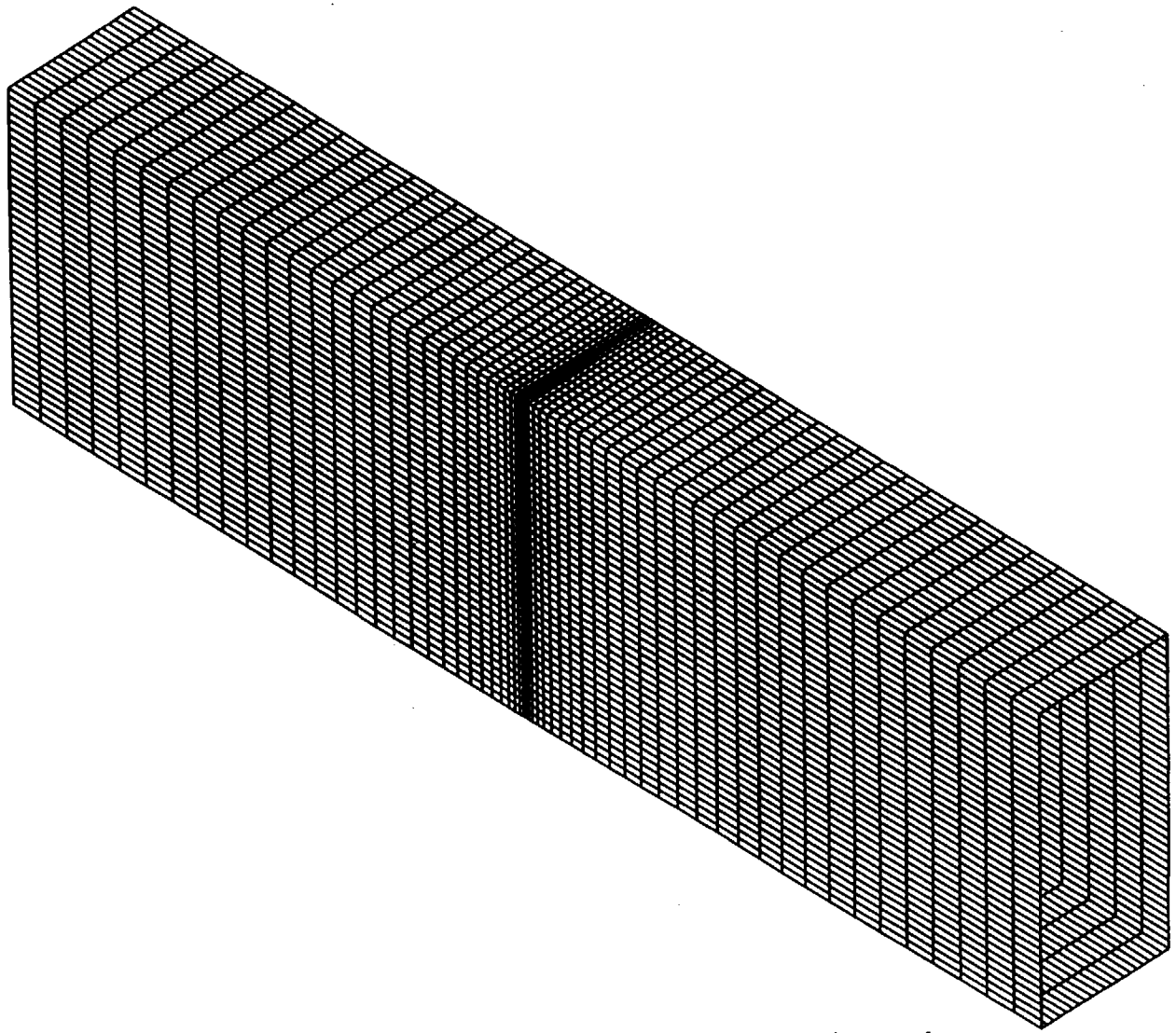

Fig. 8 Panel representation of rectangular wind tunnel.

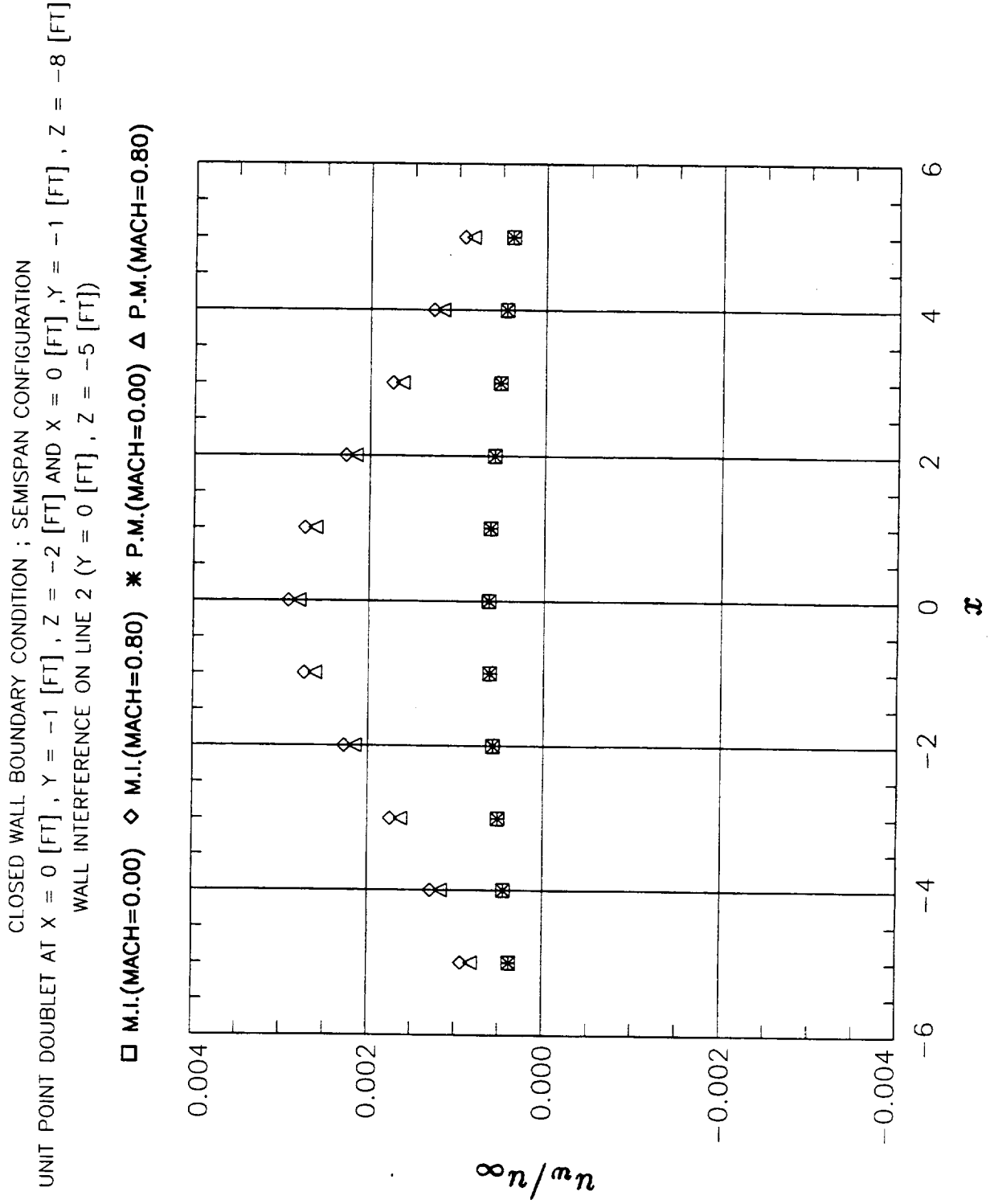

Fig. 9a Wall interference velocity component u_w/u_∞ due to two unit point doublets in rectangular tunnel; Method of Images (M.I.) versus panel method code (P.M.).

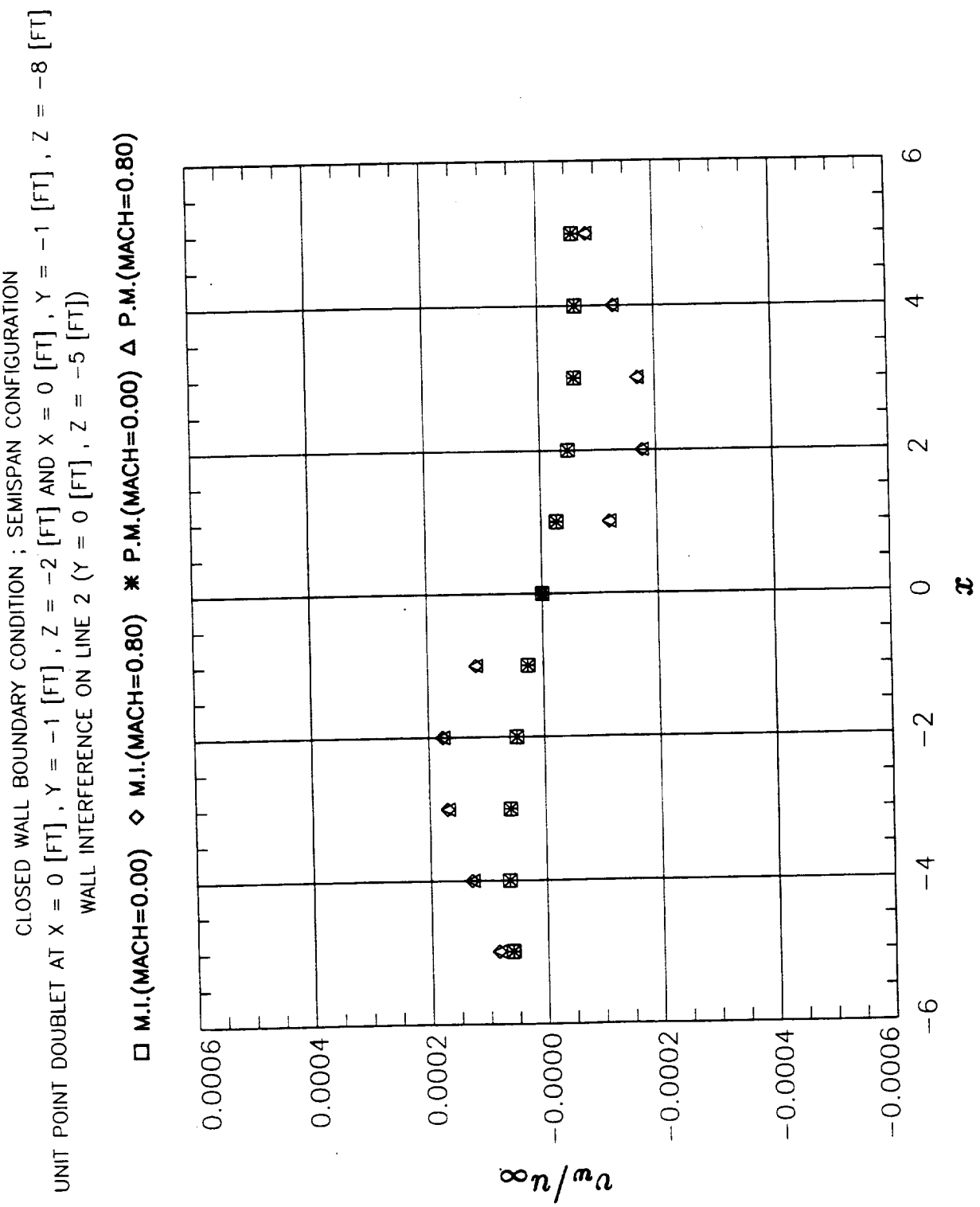

Fig. 9b Wall interference velocity component v_w/u_∞ due to two unit point doublets in rectangular tunnel; Method of Images (M.I.) versus panel method code (P.M.).

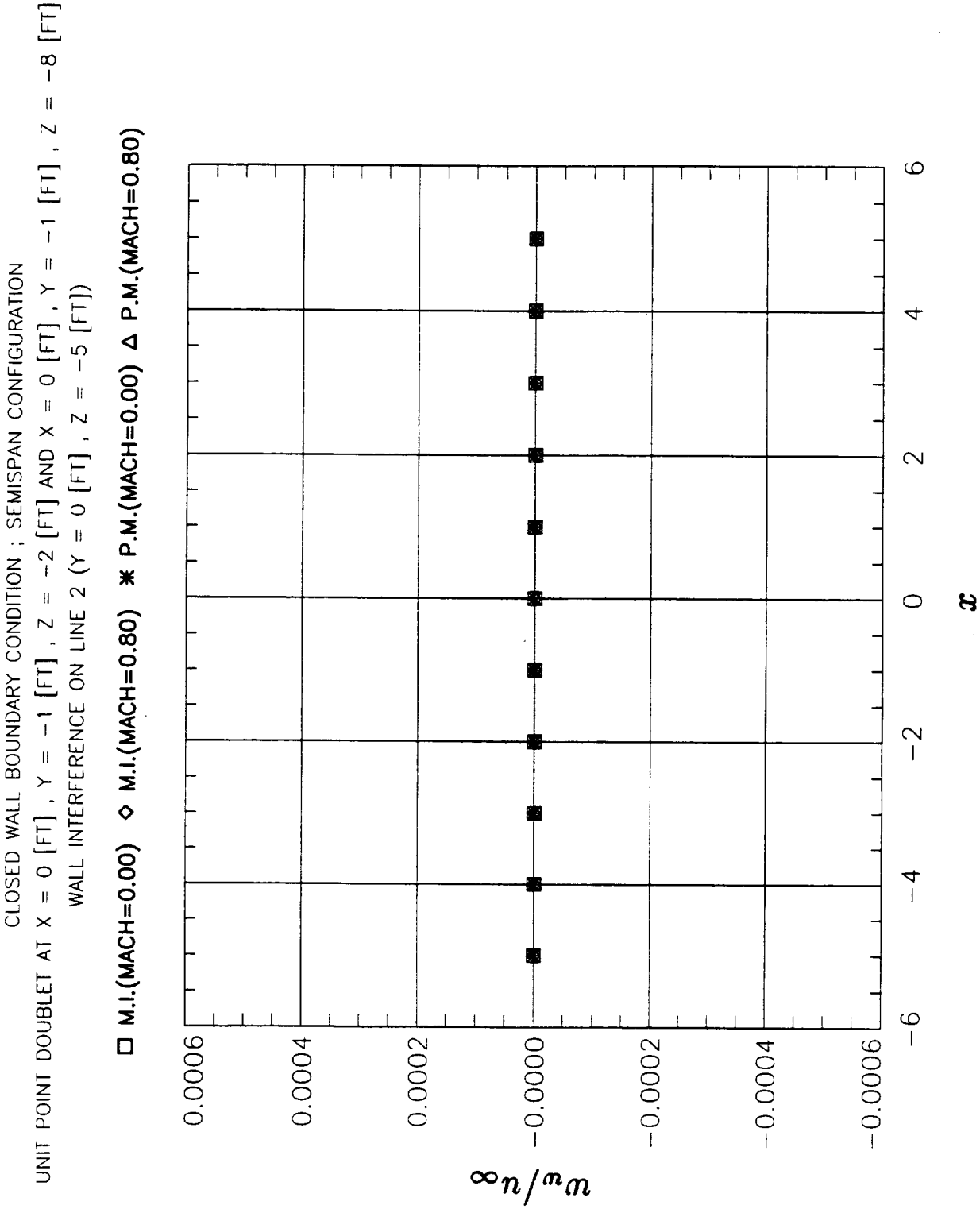

Fig. 9c Wall interference velocity component w_w/u_∞ due to two unit point doublets in rectangular tunnel; Method of Images (M.I.) versus panel method code (P.M.).

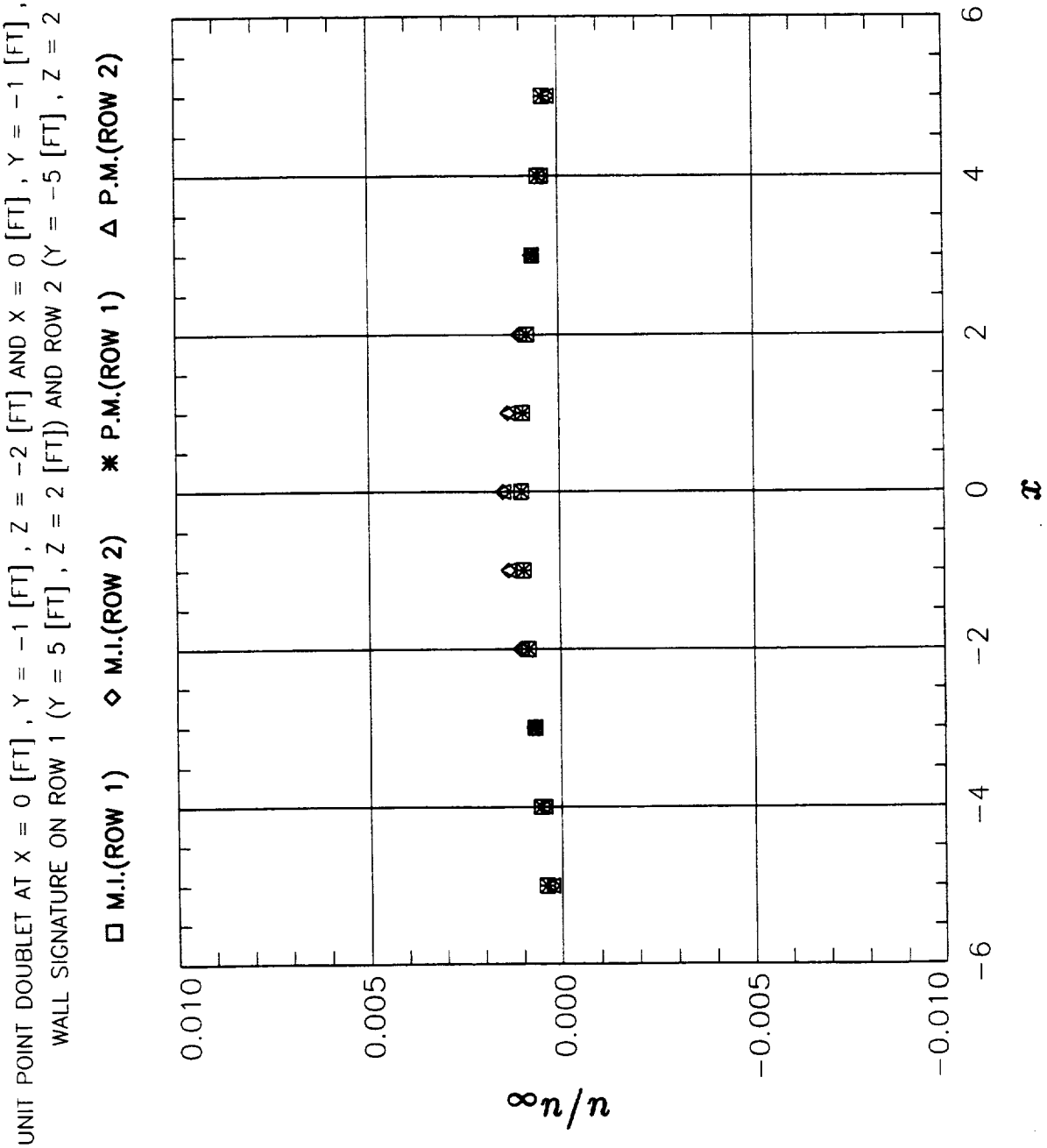

Fig. 9d Velocity component u/u_∞ ($M_\infty = 0.00$) due to two unit point doublets in rectangular tunnel; Method of Images (M.I.) versus panel method code (P.M.).

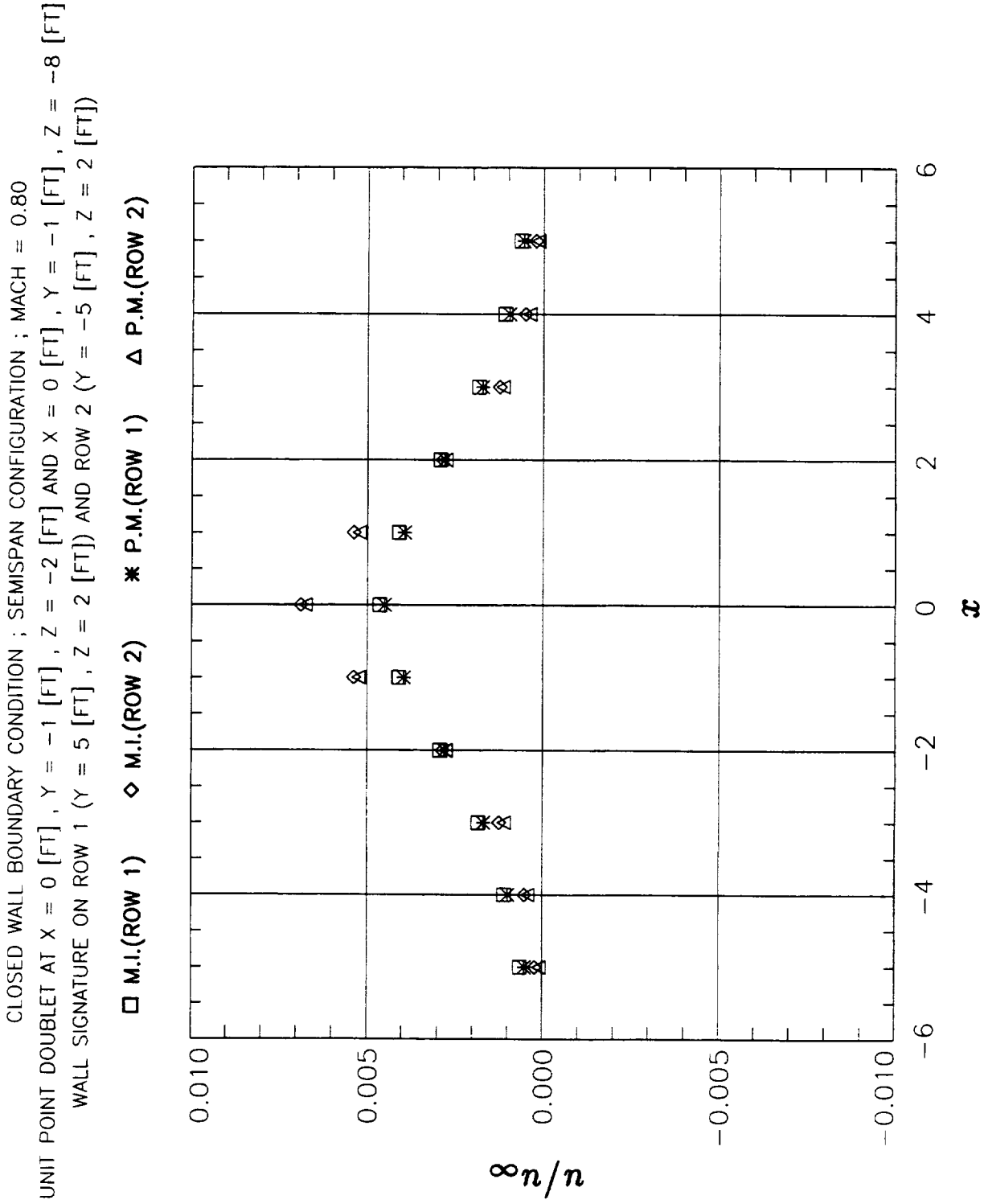

Fig. 9e Velocity component u/u_∞ ($M_\infty = 0.80$) due to two unit point doublets in rectangular tunnel; Method of Images (M.I.) versus panel method code (P.M.).

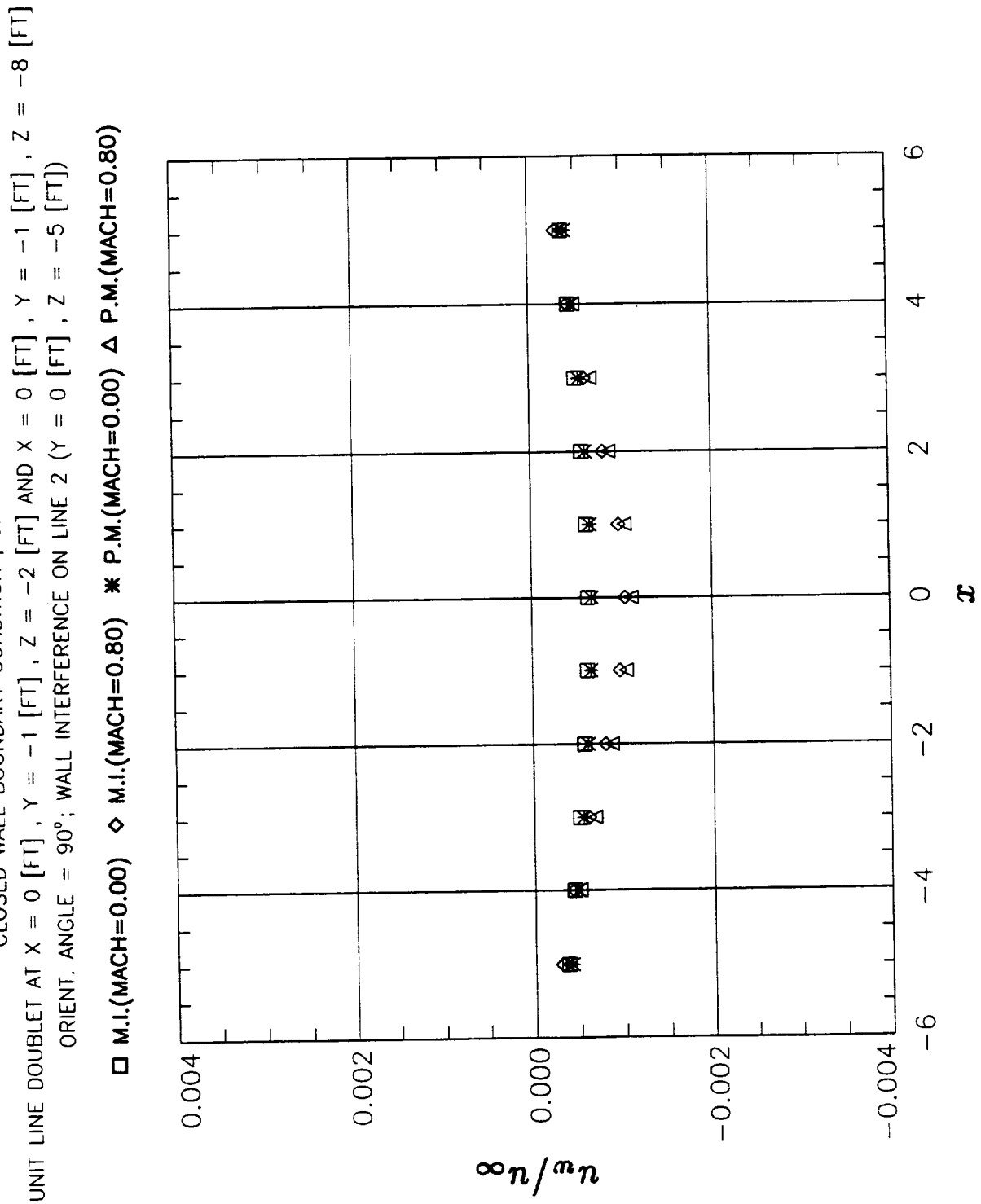

Fig. 10a Wall interference velocity component u_w/u_∞ due to two unit line doublets in rectangular tunnel; Method of Images (M.I.) versus panel method code (P.M.).

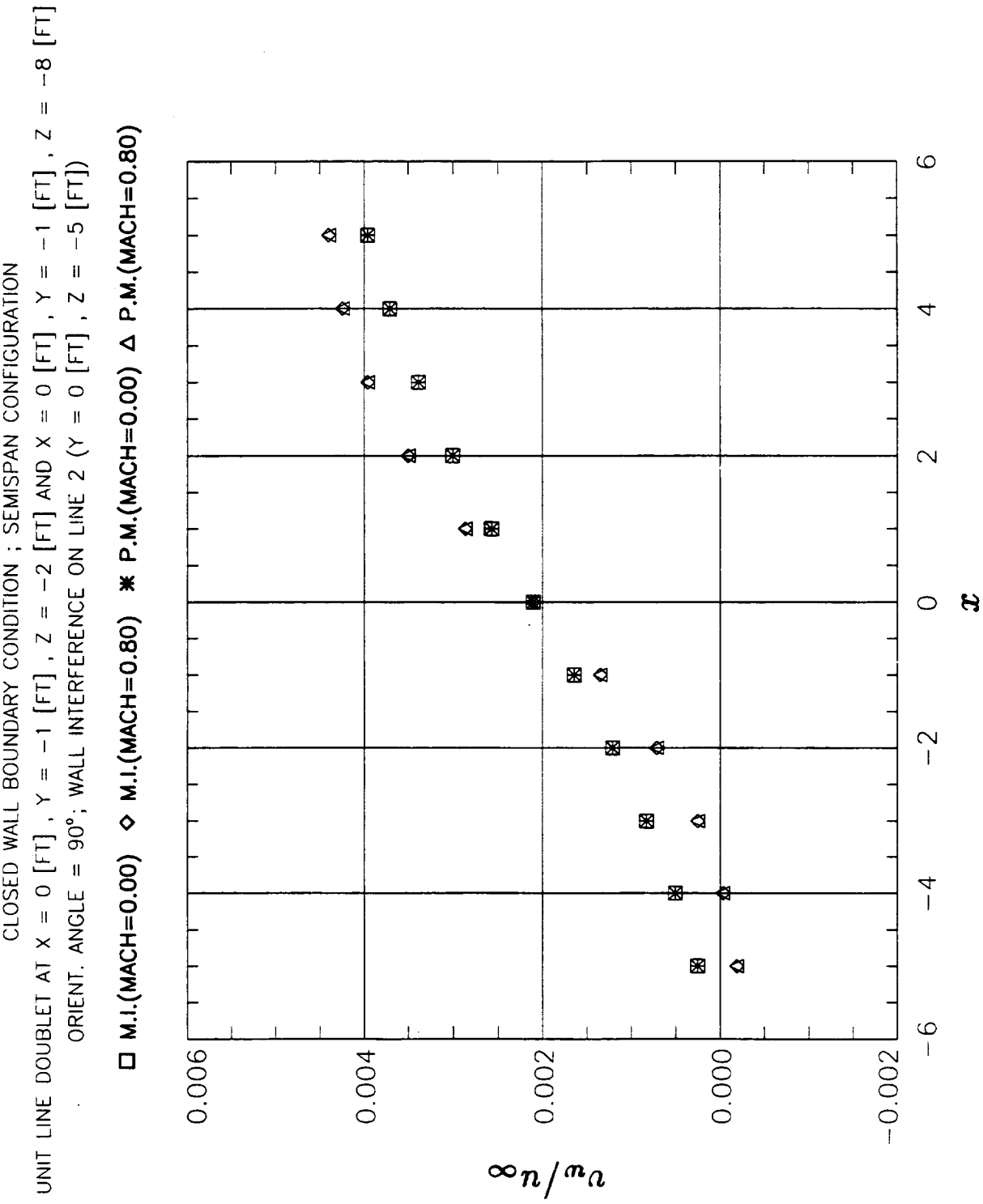

Fig. 10b Wall interference velocity component v_w/u_∞ due to two unit line doublets in rectangular tunnel; Method of Images (M.I.) versus panel method code (P.M.).

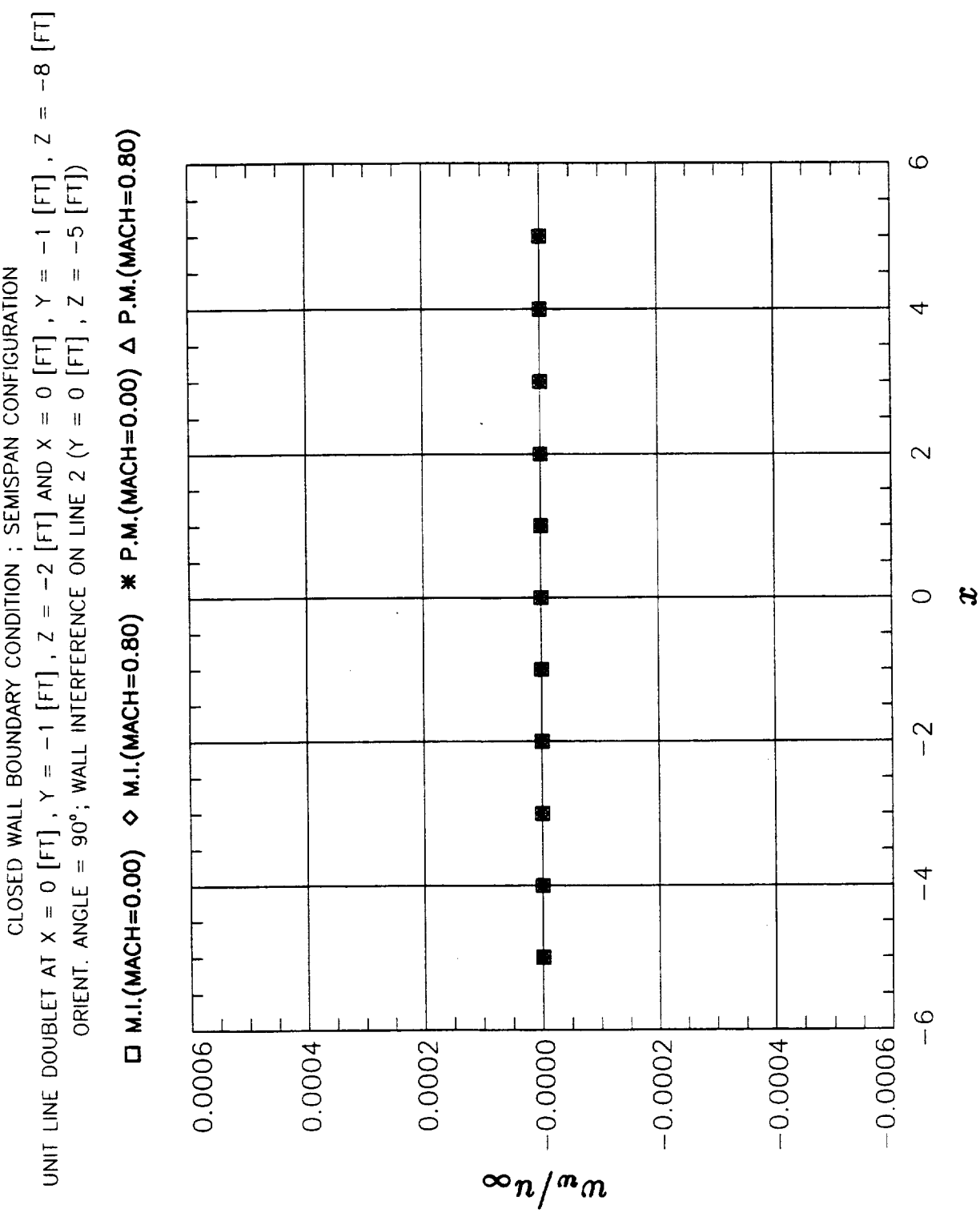

Fig. 10c Wall interference velocity component w_w/u_∞ due to two unit line doublets in rectangular tunnel; Method of Images (M.I.) versus panel method code (P.M.).

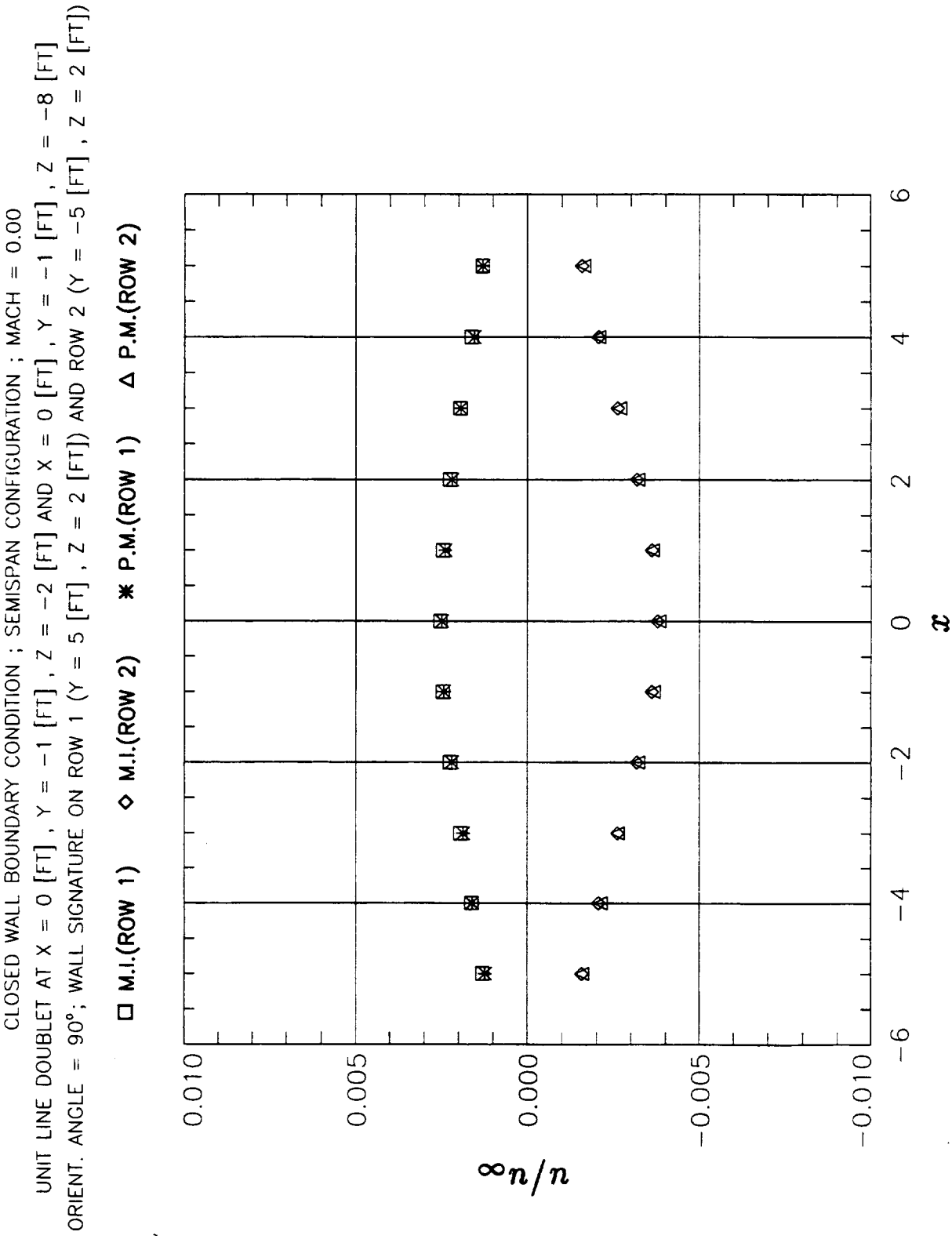

Fig. 10d Velocity component u/u_∞ ($M_\infty = 0.00$) due to two unit line doublets in rectangular tunnel; Method of Images (M.I.) versus panel method code (P.M.).

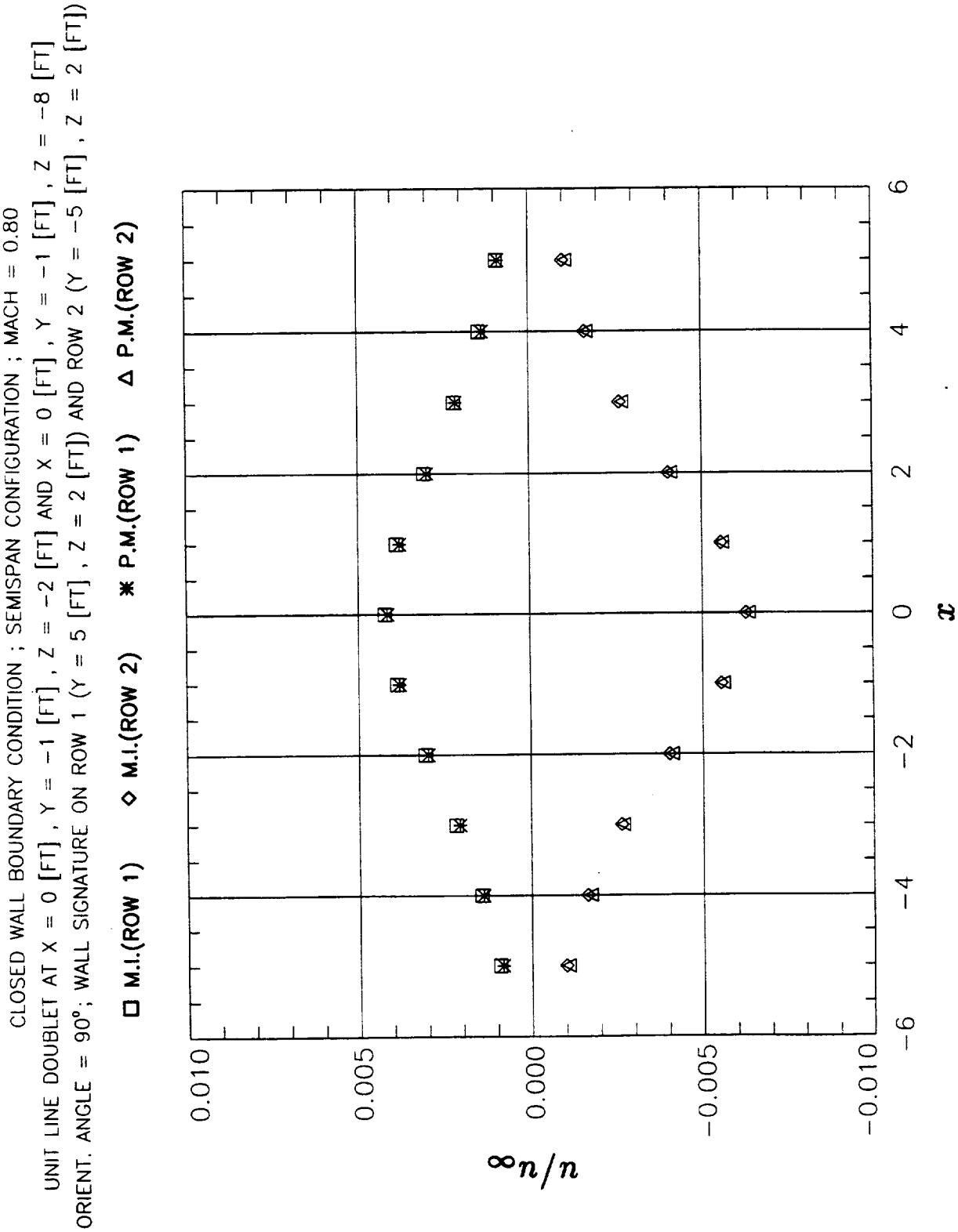

Fig. 10e Velocity component u/u_∞ ($M_\infty = 0.80$) due to two unit line doublets in rectangular tunnel; Method of Images (M.I.) versus panel method code (P.M.).

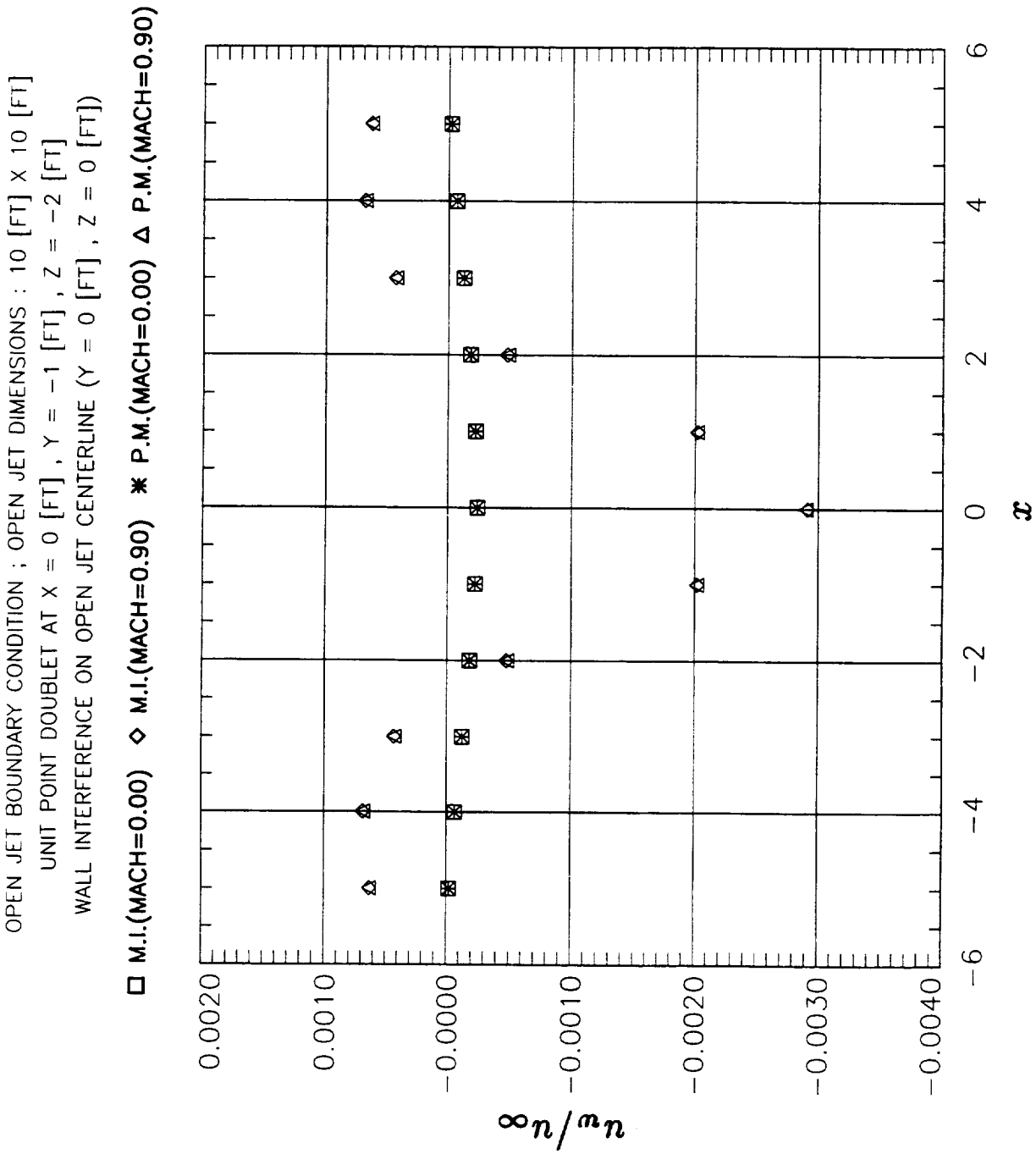

Fig. 11a Wall interference velocity component u_w/u_∞ due to unit point doublet in open jet; Method of Images (M.I.) versus panel method code (P.M.).

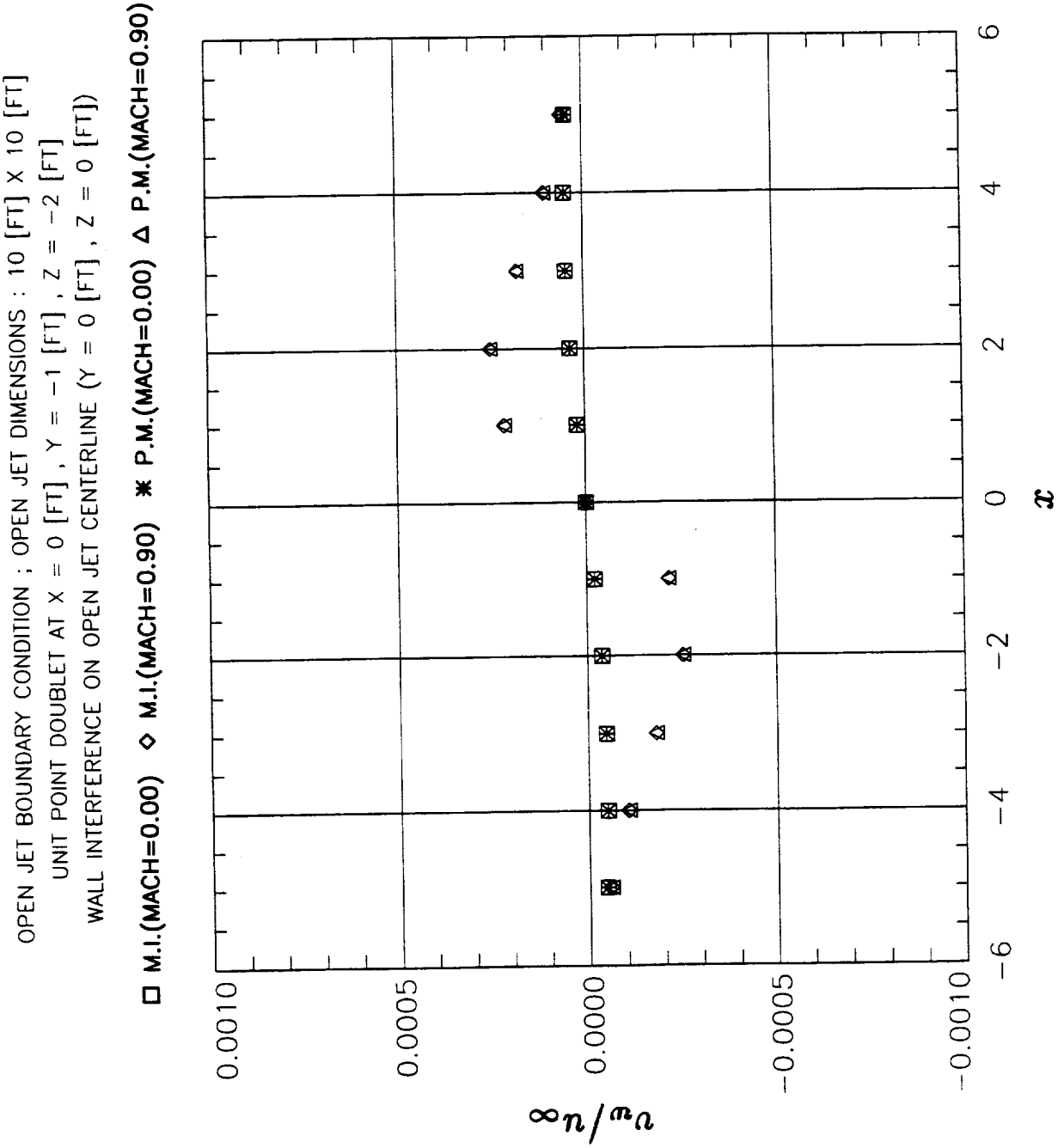

Fig. 11b Wall interference velocity component v_w/u_∞ due to unit point doublet in open jet; Method of Images (M.I.) versus panel method code (P.M.).

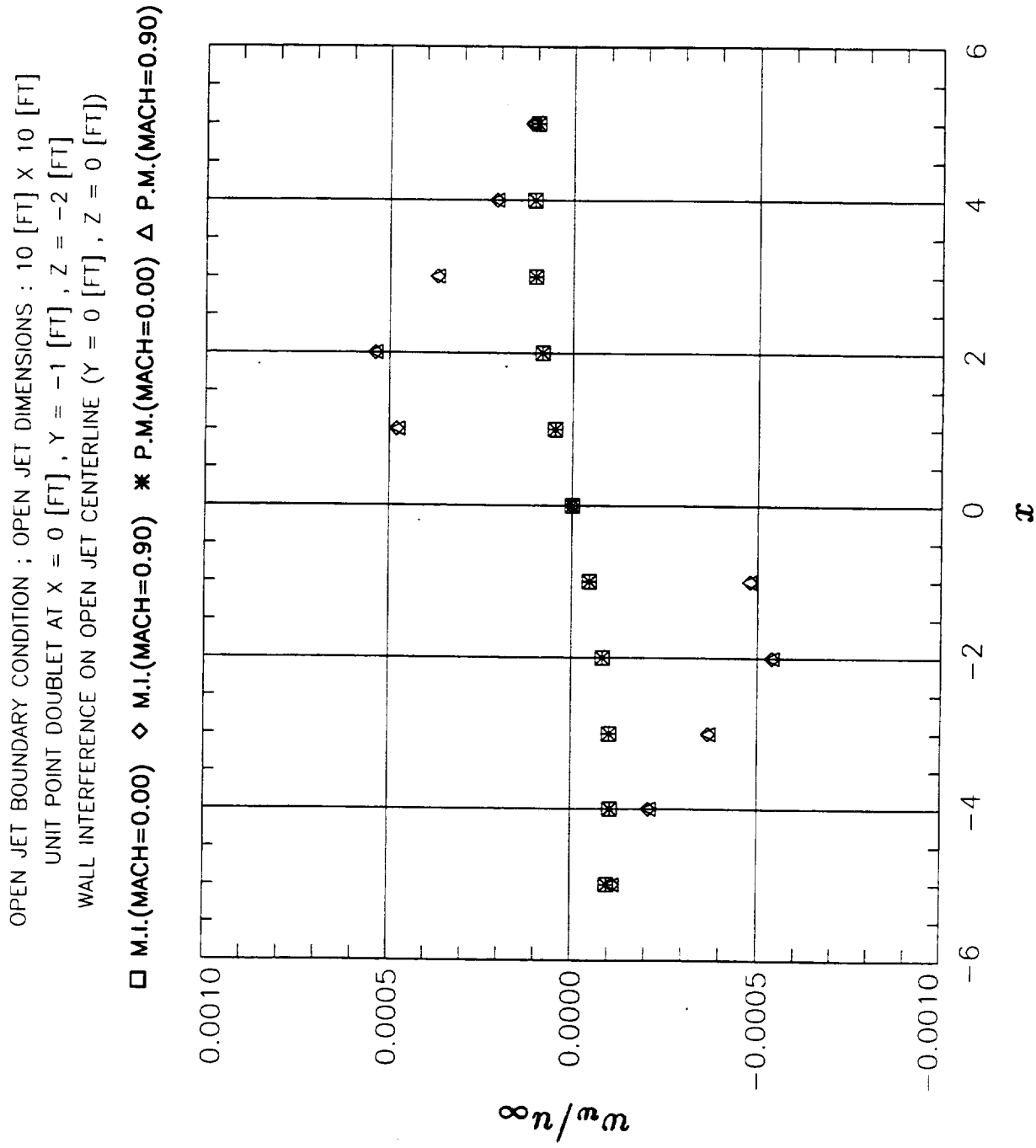

Fig. 11c Wall interference velocity component w_w/u_∞ due to unit point doublet in open jet; Method of Images (M.I.) versus panel method code (P.M.).

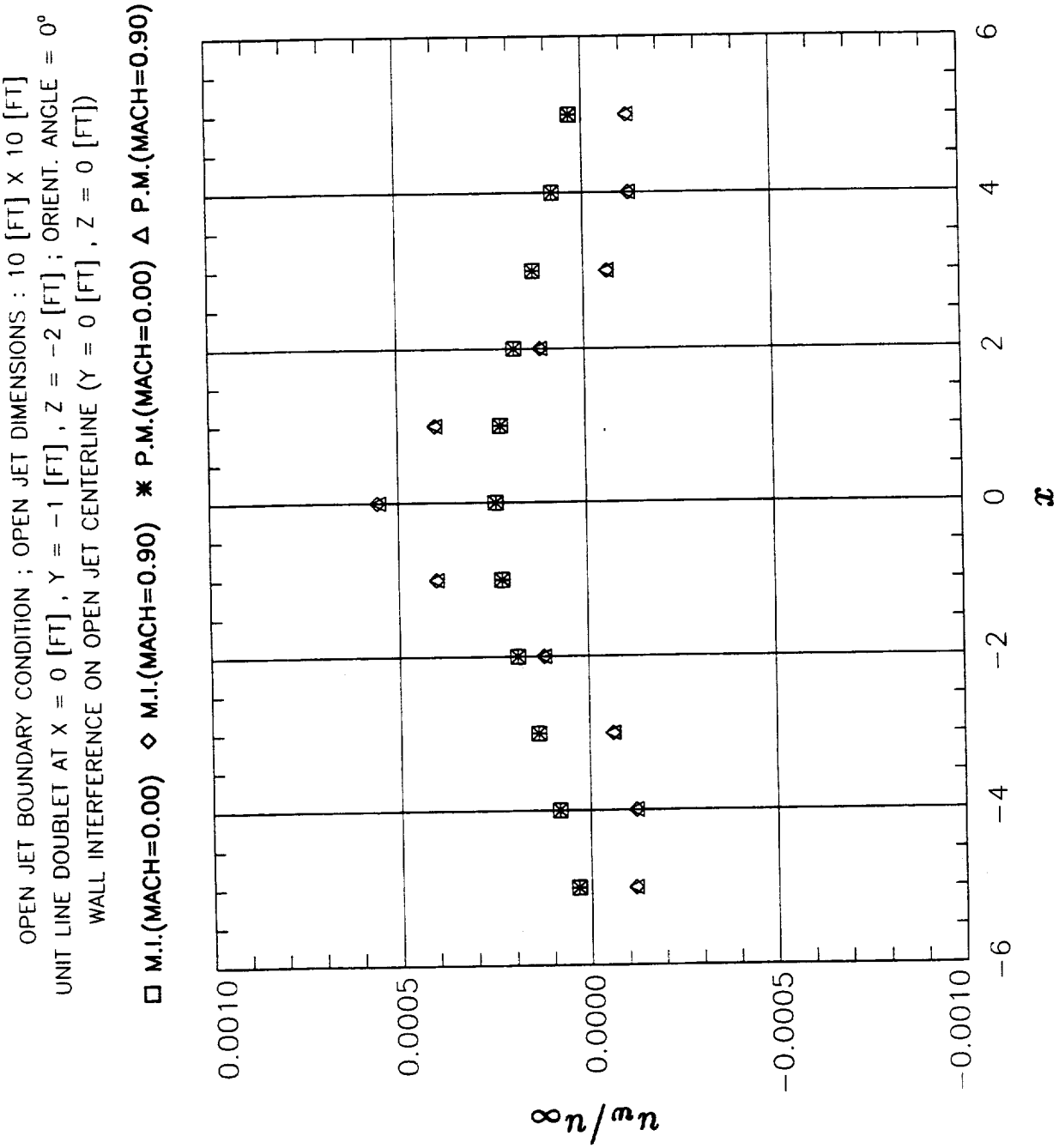

Fig. 12a Wall interference velocity component u_w/u_∞ due to unit line doublet in open jet; Method of Images (M.I.) versus panel method code (P.M.).

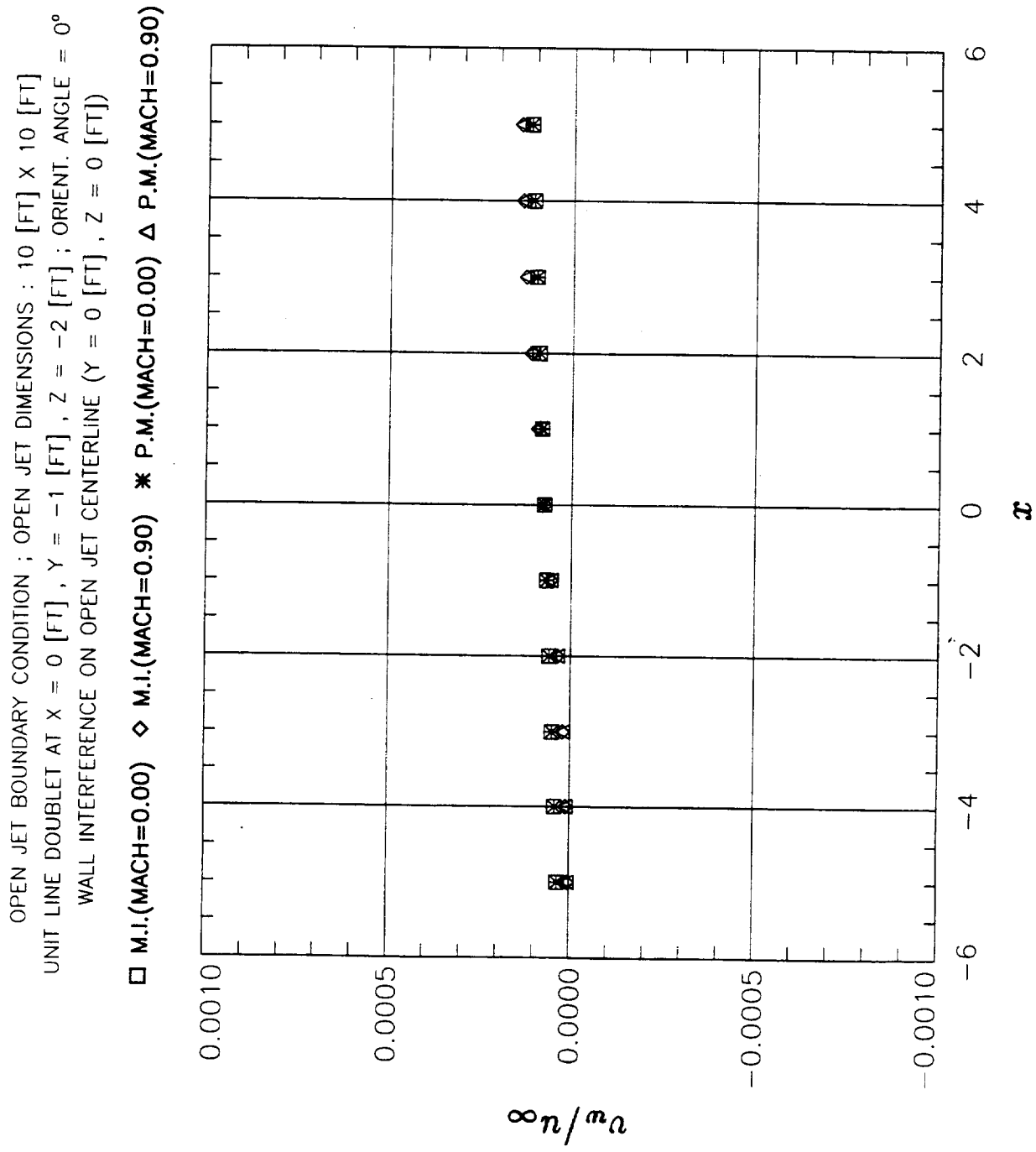

Fig. 12b Wall interference velocity component v_w/u_∞ due to unit line doublet in open jet; Method of Images (M.I.) versus panel method code (P.M.).

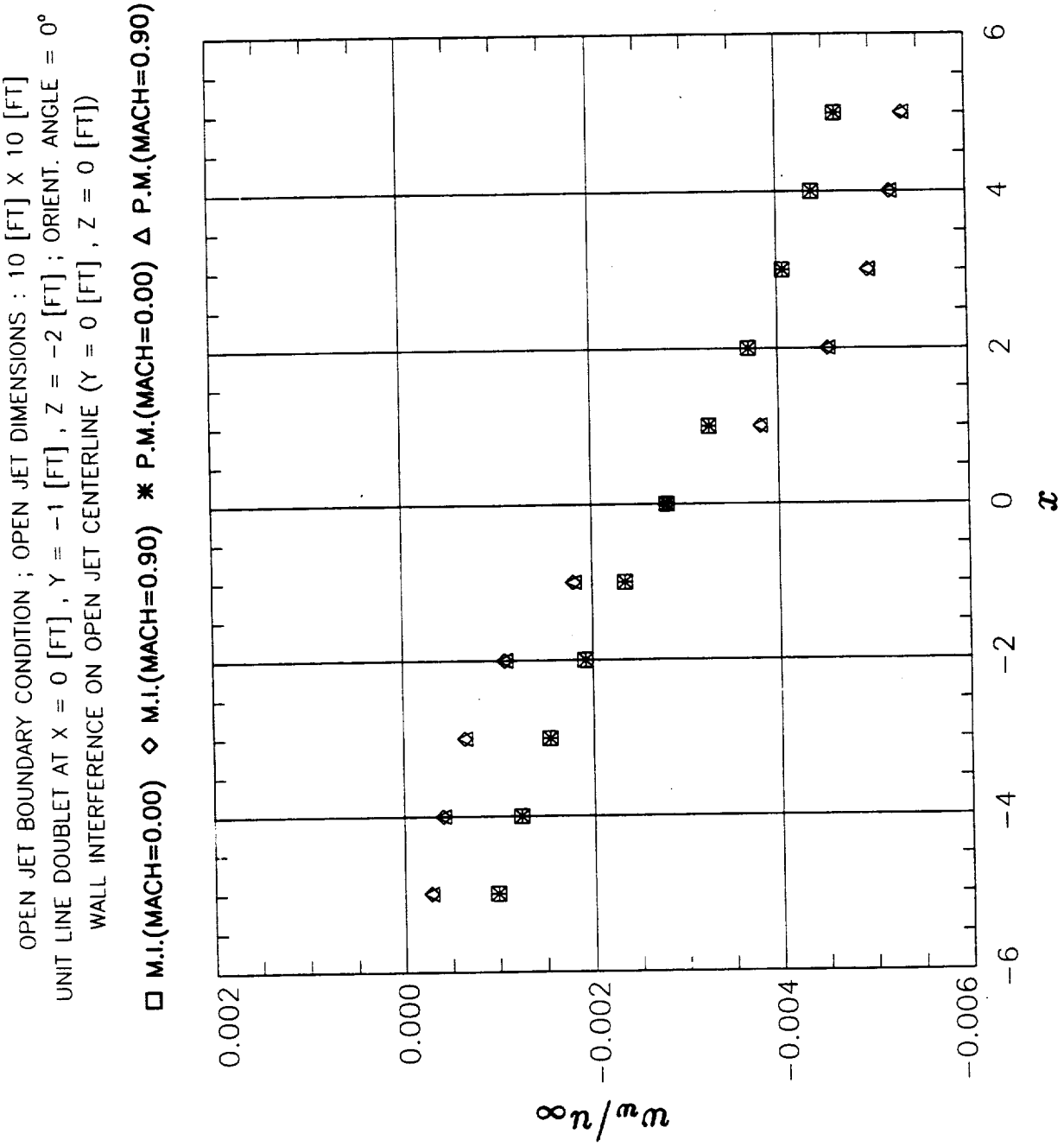

Fig. 12c Wall interference velocity component w_w/u_∞ due to unit line doublet in open jet; Method of Images (M.I.) versus panel method code (P.M.).

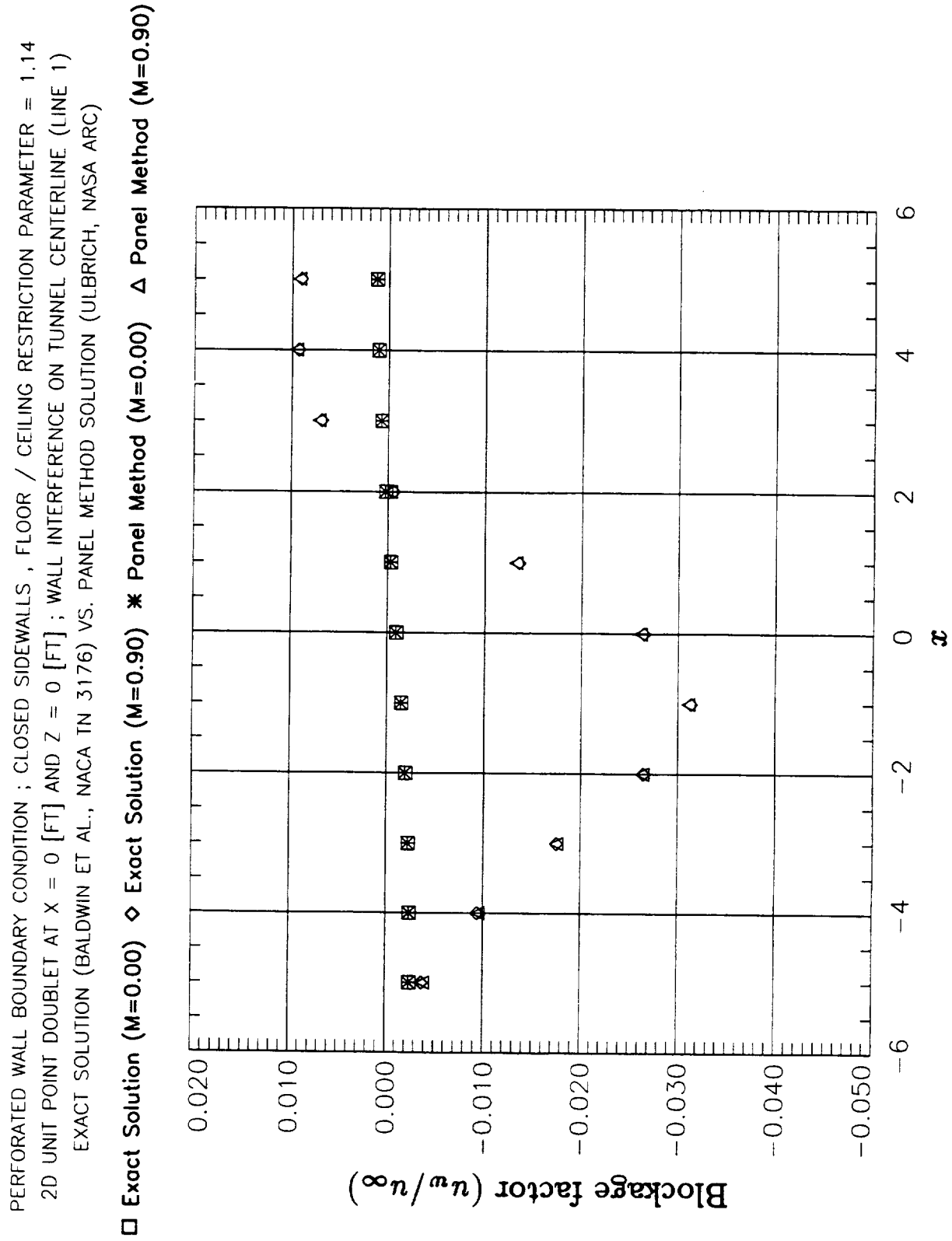

Fig. 13 Blockage factor (u_w/u_∞) on tunnel centerline due to 2D unit point doublet in 2D wind tunnel; NACA TN 3176 (Exact Solution) versus ANTARES (Panel Method).

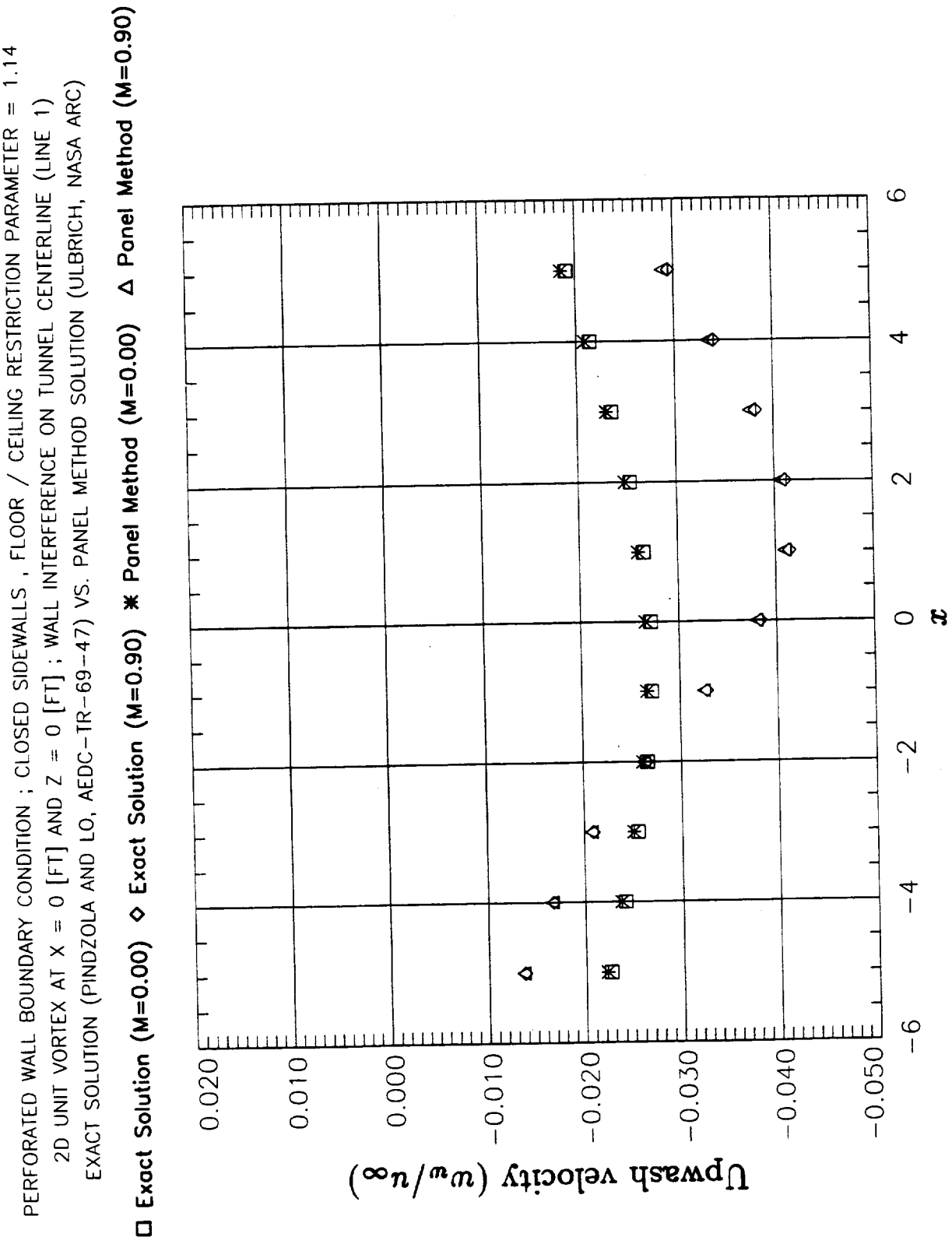

Fig. 14 Upwash velocity (w_w/u_∞) on tunnel centerline due to 2D unit vortex in 2D wind tunnel; AEDC-TR-69-47 (Exact Solution) versus ANTARES (Panel Method).

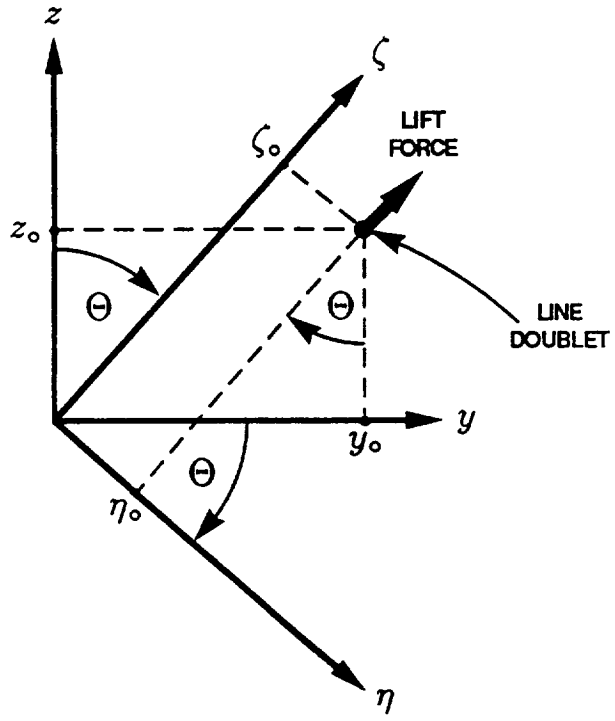

Fig. 15a Coordinate system rotation as a function of line doublet orientation angle.

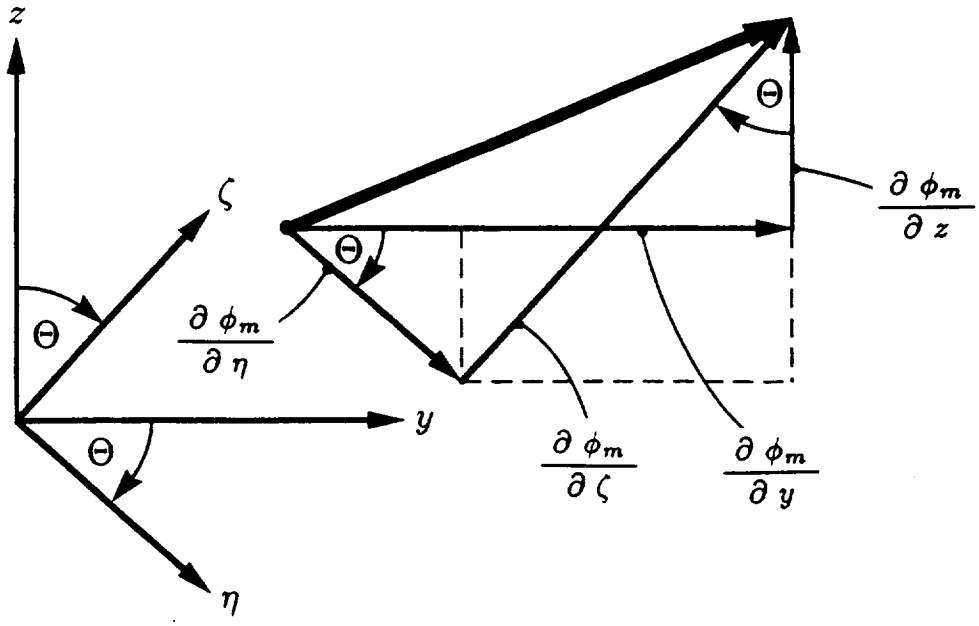

Fig. 15b Perturbation velocity component transformation.

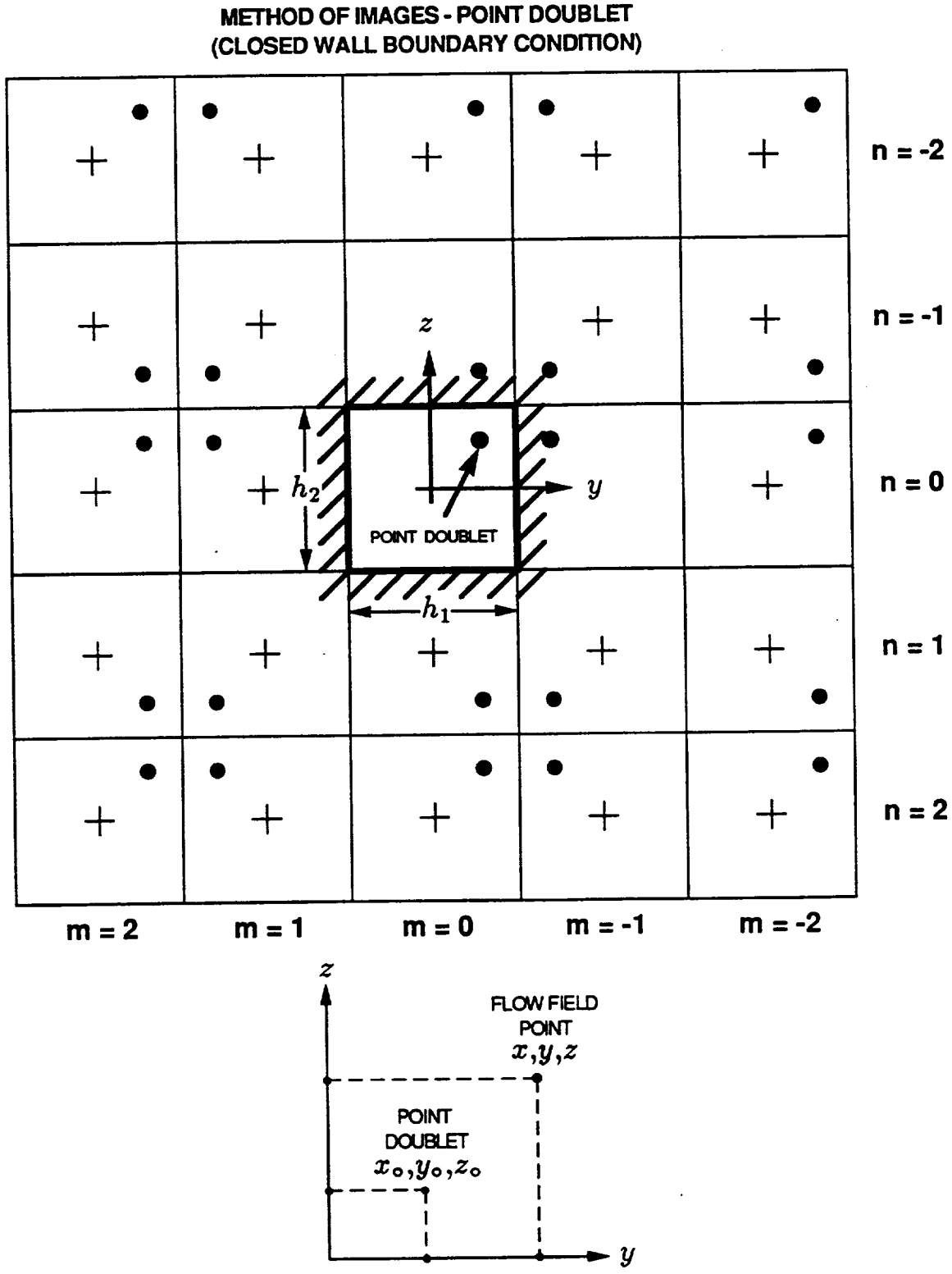

Fig. 16a Image system of point doublet for closed wall boundary condition.

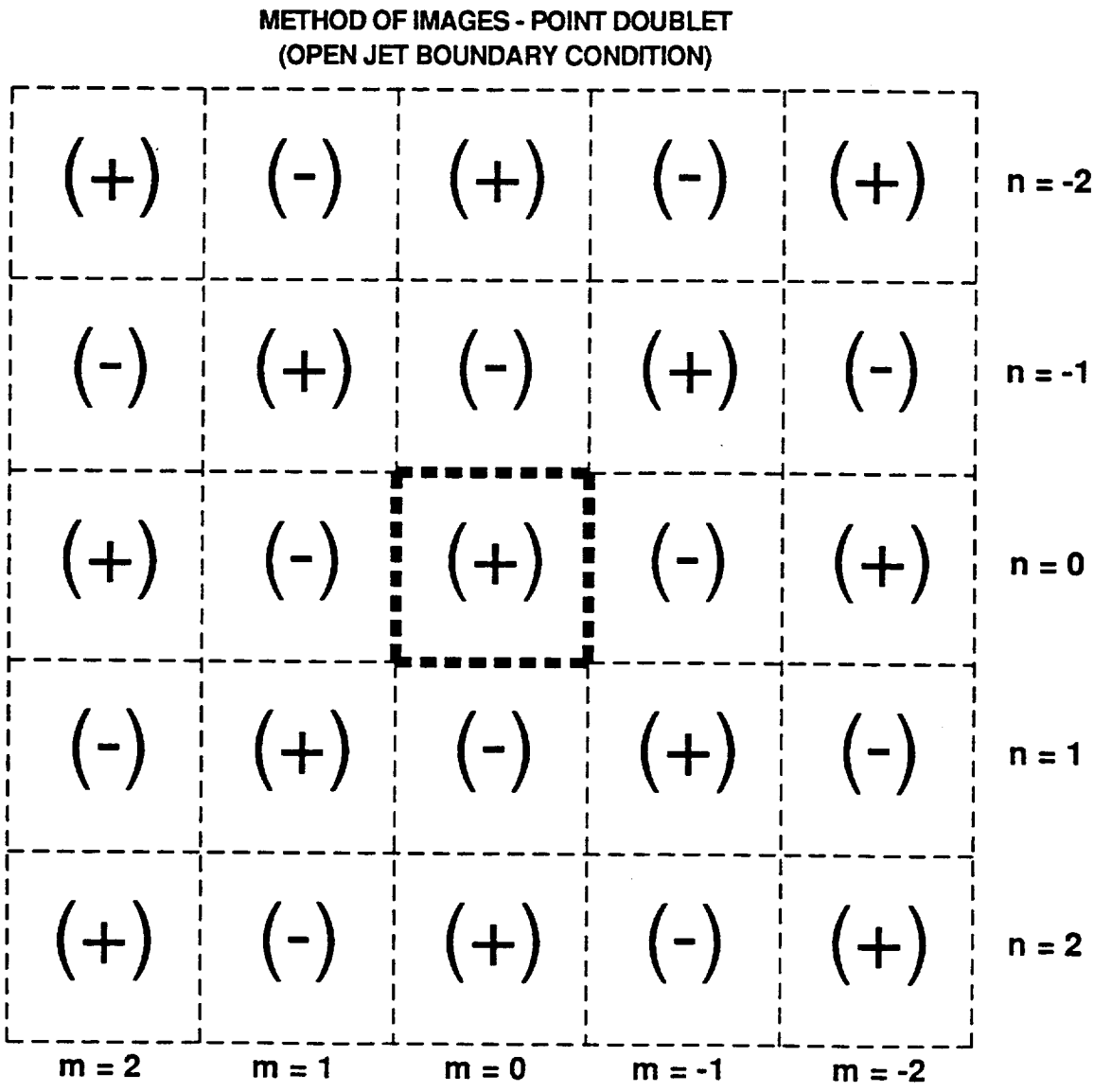

Fig. 16b Image system of point doublet for open jet wall boundary condition.

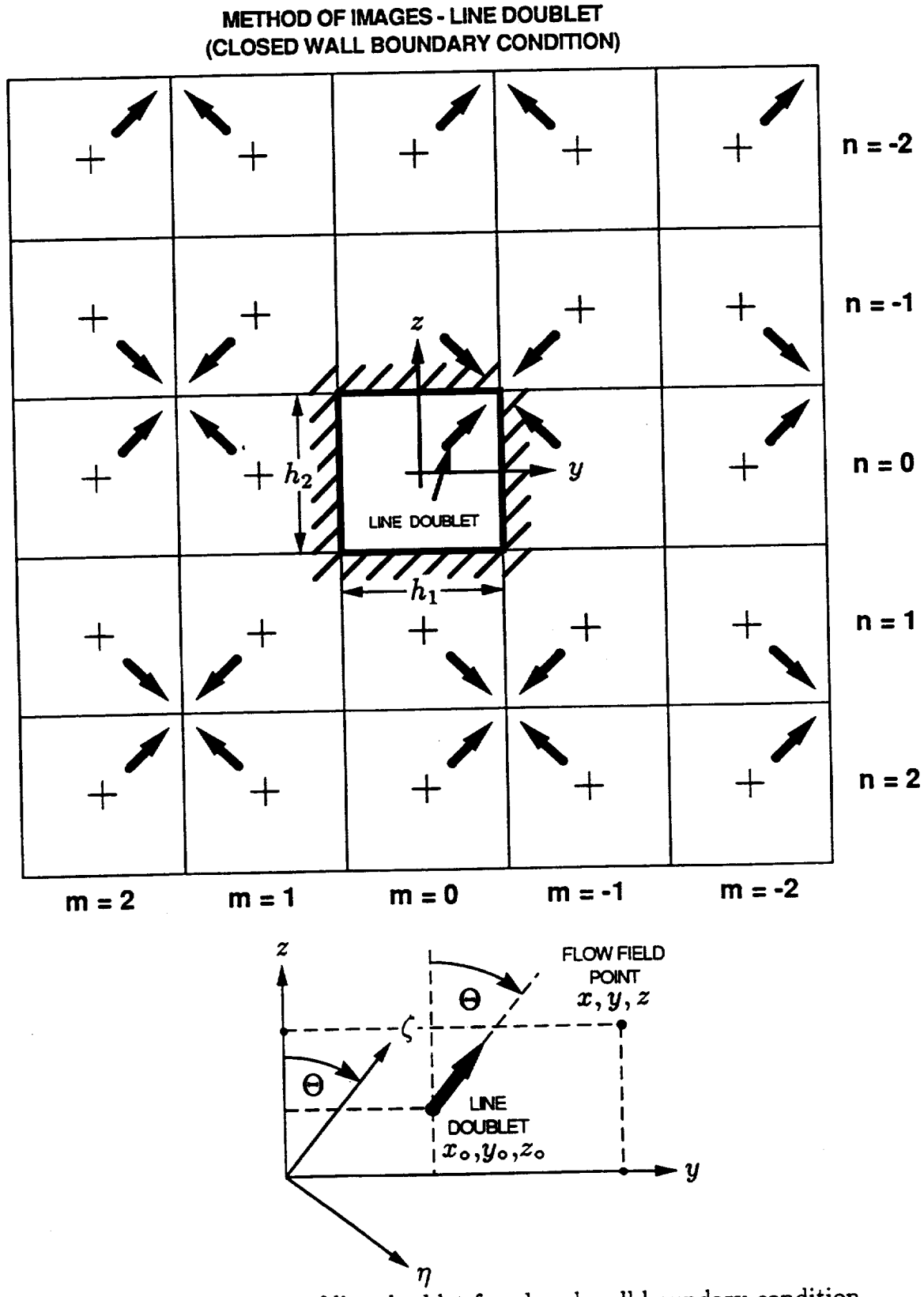

Fig. 17a Image system of line doublet for closed wall boundary condition.

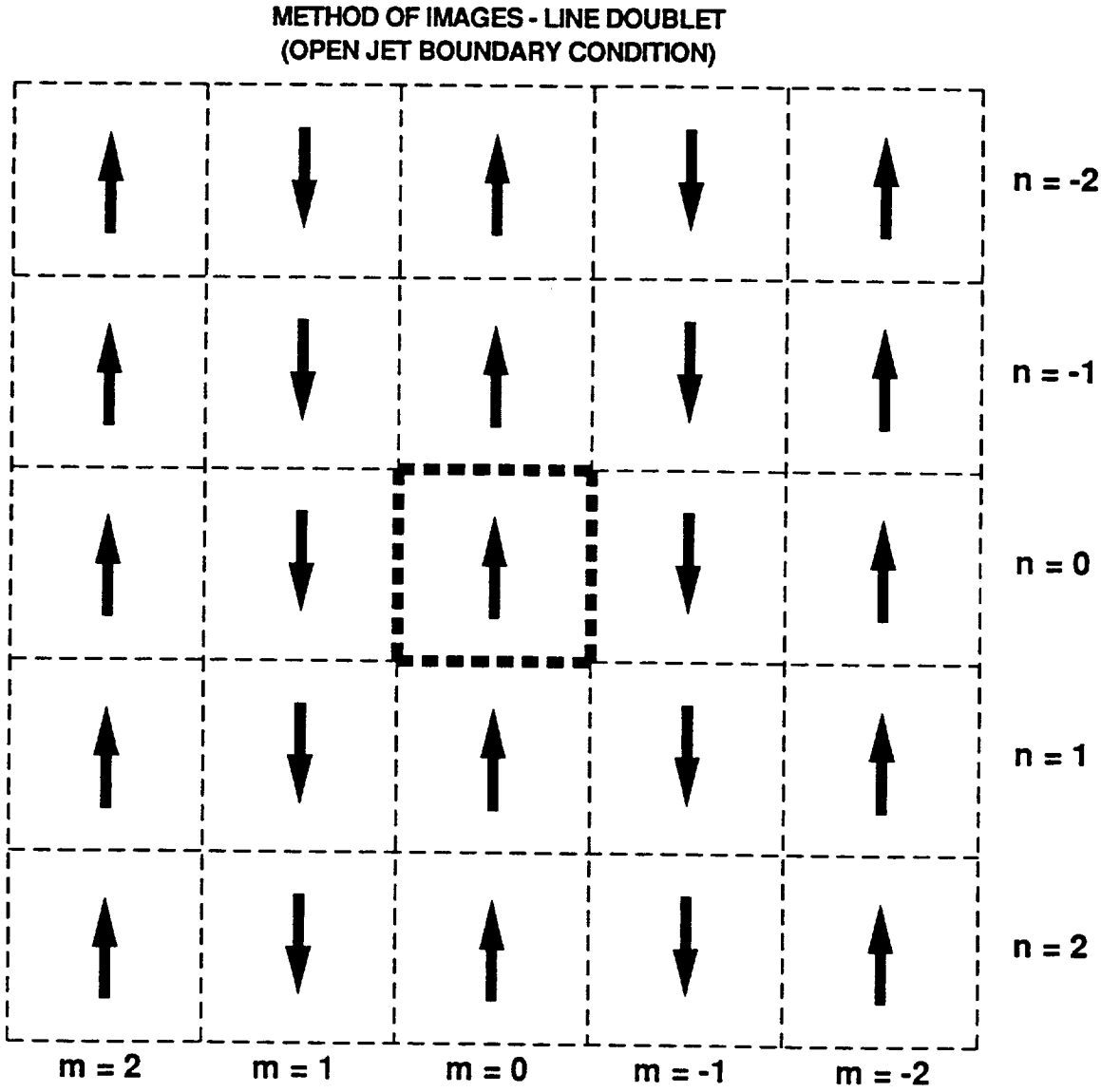

Fig. 17b Image system of line doublet for open jet wall boundary condition.

REPORT DOCUMENTATION PAGE

Form Approved
OMB No. 0704-0188

1. AGENCY USE ONLY *(Leave blank)*	2. REPORT DATE	3. REPORT TYPE AND DATES COVERED
	May 2000	Contractor Report

4. TITLE AND SUBTITLE
Description of Panel Method Code ANTARES

5. FUNDING NUMBERS
NAS2-98083

6. AUTHOR(S)
Norbert Ulbrich

7. PERFORMING ORGANIZATION NAME(S) AND ADDRESS(ES)
Sverdrup Technology, Inc.
P.O. Box 366, M/S 227-4
Moffett Field, CA 94035-1000

8. PERFORMING ORGANIZATION REPORT NUMBER
A-00V0017

9. SPONSORING/MONITORING AGENCY NAME(S) AND ADDRESS(ES)
National Aeronautics and Space Administration
Washington, DC 20546-0001

10. SPONSORING/MONITORING AGENCY REPORT NUMBER
NASA/CR-2000-209592

11. SUPPLEMENTARY NOTES
Point of Contact: Norbert Ulbrich, Ames Research Center, M/S 227-3, Moffett Field, CA 94035-1000
(650) 604-6893

12a. DISTRIBUTION/AVAILABILITY STATEMENT
Unclassified — Unlimited
Subject Category 09 Distribution: Standard
Availability: NASA CASI (301) 621-0390

12b. DISTRIBUTION CODE

13. ABSTRACT ***(Maximum 200 words)***

Panel method code ANTARES was developed to compute wall interference corrections in a rectangular wind tunnel. The code uses point doublets to represent blockage effects and line doublets to represent lifting effects of a wind tunnel model. Subsonic compressibility effects are modeled by applying the Prandtl-Glauert transformation. The closed wall, open jet, or perforated wall boundary condition may be assigned to a wall panel centroid. The tunnel walls can be represented by using up to 8000 panels. The accuracy of panel method code ANTARES was successfully investigated by comparing solutions for the closed wall and open jet boundary condition with corresponding Method of Images solutions. Fourier transform solutions of a two-dimensional wind tunnel flow field were used to check the application of the perforated wall boundary condition. Studies showed that the accuracy of panel method code ANTARES can be improved by increasing the total number of wall panels in the circumferential direction. It was also shown that the accuracy decreases with increasing free-stream Mach number of the wind tunnel flow field.

14. SUBJECT TERMS	15. NUMBER OF PAGES
Subsonic flow, Wind tunnel wall interference, Panel method code	109
	16. PRICE CODE: A06

17. SECURITY CLASSIFICATION OF REPORT	18. SECURITY CLASSIFICATION OF THIS PAGE	19. SECURITY CLASSIFICATION OF ABSTRACT	20. LIMITATION OF ABSTRACT
Unclassified	Unclassified		